Chem Soc Rev

Structural modification strategies for the rational design of Red/NIR region BODIPYs

Journal:	*Chemical Society Reviews*
Manuscript ID:	CS-REV-01-2014-000030.R1
Article Type:	Review Article
Date Submitted by the Author:	14-Mar-2014
Complete List of Authors:	Lu, Hua; Hangzhou Normal University, Key Laboratory of Organosilicon Chemistry and Material Technology Mack, John; Rhodes University, Yang, Yongchao; Nanjing University, Department of Chemistry Shen, Zhen; Nanjing University, Department of Chemistry

Structural modification strategies for the rational design of Red/NIR region BODIPYs†

Hua Lu,[a,b] John Mack,[c] Yongchao Yang,[a] Zhen Shen*[a]

[a] State Key Laboratory of Coordination Chemistry, Nanjing National Laboratory of Microstructures, Nanjing University, Nanjing, 210093, P. R. China. zshen@nju.edu.cn

[b] Key Laboratory of Organosilicon Chemistry and Material Technology, Ministry of Education, Hangzhou Normal University, Hangzhou, 310012, P. R. China.

[c] Department of Chemistry, Rhodes University, Grahamstown, 6140, South Africa.

†This review is dedicated to Professor Xiaozeng You on the occasion of his 80th birthday.

Table of Contents:

1. Introduction

2. Electronic structures and optical properties of BODIPY chromophores

2.1 BODIPY π-conjugation system

2.2 Optical properties of BODIPY

2.3 The formation of nonradiative S_1 states.

3. General synthetic methods

3.1 Peripheral substitution of the BODIPY core

3.1.1 Nucleophilic and transition metal catalyzed cross coupling reactions

3.1.2 C–H activity and oxidative nucleophilic reactions

3.1.3 Condensation reactions with benzaldehyde derivatives

3.2 Aromatic ring fusion

3.2.1 Reactions of aromatic ring-fused pyrroles with aldehydes

3.2.2 Reactions of acylpyrroles with structurally modified pyrroles

3.3 Aza-substitution at the *meso*-position

3.3.1 Reactions of pyrroles with nitrosopyrroles

3.3.2 Reactions of phthalonitriles with arylmagnesium bromides

4 Theoretical descriptions of the electronic structures of a series of structurally modified BODIPY dyes

5. Wavelength tuning strategies

5.1 Aryl-substituted BODIPYs

5.1.1 Diaryl-substituted BODIPYs

5.1.2 Polyaryl-substituted BODIPYs

5.2 Alkynyl-substituted BODIPYs

5.3 Styryl-substituted BODIPYs

5.3.1 Monostyryl-substituted BODIPYs

5.3.2 Distyryl-substituted BODIPYs

5.3.3 Multi-π-styryl-substituted BODIPYs

5.3.4 *Meso*-vinyl substituted BODIPYs

5.4 Heteroatom substituted BODIPYs

5.5 Fused-ring systems

5.5.1 Fused-ring systems with sp^3 hybridized carbons

5.5.2 Fused-ring systems with heteroatoms

5.5.3 Fused-ring systems with B–O chelation

5.6 Fused-ring-expansion systems

5.6.1 Fused-ring-expansion at the α, and β-positions

5.6.2 *Meso*-, β- and porphyrin-fused-BODIPYs

5.7 β-Aromatic ring-fused and α-substituted BODIPYs

5.8 Aza-BODIPYs

5.8.1 Tetra-aryl systems

5.8.2 Conformationally restricted systems

5.8.3 β-aromatic-fused α-substituted aza-BODIPYs

5.9 *Bis*-BODIPYs

5.9.1 Directly linked *bis*-BODIPYs

5.9.2 Aromatic-fused *bis*-BODIPYs and their analogues

5.10 BODIPY analogues

5.10.1 N–B–O analogues

5.10.2 N–B–N analogues

6 Conclusions and perspectives

7 Glossary of abbreviations

8 Acknowledgements

9 Reference

Abstract: This review focuses on classifying different types of long wavelength absorbing BODIPY dyes based on the wide range of structural modification methods that have been adopted, and on tabulating their spectral and photophysical properties. The structure-property relationships are analyzed in depth with reference to molecular modeling calculations, so that the effectiveness of the different structural modification strategies for shifting the main BODIPY spectral bands to longer wavelengths can be readily compared, along with their effects on the fluorescence quantum yield (Φ_F) values. This should facilitate the future rational design of red/NIR region BODIPY dyes for a wide range of different applications.

1. Introduction

Over the past decade there has been considerable interest in the synthesis of organic chromophores with strong absorption and fluorescence bands in the near-IR (NIR) region primarily because of advances in optical techniques for imaging, in microarrays, and in electrophoresis, and the need for

labels and optical sensors for biological and medical applications.[1-6] For the latter, it is advantageous to work in the red/NIR region of the spectrum because of the so-called biological window in the 650–1000 nm region, where autofluorescence, and absorption by water, tissues and cells are minimized, and there is less light scattering. This means that deeper penetration by incident laser light (2–5 cm) can be achieved in what is sometimes also described as the therapeutic window.[7-11] These factors, together with the development of low-cost NIR region excitation sources and detectors, have inspired the design of new fluorophores or fluorescent materials,[12-22] with high molar absorption coefficients and fluorescence quantum yield (Φ_F) values in this spectral region.[23]

Until recently, cyanine dyes, such as Cy3 or Cy5, have been the fluorochrome of choice in many biological applications, but issues related to their poor photostability and low Φ_F values are often encountered. Rotation and photoisomerization of their flexible structures often result in nonradiative deactivation pathways.[24-26] Even for more rigid or bridged cyanines, the remaining flexible bonds can still provide effective funnels for nonemissive deactivation.[27-28] Rhodamine dyes are often used as alternatives, owing to their structural rigidity. Rhodamine and fluoresceine dyes exhibit high Φ_F values, even in aqueous solvents. Their use in biological applications is problematic, however, since their absorption and emission maxima lie well below 600 nm.[3,29-30] Moreover, since they are positively charged ions, the solubility of rhodamines is generally restricted to highly polar solvents and the effect of the counter ion for the dye also has to be taken into consideration in any application.[31]

Boron-dipyrromethene (4,4-difluoro-4-bora-3a,4a-diaza-*s*-indacene, BDP or BODIPY) fluorescent dyes, a structural analogue of the porphyrins, have been the focus of considerable research interest over the last three decades.[32-41] The synthesis of BODIPY dyes was first described by Treibs and Kreuzer in 1968.[42] Since the mid-1980s, their use as solid-state solar concentrators has also been explored.[43-49] BODIPYs subsequently started to be used extensively as laser dyes, fluorescent stains and labels in fluorescence imaging, and as indicator dyes in sensory applications. In recent years, the number of papers being published on the synthesis and properties of BODIPY dyes has been growing

rapidly.[34,37-41] This has been related to, (i) their facile synthesis and structural versatility, (ii) their excellent spectroscopic properties (narrow Gaussian-shaped absorption and emission bands, high molar extinction coefficients (usually $\varepsilon > 80\ 000\ M^{-1}.cm^{-1}$) and Φ_F values (commonly $\Phi > 0.50$), moderate redox potentials, negligible triplet-state formation and negligible sensitivity to solvent polarity, excellent photostability, and high solubility in commonly used organic solvents of differing polarities), and (iii) their wide range of potential applications in numerous research fields.[32,33,37-40] A major drawback, however, is that the spectral properties of the classic BODIPY chromophore are typically limited to the 470 – 530 nm region.[50-55] Marked red-shifts of the absorption and emission maxima have been achieved through aryl, ethynylaryl and styryl substitution at the 1-, 3-, 5-, and/or 7-positions, aromatic ring fusion, by replacing the *meso*-carbon atom with an aza-nitrogen atom to form an aza-BODIPY, or combinations thereof.[50]

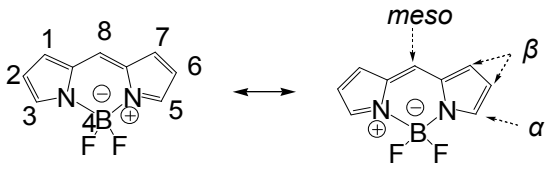

Fig. 1 The "BODIPY" fluorophore and its IUPAC numbering system. The 8-position is often referred to as the *meso*-carbon, while the 3,5-positions, and the 2,6- and 1,7-positions are referred to as the α- and β-carbons. Delocalized resonance structures of BODIPY are provided with the formal charges indicated.

Earlier reviews on BODIPY chemistry have covered the synthesis and spectroscopic properties of BODIPY dyes, as well as their applications in fluorescent indicators, photodynamic therapy, luminescent devices and energy transfer cassettes.[32-37,39-40] There has also been a strong focus on the versatility of the BODIPY core with respect to functionalization.[35] This review is dedicated to classifying different types of long wavelength BODIPY based on the wide range of structural modification strategies that have been adopted and on tabulating their spectral properties. The structure-property relationships are analyzed in depth with reference to molecular modeling calculations, so that the effectiveness of the different strategies can be readily compared, along with their impact on the Φ_F values. This should greatly facilitate the future rational design of red/NIR BODIPY dyes with properties suitable for applications.

In recent years, there has also been a considerable interest in the incorporation of BODIPY fluorophores into energy-transfer cassettes and polymers,[22,34,56-57] but this research is not included since this review focus on the modification of the BODIPY to long wavelength. The exchange of the two fluorine atoms at the boron centre with another anion provides another route for functionalizing these dyes.[58-70] Since this typically results in almost no change in the wavelength maxima, however, these structures are not included here. Readers interested in these topics should consult the relevant literature.

2. Electronic structures and optical properties of BODIPY chromophores

2.1 BODIPY π-conjugation system

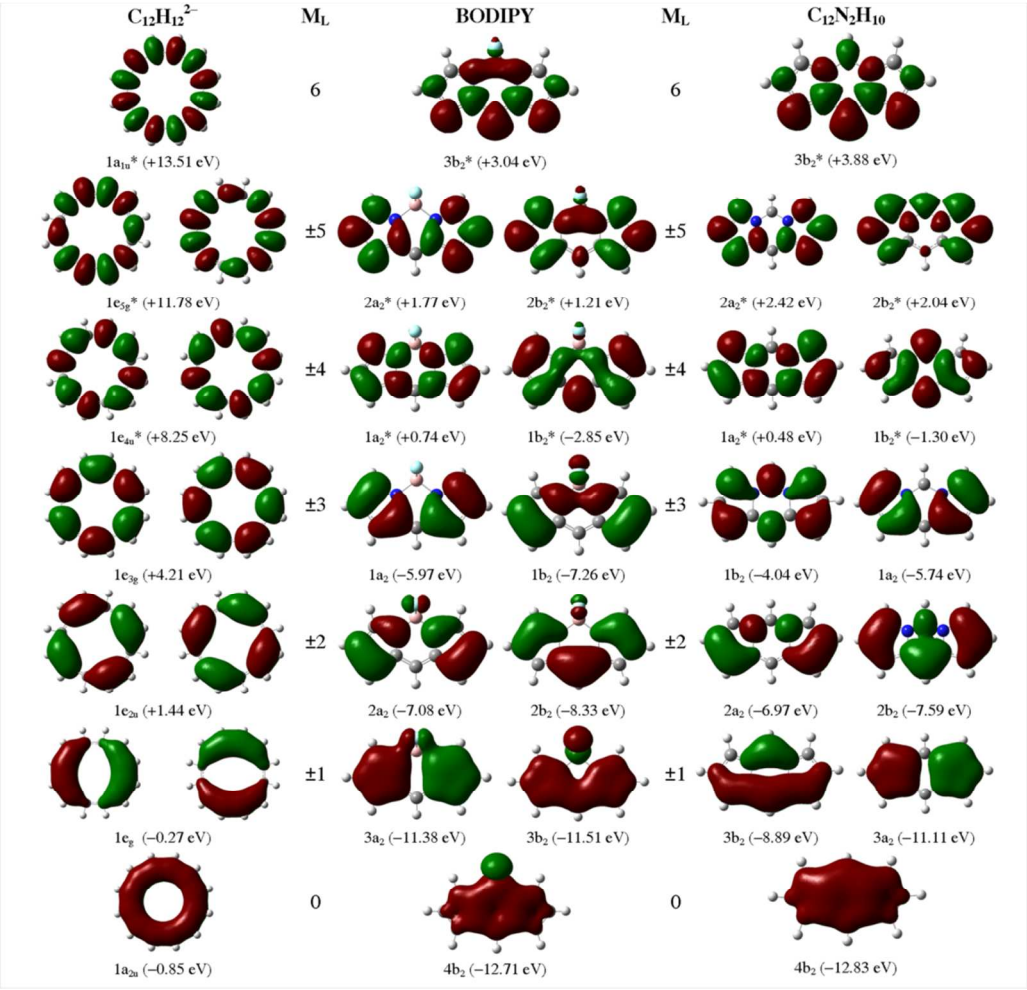

Fig. 2 MO energies of a $C_{12}H_{12}^{2-}$ cyclic perimeter, BODIPY and a $C_{12}H_{10}N_2$ model compound.

Although BODIPY dyes do not formally fit Hückel's rule for aromaticity, their properties are broadly similar to those of aromatic π-systems, since the coordination of the boron atom holds the dipyrromethene ligand in a rigidly planar conformation. The π-MOs associated with the indacene plane can be compared to those of an aromatic $C_{12}H_{12}^{2-}$ cyclic perimeter, which has MOs arranged in a $M_L = 0, \pm1, \pm2, \pm3, \pm4, \pm5, 6$ sequence in ascending energy terms. The angular nodal patterns for the π-MOs of an unsubstituted BODIPY dye follow a similar sequence, but the introduction of the BF_2 moiety, the cross links and pyrrole nitrogen atoms results in a marked lifting of the degeneracies of the MO energies due to the C_{2v} symmetry. This results in a HOMO and LUMO that are well-separated in energy terms from the other π-system MOs. Theoretical calculations predict that the lowest-lying $S_0 \rightarrow S_1$ transition is almost entirely associated with the HOMO → LUMO transition.[71] The a_2 MOs with a short-axis nodal plane passing through the boron atom are largely unaffected in energy terms relative to a $C_{12}H_{10}N_2$ heteroaromatic model compound, while the b_2 MOs with nodal planes aligned with the long-axis are significantly stabilized due to stronger bonding interactions between the two pyrrole moieties, larger MO coefficients on the electronegative nitrogen atoms, and the crosslinking between atoms on the outer perimeter due to the incorporation of the two pyrrole moieties. [71]

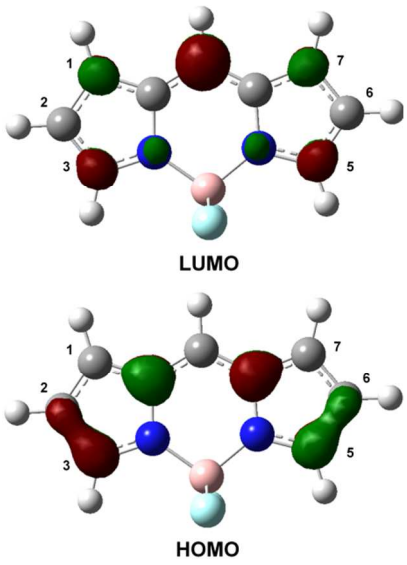

Fig. 3 Nodal patterns of the HOMO and LUMO of an unsubstituted BODIPY model compound at an isosurface of 0.07 a.u.

From the standpoint of obtaining a red-shift of the main absorption and emission spectral band, a structural modification must alter the energies of the two frontier π-MOs in a manner that narrows the HOMO–LUMO gap. Aryl-substituents can be added at the *meso*-carbon. Although the inductive effect of these substituents will usually have a similar effect on the energies of the HOMO and LUMO, the mesomeric effects can differ significantly.[72-74] The interaction between the π-systems typically has only a minor effect on the energy of the HOMO, since there is a nodal plane at the *meso*-carbon, but changes to the *para*-substituent on a phenyl substituent can have a significant impact on the energy of the LUMO, since there is a large MO coefficient at this position. The effects of substituents at the 1,7-, 2,6- and 3,5-positions of the BODIPY structure (Fig. 3) can be rationalized in a similar manner. There is a nodal plane near the 2,6-positions in the LUMO but not in the HOMO, while there are nodal planes near the 1,7-positions in the HOMO but not in the LUMO. Although there are no nodal planes, there are larger MO coefficients at the 3,5-positions in the HOMO than in the LUMO. In each case, there is scope for narrowing the HOMO–LUMO gap based on the mesomeric effects of substituents when there is an extension of the π-conjugation system.[71]

2.2 Optical properties of BODIPY

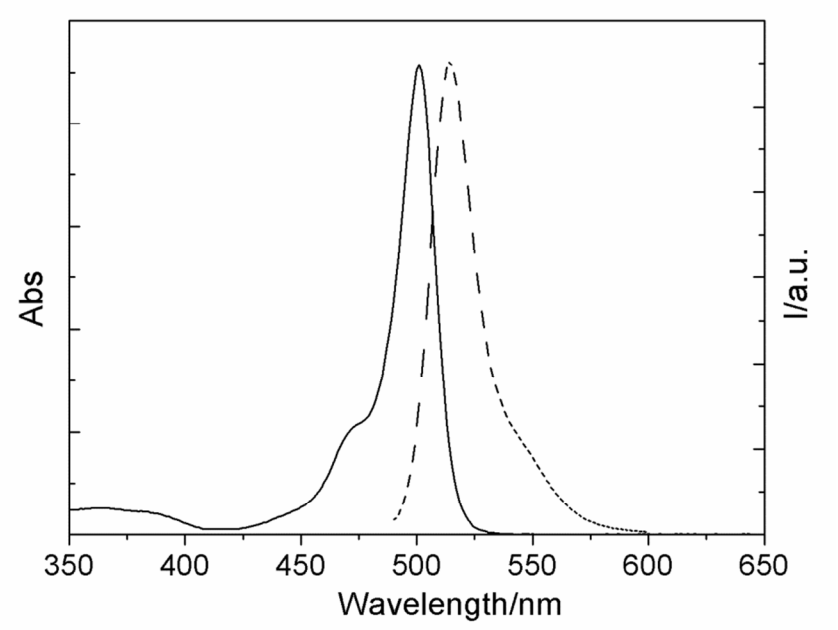

Fig. 4 Absorption and emission spectra of 1,3,5,7-tetramethyl-*meso*-phenyl-BODIPY, λ_{ex} = 470 nm.

Generally, the absorption spectra of BODIPY dyes contain narrow spectral bands with two absorption maxima in the visible region: (i) the intense 0-0 band of the S_0–S_1 transition and (ii) a more or less pronounced shoulder on the high-energy side of the main band, which is attributed to the 0-1 vibrational transition. Additionally, weaker broad absorption bands at shorter wavelengths can be assigned to S_0–S_n ($n \geq 2$) transitions.[75-82] When the BF_2 moiety is removed from the BODIPY structure, the structure is converted into the all-*trans* conformation and the chromophore is converted into a type of cyanine dye. Cyanine dyes undergo *trans-cis* isomerization upon electronic excitation, which quenches the fluorescence.[83] The favorable properties of BODIPY dyes for fluorescent dye applications can largely be attributed to their rigid planar structures. The potential energy surfaces of the S_0 and S_1 states are very similar, so narrow Gaussian-shaped absorption and emission bands are typically observed for the lowest energy transition. The rigidity of the π-system also leads to high Φ_F values, since there is a very low rate of nonradiative decay. Any structural modification, which results in a greater degree of conformational flexibility, will tend to result in a lower fluorescence quantum yield. Another reason for the high Φ_F values is that there are relatively low rates of intersystem crossing (ISC). This is an advantage for applications that depend on the intensity of the fluorescence emission band, but there are other potential applications such as photodynamic therapy which could make use of the red/NIR region dye properties of structurally modified BODIPYs, where this is not advantageous. In the last few years, heavy-atom-functionalized BODIPY dyes have been reported which exhibit enhanced rates of ISC and hence higher singlet oxygen quantum yields.[37,39]

2.3 The formation of nonradiative S_1 states.

The fluorescence intensity of structurally modified BODIPY dyes can be quenched in polar solvents due to an enhancement of the rate of nonradiative decay via what are often referred to as intramolecular charge transfer (ICT) states.[84-87] ICT states are derived from the S_1 state of the fluorophore and are caused by a separation of charge on different portions of the structure upon electronic excitation. The rate of nonradiative decay is believed to be enhanced by the formation of

conical intersections between this low-lying non-emissive S_1 state and the ground state.[84-87] It has been demonstrated that the charge-separated character of non-emissive S_1 state is enhanced when there is a twisting of the bond linking the donor and acceptor moieties.[85,86]

Another important quenching mechanism for the S_1 state is referred to as photoinduced electron transfer (PET).[73,88-96] In this context, an electron receptor and the fluorophore are usually separated by a short alkyl spacer, electronically disconnecting the π-electron systems of the receptor and fluorophore. The PET process is followed by nonradiative decay to the ground state. The Marcus theory[97] gives a quantitative description of the kinetics of electron transfer if the coupling between the initial and final states is well accounted. The PET process can be described pictorially in terms of molecular orbital (MO) theory,[98] and this has become a powerful tool for analyzing the fluorescence "on-off" problem.[99,100] In the unbound state, after excitation, the fast electron transfer from the receptor to the fluorophore quenches the fluorescence of the system. When the receptor is bound, the receptor redox potential is perturbed and slows down the PET process, reviving fluorescence emission. This logic indication process can also be reversed.[92] From the standpoint of Kasha's rule,[101] the "on-off" process of the fluorescence intensity can be considered as being due to the transformation of a radiative S_1 state into a nonradiative S_1 state.

3. General synthetic methods

The synthesis methods and structural modification strategies that have been used to shift the main absorption and emission bands to longer wavelengths will be briefly described. Three main approaches have been identified for the modification of the BODIPY structure through peripheral substitution. The BODIPY structure can also be modified through fused-ring-expansion of the pyrrole moiety and aza-substitution at the *meso*-position (Scheme 1).

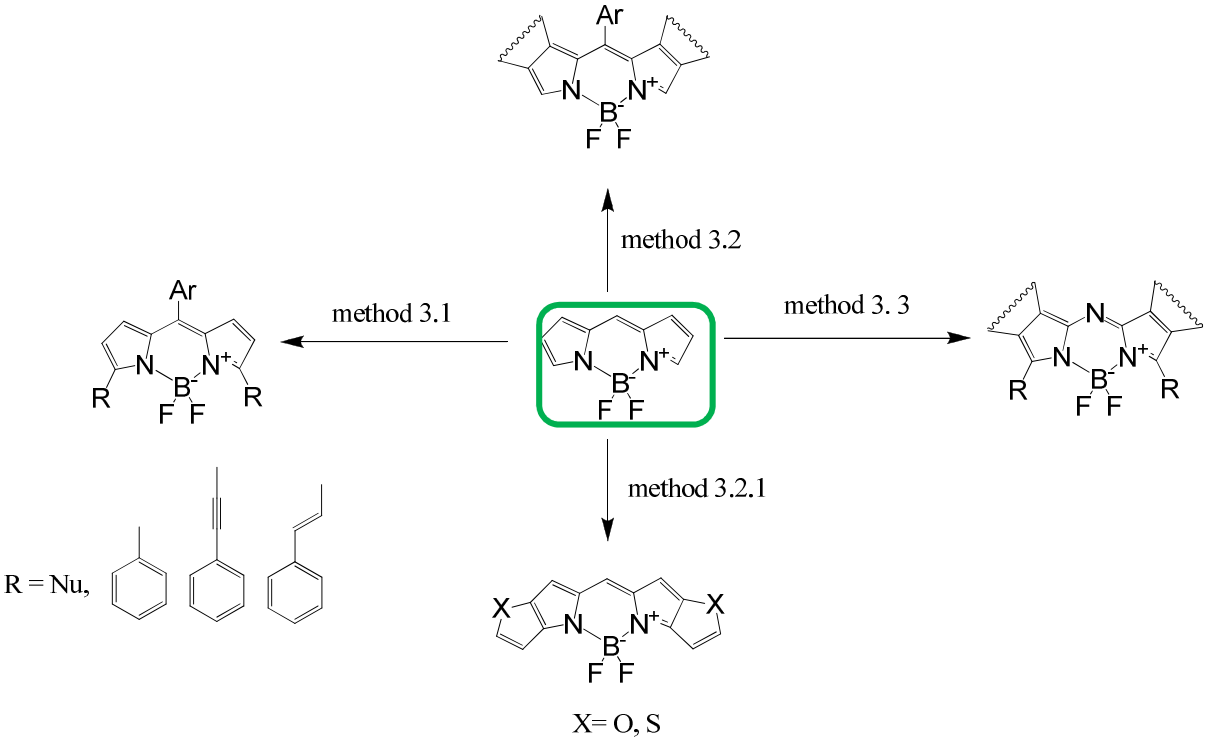

Scheme 1 General synthetic methods of the Red/ NIR BODIPY derivatives.

3.1 Peripheral substitution of the BODIPY core

3.1.1 Nucleophilic and transition metal catalyzed cross coupling reactions

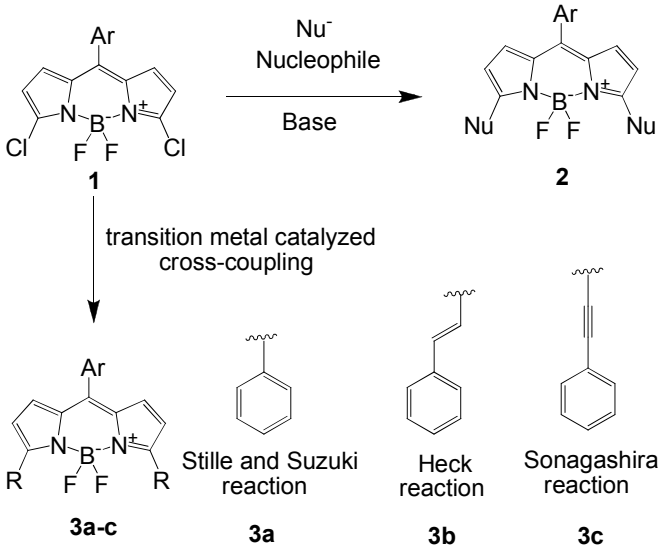

Scheme 2 The structural modification of 3,5-dichloroBODIPY via metal catalysis and nucleophilic substitution reactions. The R and Nu^- group are used to denote a wide range of different substituents.

3,5-Dichloro-BODIPY and other 3,5-dihalogenated BODIPYs are reactive towards aromatic substitution by oxygen, nitrogen, sulfur, selenium and tellurium nucleophiles,[102-112] and can also be reacted in various transition metal catalyzed cross-coupling reactions, such as Suzuki and Stille arylations, Heck reactions and Sonogashira alkynations.[113-121] The reaction conditions can be adjusted

so that either mono- or disubstituted products are formed. These nucleophilic substitution and cross-coupling reactions of 3,5-dichloroBODIPY represent a very successful approach for preparing a wide variety of BODIPY compounds, which absorb and emit in the red/NIR region. These types of reactions can also be utilized with BODIPYs that have been halogentated at the 2,6- and 1,7-positions.[122-126]

3.1.2 C–H activity and oxidative nucleophilic reactions

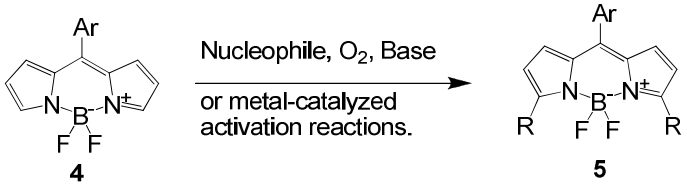

Scheme 3 Formation of α-substituted BODIPYs via a metal-catalyzed C–H bond activation and oxidative nucleophilic substitution reactions.

BODIPYs with no substituents at the α-pyrrole carbons (i.e. the 3,5-positions) are prone to oxidative nucleophilic attack. Substituents can be introduced in a single step under an oxygen atmosphere, based on the strength of their nucleophilicity.[127-133] Metal-mediated C–H functionalization can also be applied, and mono- or disubstituted dyes can be obtained.[134-136] A water soluble, sulfonated BODIPY dye has been prepared via this route in low yield.[134]

3.1.3 Condensation reactions with benzaldehyde derivatives

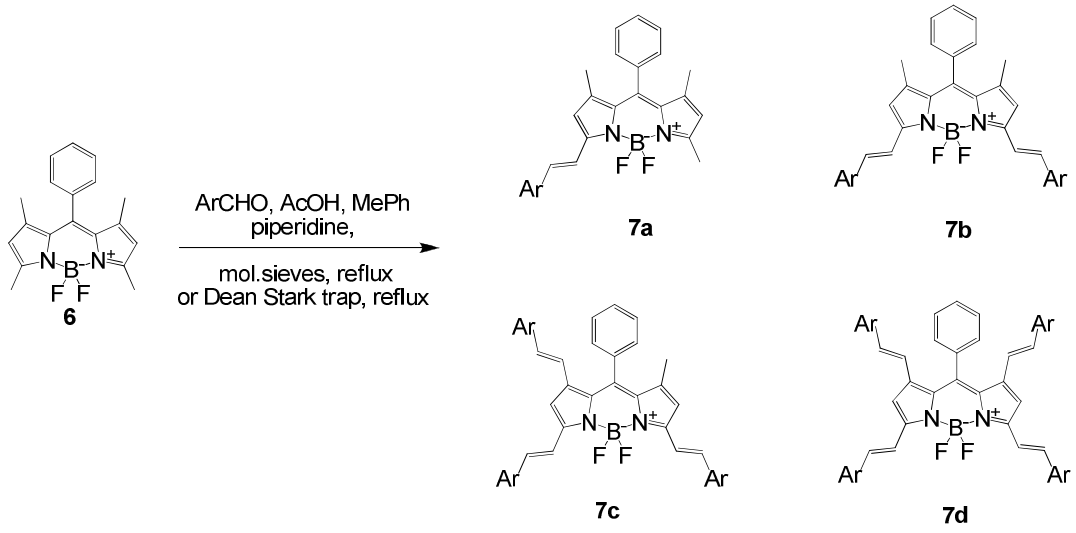

Scheme 4 The condensation reaction of 1,3,5,7-tetramethyl-BODIPYs with aromatic aldehydes.

3,5-Methyl BODIPY substituents have long been known to be sufficiently acidic to participate in

Knoevenagel reactions.[137] Recent research has demonstrated that methyl groups at the 1,7-positions can be almost as acidic as those at the 3,5-positions.[138] Tetrastyryl-substituted BODIPY derivatives can, therefore, be obtained via condensation reactions of 1,3,5,7-tetramethyl-BODIPYs with aromatic aldehydes. The water that is formed as a byproduct can be removed by using a Dean-Stark apparatus or dry molecular sieves. Usually, this reaction affords mixtures of products. The relative yields of the mono- to tetra-styryl-substituted BODIPYs can be adjusted by modifying the concentrations of the reactants, the amount of aromatic aldehyde added, and the reaction time. When *p*-dimethylaminobenzaldehyde is used, however, the reaction can be restricted to the mono-substituted compound.[139] The methyl groups at the 1,3,5,7-positions can be reacted in a stepwise manner, which enables the attachment of three different additional substituents in a tetravinyl configuration.[140-142] Knoevenagel condensation reactions with aromatic aldehydes have been identified as one of the best strategies for obtaining red/NIR region absorbing BODIPY derivatives that are suitable for use in applications such as labeling reagents,[143-146] energy concentration,[147-161] photodynamic therapy,[162,163] molecular switching,[164-167] chemosensors[31,168-171] and laser dyes.[172-174.]

3.2 Aromatic ring fusion

3.2.1 Reactions of aromatic ring-fused pyrroles with aldehydes

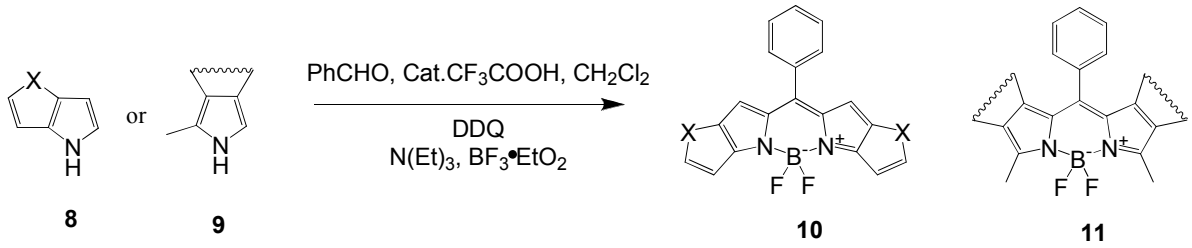

8 **9** **10** **11**

Scheme 5 Synthesis of BODIPY dyes through the pyrroles with aldehydes or benzoyl chlorides.

Aromatic ring-fused pyrroles can be synthesized through Michael addition or Paal-Knorr reactions.[175-179] The reaction of modified pyrroles with aldehydes under acid-catalyzed conditions affords dipyrromethenes, which can be oxidized with DDQ and coordinated with a boron atom under alkaline conditions.[43] Modified pyrroles can be reacted with acid chlorides or anhydrides to directly afford dipyrrolemethenes and BODIPY products with no DDQ oxidation step.[43,46,180,181]

3.2.2 Reactions of acylpyrroles with structurally modified pyrroles

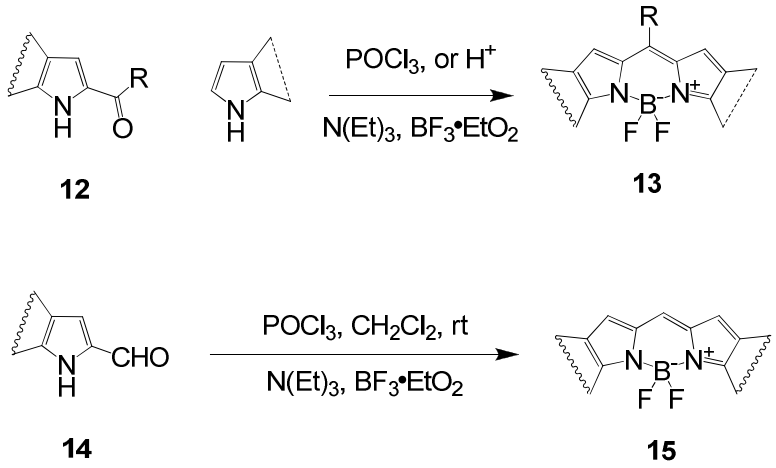

Scheme 6 Synthesis of BODIPY dyes through a reaction of acylpyrroles with another pyrrole (top) and through the condensation of only the acylated pyrrole (bottom).

The synthesis of asymmetric BODIPY dyes has been achieved via condensation of acylpyrrole **12** with a second modified-pyrrole under Lewis acid catalyzed conditions, followed by a reaction with an excess of base and BF_3•OEt_2.[182] Recently, it has been reported that dipyrromethenes can be prepared from a condensation reaction involving only the acylated pyrrole.[183] This new route for forming BODIPYs is a one-pot procedure. Since only facile purification steps are required and the products are obtained in good yield, this approach is likely to be increasingly used to form red/NIR region dyes in future.

3.3 Aza-substitution at the *meso*-position

3.3.1 Reactions of pyrroles with nitrosopyrroles

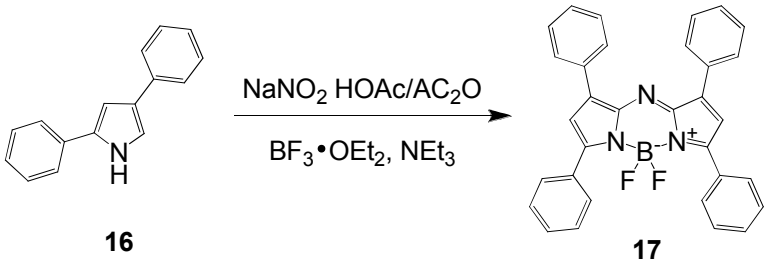

Scheme 7 Synthesis of aza-BODIPY dyes via the reaction of a pyrrole with a nitrosopyrrole.

Aza-BODIPY dyes can be prepared by reacting a pyrrole with a nitrosopyrrole, followed by a reaction with BF_3•OEt_2, either in a separate step or *in situ*, or by the formation of aza-dipyrrins structures from chalcones and nitromethane, or cyanide, followed by a condensation reaction with ammonium acetate.

One-pot synthetic routes for aza-dipyrrins have been known since 1943,[184-186] but it was not until 1994 that aza-BODIPY **17** was reported in the literature and its remarkable spectroscopic properties were highlighted.[187] In recent years, aza-BODIPY dyes have been studied extensively by the O'Shea research group.[188-194] The key advantage of aza-BODIPY dyes is that a marked red shift of the absorption and emission bands can be achieved without modifying the most important optical and photophysical properties of BODIPY dyes, such as their high molar absorption coefficients, narrow absorption and emission bands, small Stokes shifts, and excellent photostability.

3.3.2 Reactions of phthalonitriles with arylmagnesium bromides

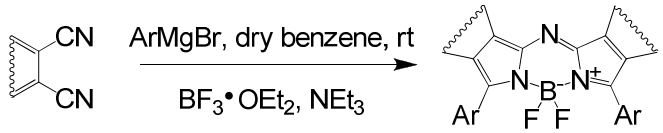

18 **19**

Scheme 8 Synthesis of an aza-BODIPY dye via the reaction of a phthalonitrile with an aryl magnesium bromides.

Aza-dipyrrins can be prepared in moderate yield through a one-pot reaction by reacting a phthalonitrile with 2.5 eq. of an aryl magnesium bromide by steam distillation, followed by recrystallization of the crude product from pyridine.[195] BF_3•OEt_2 can be used to convert the aza-dipyrrins into the corresponding aza-BODIPY dye.[196,197] This method, developed by the Shen, Luk'yanets and Kobayashi groups, is both facile and commercially viable, since phthalonitrile is commercially available and arylmagnesium bromides are easily prepared. A marked red shift of the absorption and emission bands was observed relative to the spectra of conventional 1,3,5,7-tetraaryl aza-BODIPY dyes. The introduction of additional substituent groups on the precursors is straightforward, so the spectral properties of the aza-BODIPY products can potentially be further fine-tuned. In recent studies, aza-dipyrrins have also been obtained by reacting a phthalonitrile with 1 eq. of an aryl magnesium bromide with no water steam distillation.[198]

4 Theoretical descriptions of the electronic structures of a series of structurally-modified BODIPY dyes

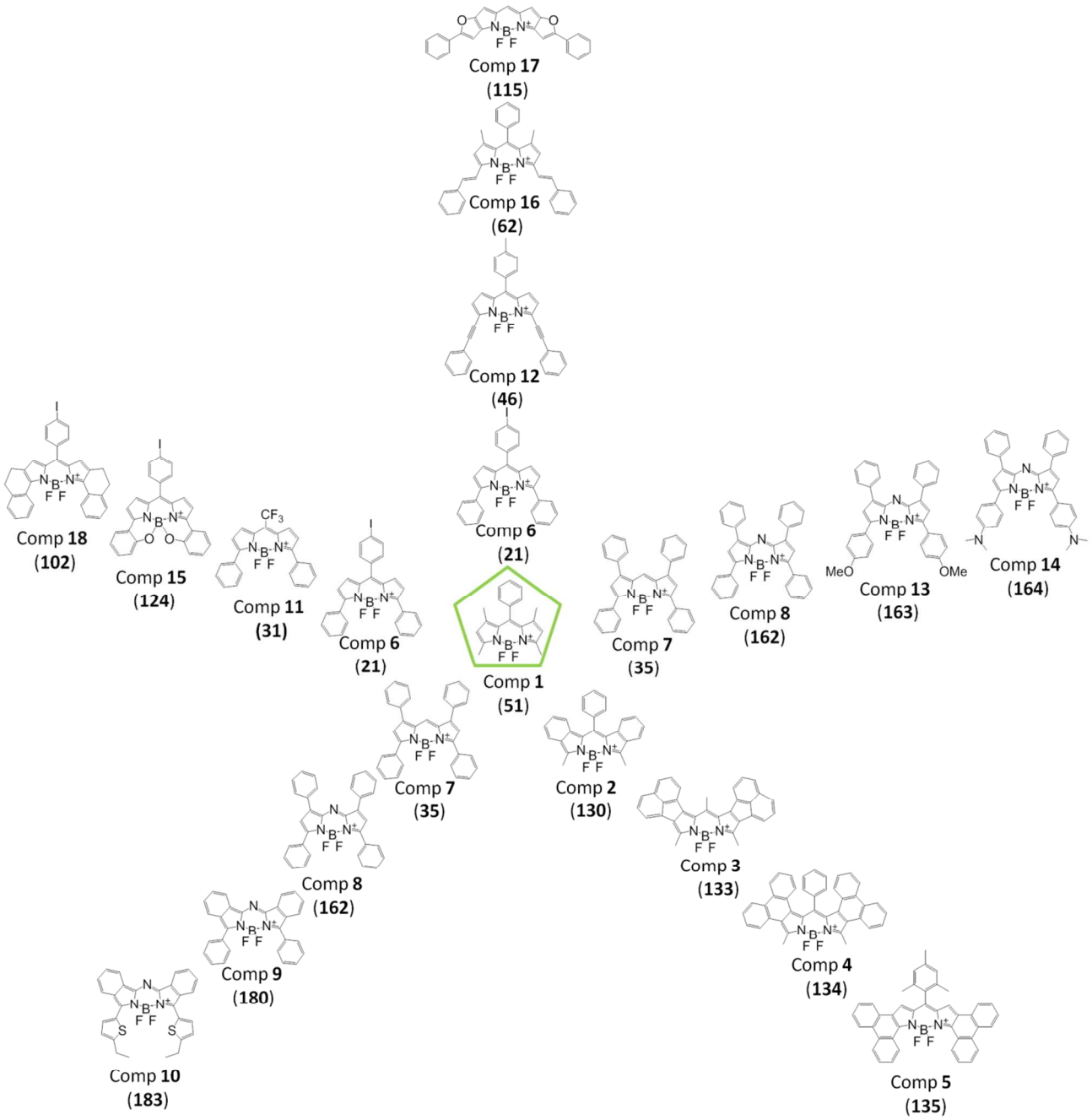

Fig. 5 The molecular structures for a series of BODIPY dyes selected to demonstrate trends in the energies of the HOMO and LUMO of the π-system and hence in the magnitude of the HOMO–LUMO gaps and the wavelengths of the main spectral bands. The numbering used for each dye in the remainder of the text is provided in each case.

The aim of this review is to examine the electronic structures of different types of long wavelength absorbing BODIPYs to identify the key trends observed in the spectral and redox properties and in theoretical calculations, in a manner that will facilitate the future rational design of red/NIR region BODIPY dyes with properties suitable for specific applications. A series of eighteen BODIPY

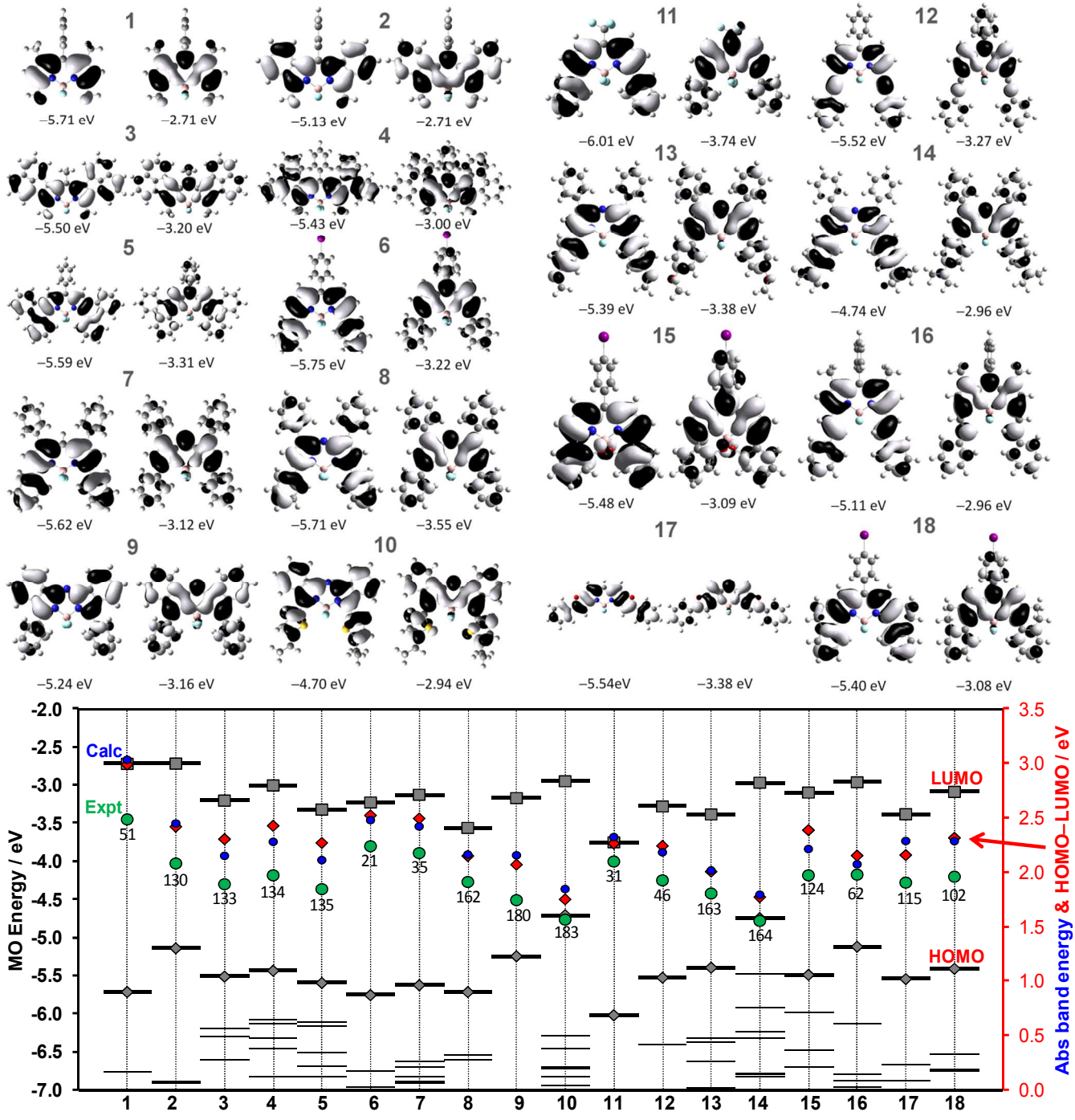

Fig. 6 The angular nodal patterns of **1-18** (Fig. 5) at an isosurface value of 0.02 a.u. (TOP). The energies of the frontier π-MOs (BOTTOM). Thicker lines with diamonds and squares are used to denote the HOMO and LUMO. Blue circles and red diamonds are used to denote the predicted absorption band energies and the HOMO–LUMO gaps. The trends observed in these values closely follow those of the observed absorption band energies that are highlighted with larger green circles. The numbering used for each dye in the remainder of the text is provided in each case.

derivatives have been selected for study by DFT and TD-DFT, Fig 5, so that the most important trends in the electronic structures and optical properties can be clearly demonstrated. The Gaussian 09 software package[199] was used to carry out B3LYP [200-204] geometry optimizations with SDD basis sets.[205] The same approach was then used to carry out TD-DFT for each of the optimized structures,

Fig 5. The trends predicted in the HOMO–LUMO gaps and in the energies of the main spectral bands are broadly similar to that observed experimentally in the energy of the main absorption band. A detailed consideration of the alignments of the angular nodal patterns of the HOMO and LUMO can therefore be expected to provide insight as to why particular structural modifications result in red shifts of the main spectral bands in a similar manner to the perimeter model approach developed by Michl to study trends in the optical spectra of aromatic and heteroaromatic cyclic polyenes.[72-74]

5. Wavelength tuning strategies

The effects of ten major structural modification strategies will be examined so that their relative effectiveness can be assessed: (i) aryl substitution, (ii) alkynyl substitution, (iii) styryl substitution, (iv) heteroatom substitution, (v) rigidization with fused-rings, (vi) fused-ring expansion of the π-system, (vii) β-aromatic ring-fusion combined with α-substitution (viii) the incorporation of an aza-nitrogen atom, (ix) formation of BODIPY dimers, and (x) core modification to form BODIPY analogues.

5.1 Aryl-substituted BODIPYs

The introduction of aryl substituents has proven to be effective strategies for achieving a red shift of the main spectral bands. The usefulness of this strategy will be explored by examining the properties of diaryl compounds with substituents at the 3,5-positions and polyaryl compounds.

5.1.1 Diaryl-substituted BODIPYs

The absorption and emission maxima of diaryl-substituted BODIPYs **21-34** are shifted to longer wavelengths, relative to those of the unsubstituted BODIPY **20**.[206] The bathochromic shift for **21** is approximately 52 nm. A destabilization of the HOMO of **21** would normally be anticipated since phenyl rings are incorporated at the 3,5-positions of the pyrrole rings (Fig. 6), where there are large MO coefficients (Fig. 3). Although the differing substitution patterns on the pyrrole rings and the electron withdrawing properties of the *para*-iodo group on the *meso*-substituent makes direct comparison with the classic BODIPY structure of **51** problematic in this regard. It is noteworthy that

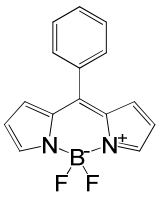

20
Toluene Φ 0.053
λ_{abs} 503 nm λ_{em} 521 nm
ε = 54 000 $M^{-1}cm^{-1}$

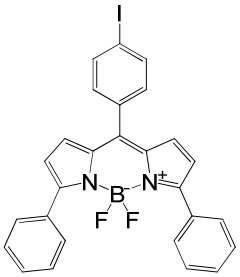

21
$CHCl_3$ Φ 0.20
λ_{abs} 555 nm λ_{em} 588 nm
ε = 52 400 $M^{-1}cm^{-1}$

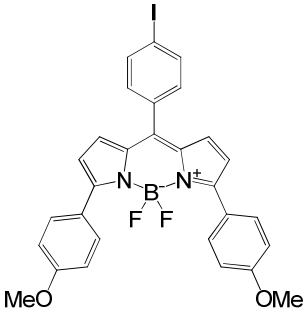

22
$CHCl_3$ Φ 0.42
λ_{abs} 582 nm λ_{em} 626 nm
ε = 54 100 $M^{-1}cm^{-1}$

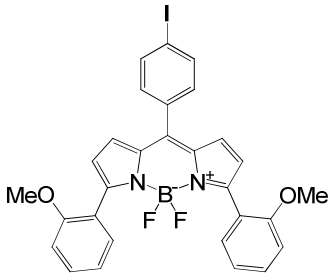

23
$CHCl_3$ Φ 0.08
λ_{abs} 545 nm λ_{em} 598 nm
ε = 30 500 $M^{-1}cm^{-1}$

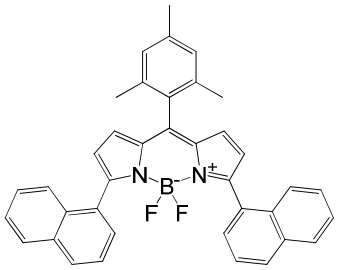

24
CH_2Cl_2 Φ 0.95
λ_{abs} 538 nm λ_{em} 601 nm
ε = 66 300 $M^{-1}cm^{-1}$

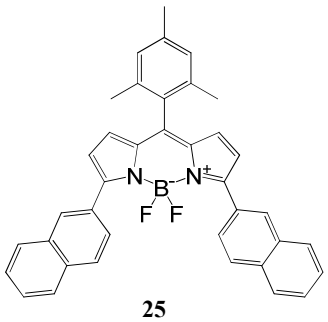

25
CH_2Cl_2 Φ 0.95
λ_{abs} 573 nm λ_{em} 618 nm
ε = 105 100 $M^{-1}cm^{-1}$

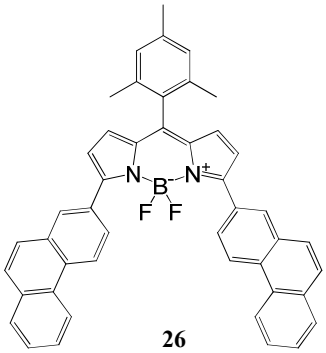

26
CH_2Cl_2 Φ 0.77
λ_{abs} 579 nm λ_{em} 624 nm
ε = 69 000 $M^{-1}cm^{-1}$

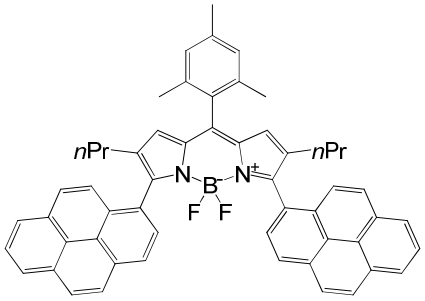

27
CH_2Cl_2 Φ 0.64
λ_{abs} 562 nm λ_{em} 626 nm
ε = 51 000 $M^{-1}cm^{-1}$

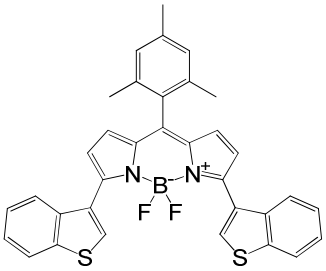

28
CH_2Cl_2 Φ 0.84
λ_{abs} 581 nm λ_{em} 625 nm
ε = 63 800 $M^{-1}cm^{-1}$

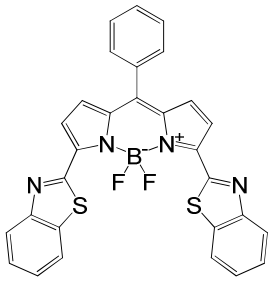

29
CH_2Cl_2 Φ 0.86
λ_{abs} 623 nm λ_{em} 643 nm
ε = 48 000 $M^{-1}cm^{-1}$

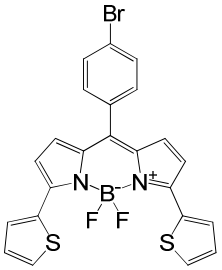

30
CH_2Cl_2 Φ 0.82
λ_{abs} 622 nm λ_{em} 643 nm
ε = 69 700 $M^{-1}cm^{-1}$

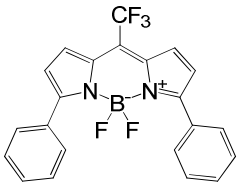

31
hexane Φ 0.74
λ_{abs} 592 nm λ_{em} 622 nm
ε = 48 000 $M^{-1}cm^{-1}$

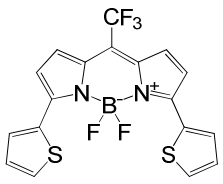

32
hexane Φ 1.00
λ_{abs} 665 nm λ_{em} 674 nm
ε = 85 000 $M^{-1}cm^{-1}$

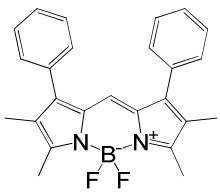

33
MeCN Φ 0.93
λ_{abs} 538 nm λ_{em} 549 nm

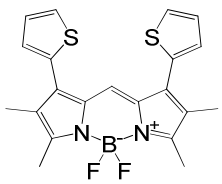

34
MeCN Φ 0.52
λ_{abs} 548 nm λ_{em} 571 nm

the *para*-electron-donating group of **22** results in an even larger red shift.[207,208] The introduction of *ortho*-methoxy-phenyl rings onto the BODIPY core at the 3,5-positions to form **23** results in a decrease in the molar extinction coefficient and Φ_F value, and shortens the wavelengths of the maxima of the main absorption and emission bands.[207,208] The incorporation of fused-ring-expanded aromatic substituents to form **24-27** leads to a red-shift of the absorption and emission maxima and an increase in the Φ_F values.[209] There is a 35 nm red shift of the absorption band compared to those of **24** and **25** based on a change of the attachment position by one carbon atom. This can be rationalized based on changes in the properties of the frontier π-MOs. The relative orientations of the indacene plane and the attached aromatic rings are determined by the size of the substituent. When larger fused ring systems are introduced at the 3,5- positions, the two π-systems cannot remain coplanar due to the constraints imposed by the BF_2 moiety. For example, **25** has been found to retain a higher level of co-planarity than **24**.[209]

The spectral bands of 3,5-di(benzo[*b*]thiophen-3-yl)-substituted BODIPY **28** lie at the same wavelengths as those of **22**, but there is a much higher Φ_F value. This difference is related to the incorporation of a mesityl group at the *meso*-position and the bulky benzothiophene moiety at the 3,5-positions, since there is no free rotation of the substituents and this limits the rate of nonradiative decay. In the solid state, the spectroscopic properties of **28** are close to those observed in solution, due to weak intermolecular interactions.[210] The 3,5-di-(benzothiazolyl)-substituted BODIPY **29** has an intense emission band at 643 nm with a high Φ_F value that is insensitive to solvent polarity.[211] There is a 67 nm red-shift of the band maxima of **30** when compared to those of **21**. These spectral differences can best be explained in terms of differences in the degree of steric hindrance on changing from a 6- to a 5-membered ring. Furthermore, the electronic properties of thiophene rings are very similar to those of *para*-methoxy-phenyl rings.[212]

Modifications at the *meso*-position usually do not influence the position of the absorption and fluorescence emission bands, since there normally is little scope for a mesomeric interaction between

aryl substituents and the BODIPY chromophore. However, the incorporation of a strongly electron-withdrawing CF_3 substituent at the *meso*-position in the structures of **31** and **32** causes a large ca. 35 nm bathochromic shift relative to the main spectral bands of the aryl-substituted **21** and **30** dyes.[213] There is a marked stabilization of both the HOMO and LUMO of **31** (Fig. 6) due to the inductive effect associated with the electron withdrawing CF_3 group. The narrowing of the HOMO–LUMO gap that leads to the red shift of the main absorption band is related to there being a larger stabilization of the LUMO, which has a large MO coefficient on the *meso*-carbon, due to a mesomeric interaction related to hyperconjugation. **31** and **32** have high Φ_F values and are likely to have at least two advantages in the context of biochemical probe applications. Firstly, the relatively small size of **31** and **32**, and secondly, the usefulness of CF_3 group as an NMR marker.[213]

The bathochromic shifts observed after diaryl substitution at the 1,7-positions to form **33** and **34**, are not as large as those observed for the corresponding 3,5-disubstituted dyes.[122] The absorption and fluorescence emission maxima of **34** are blue-shifted by about 74 and 72 nm, respectively, relative to those observed for its 3,5-dithiophene BODIPY analogue **30**. The 1,7-disubstituted dye **33** has similar spectroscopic properties to its 3,5-diphenyl analogue **21** with blue-shifts of ca. 17 and 39 nm, respectively. The smaller effects observed when substituents are introduced at the 1,7-positions seem to be attributable to the HOMO having smaller MO coefficients at the 1,7-positions, Fig 3.[122]

5.1.2 Polyaryl-substituted BODIPYs

Polyphenylated BODIPYs **35-39** have intense absorption and fluorescence bands with maxima between 561–597 nm and 597–640 nm, respectively, which are red-shifted by 70–120 nm compared to those of **20**, the unsubstituted BODIPY dye.[117,214-219] When the MO energies of **35** are compared to those of a classic tetramethyl-BODIPY dye such as **51** (Fig. 6) it is clear that the narrowing of the HOMO–LUMO gap is due primarily to a stabilization of the LUMO. This is probably related to the absence of the inductive and mesomeric interactions between the BODIPY fluorophore and a *meso*-phenyl substituent. Any stabilization of the HOMO in this regard is cancelled out by the effect of

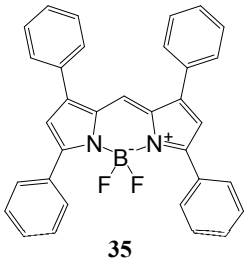

35
THF Φ 0.92
λ_{abs} 571 nm λ_{em} 601 nm
ε = 74 100 $M^{-1}cm^{-1}$

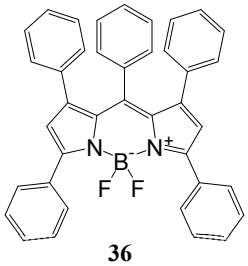

36
THF Φ 0.31
λ_{abs} 561 nm λ_{em} 597 nm
ε = 60 200 $M^{-1}cm^{-1}$

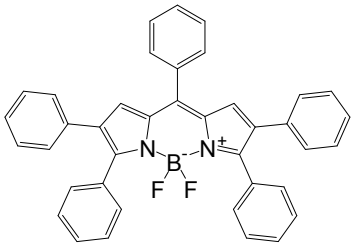

37
CH_2Cl_2 Φ 0.40
λ_{abs} 584 nm λ_{em} 628 nm
ε = 58 900 $M^{-1}cm^{-1}$

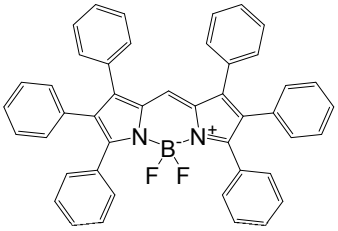

38
THF Φ 0.96
λ_{abs} 576 nm λ_{em} 608 nm
ε = 61 600 $M^{-1}cm^{-1}$

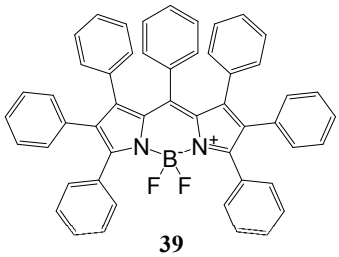

39
THF Φ 0.20
λ_{abs} 573 nm λ_{em} 613 nm
ε = 74 100 $M^{-1}cm^{-1}$

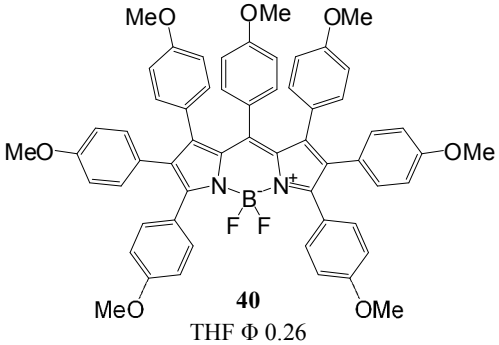

40
THF Φ 0.26
λ_{abs} 597 nm λ_{em} 640 nm
ε = 40 700 $M^{-1}cm^{-1}$

incorporating phenyl groups as the 3,5- and 1,7-positions. Although the emission maxima of **35-39** lie close to each other, significant differences are observed in their fluorescence quantum yields. Although **35** and **38** have extremely high Φ_F values, those of **36**, **37** and **39** are only moderately high. The difference is probably due to the presence of phenyl groups at the *meso* positions, since the conformational flexibility that is caused by the steric congestion can be expected to accelerate the rate of nonradiative decay. The incorporation of electron-donating OMe groups into the structure of **40**

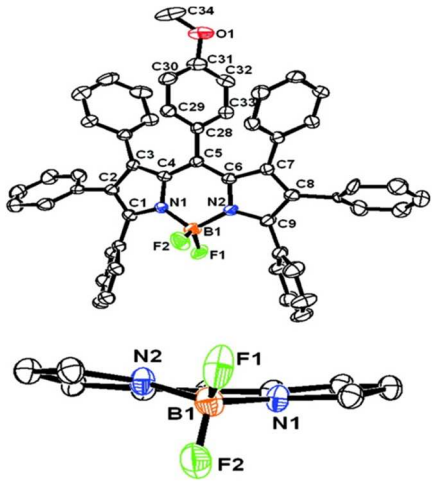

Fig. 7 X-ray structure of **39**. (Reprinted with permission from ref. 218. Copyright © 2011 American Chemical Society.)

results in only small bathochromic shifts compared to the maxima observed for **39**. This means that there is only a weak interaction between the peripheral phenyl groups and the indacene plane. X-ray structures revealed that the molecules adopt distorted and "propeller-like" conformations (Fig. 7).[218,219] **39** and **40** are brightly fluorescent in the solid state. The distorted conformations probably inhibit exciton coupling effects associated with intermolecular aggregation.[217,218]

5.2 Alkynyl-substituted BODIPYs

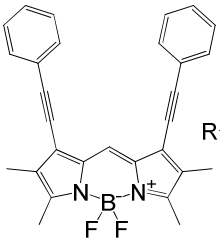

41
MeCN Φ 1.0
λ_{abs} 570 nm λ_{em} 579 nm

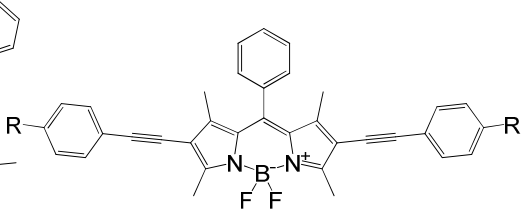

42 R=H
THF Φ 0.60
λ_{abs} 573 nm λ_{em} 594 nm
ε = 72 000 M^{-1} cm^{-1}
43 R=NPh_2
THF Φ 0.31
λ_{abs} 593 nm λ_{em} 659 nm
ε = 88 500 M^{-1} cm^{-1}
44 R=$B(Mes)_2$
CH_2Cl_2 Φ 0.65
λ_{abs} 576 nm λ_{em} 602 nm
ε = 169 000 M^{-1} cm^{-1}

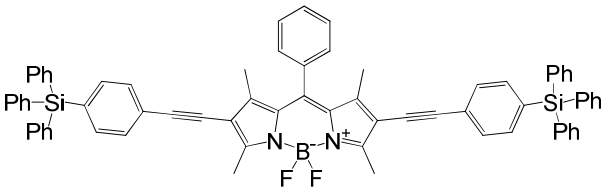

45
CH_2Cl_2 Φ 0.15
λ_{abs} 575 nm λ_{em} 600 nm
ε = 67 600 M^{-1} cm^{-1}

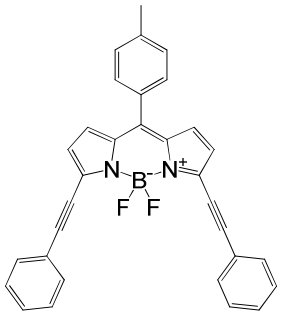

46
$CHCl_3$ Φ 1.0
λ_{abs} 614 nm λ_{em} 628 nm

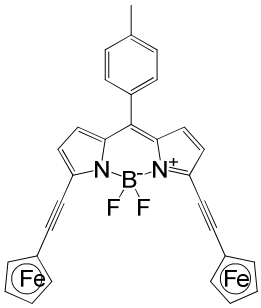

47
Toluene, N.D
λ_{abs} 558 nm ε = 16 000 M^{-1} cm^{-1}
680 nm (CT) ε = 20 000 M^{-1} cm^{-1}

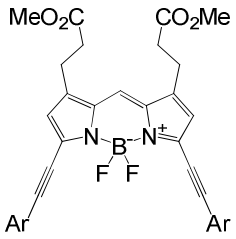

48 Ar=2-thiophene
CH_2Cl_2 Φ 0.17
λ_{abs} 649 nm λ_{em} 681 nm
ε = 29 000 M^{-1} cm^{-1}
49 Ar=3-thiophene
CH_2Cl_2 Φ 0.39
λ_{abs} 633 nm λ_{em} 653 nm
ε = 47 000 M^{-1} cm^{-1}
50 Ar=4-methoxyphenyl
CH_2Cl_2 Φ 0.29
λ_{abs} 649 nm λ_{em} 682 nm
ε = 59 000 M^{-1} cm^{-1}

Significant red shifts of the main spectral bands can also be obtained by introducing peripheral alkynyl substituents. A small Stokes shift is observed for the spectral bands of 1,7-dialkynylphenyl substituted dye **41** and there is a very high Φ_F value of 1.00.[122] The spectral bands of **41** lie at similar wavelengths to those of the 2,6-disubstituted dye **42** and are blue-shifted in comparison to those of the 3,5-disubstituted dye **46**. The probable reason is that the HOMO has smaller MO coefficients at the 1,7-positions (Fig. 3).[122] Dyes **42** and **43** have donor-π-bridge-donor structures. This results in high two photon absorption cross sections and strong emission in the red region. There is an increase in the Stokes shift and the width of the main fluorescence band on moving from **42** to **43**. This behavior is consistent with the formation of a low-lying charge separated S_1 state, prior to emission.[220,221] **44** contains two dimesitylboryl (Mes_2B) moieties and exhibits intense orange-red fluorescence with a Φ_F value of 0.65 in CH_2Cl_2 solution. **44** can be used as a "turn-off" fluorescent probe for F^-, since binding of F^- by the Mes_2B moieties results in a nonradiative PET deactivation pathway.[222,223]

The introduction of bulky triphenylsilylphenylethynyl groups to form **45** results in solid-state fluorescence at 613 nm with a quantum yield of 0.03, which is lower than the value for the corresponding monosubstituted BODIPY (0.07), most likely due to the enhanced probability of internal conversion caused by electronic coupling between the triphenylsilylphenyl ethynyl moiety and the BODIPY core.[224] However, more intense solid-state emission (Φ_F = 0.25) is observed for monotriphenylsilylphenyl BODIPY, which suggests that the introduction of the bulky arylsilyl group is an effective way to enhance the solid-state emission of BODIPY dyes.[224] The 3,5-dialkynylphenyl substituted BODIPY **46** absorbs and emits in the red region (614 nm), unlike **42**, the corresponding 2,6-disubstituted dye (573 nm).[108] The fluorescence quantum yields of **46** are extremely high (Φ_F = 1.0) and independent of solvent polarity.[108] BODIPY **47** has an intense blue color in toluene due to there being two absorption peaks. This has been attributed to the presence of a band associated with a low-lying charge-separated excited state. Negligible fluorescence is observed due to a charge transfer interaction between the ferrocenyl donor group and the boron-dipyrromethene moiety.[225] The red-

shifts of the main spectral bands of arylethynyl BODIPYs **48-50** are significantly larger.[116] Interestingly, the presence of 2-ethynylthiophenes in the structure of **48** causes larger red-shifts of the spectral bands than those observed for **49**, a 3-ethynylthiophene substituted BODIPY.[116]

5.3 Styryl-Substituted BODIPYs

Styryl substituents have proven to be a particularly useful strategy for forming red/NIR region BODIPY dyes. The properties of mono-, di-, multi-π-, and *meso*-π-styryl and *meso*-vinyl substituted BODIPYs will be examined in depth, so that their properties can be compared.

5.3.1 Monostyryl-substituted BODIPYs

When a styryl substituent is introduced to form **52** from **51**,[226] the absorption maximum shifts by ca. 60 nm into the red region of the visible spectrum.[173] When strongly electron-donating $–NMe_2$ groups are introduced at the *para*-positions of the phenyl ring to form **54**, the absorption maximum is shifted to the red by a further 34 nm.[227] The band maximum observed when weakly electron-donating –OH groups are introduced in **53** is almost unchanged, however.[228] The fluorescence emission maximum of **54** lies at 731 nm in polar solvents such as acetonitrile, due to a CT band associated with the dimethylamino group as the electron donor and the BODIPY core as the electron acceptor. Protonation of the $–NMe_2$ group eliminates this CT process and results in a blue shift of the absorption and emission bands to 555 and 565 nm. The protonated species have high fluorescence quantum yields, similar to those of **52**.[227] Generally, as is obvious when the spectra of **54** and **55** are compared, varying the substituent group at the *meso*-position has only a minor impact on the absorption spectra and there are only very minor effects on the properties of the $S_1–S_0$ fluorescence band. The first protonation of **55** is at the virtually decoupled dimethylamino group of the *meso*-substituent, followed by protonation at the dimethylamino group of the styryl fragment.[139]

When the phenyl moiety is changed to a pyrene to form **56**,[229,230] the extension of the π-conjugation system results in a red-shift of the absorption and emission bands by 38 and 49 nm, respectively, relative to those of **52**. As would be anticipated, extending the π-conjugation system with electron-

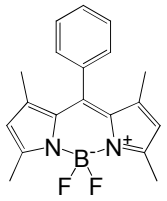

51
THF Φ 0.56
λ_{abs} 500 nm λ_{em} 510 nm

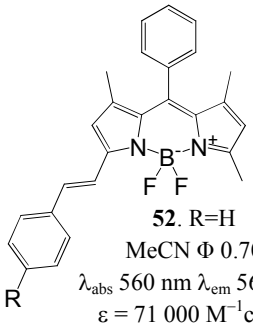

52. R=H
MeCN Φ 0.70
λ_{abs} 560 nm λ_{em} 569 nm
ε = 71 000 $M^{-1}cm^{-1}$
53. R=OH
MeMeOH/H_2O, 0.37
λ_{abs} 565 nm λ_{em} 590 nm
54. R=$N(CH_3)_2$
Et_2O Φ 0.83
λ_{abs} 594 nm λ_{em} 638 nm
ε = 98 000 $M^{-1}cm^{-1}$

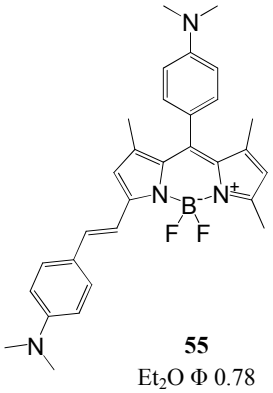

55
Et_2O Φ 0.78
λ_{abs} 591 nm λ_{em} 632 nm
ε = 91 200 $M^{-1}cm^{-1}$

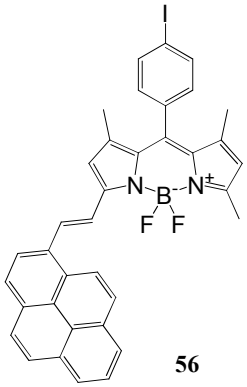

56
MTHF Φ 0.64
λ_{abs} 598 nm λ_{em} 618 nm
ε = 93 600 $M^{-1}cm^{-1}$

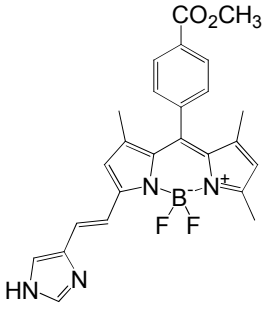

57
$CHCl_3$ Φ 0.93
λ_{abs} 572nm λ_{em} 589 nm
ε = 38 000 $M^{-1}cm^{-1}$

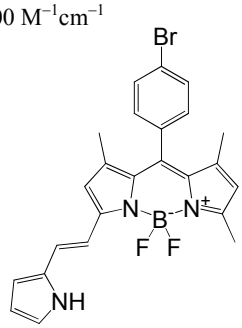

58
CH_2Cl_2 Φ 0.25
λ_{abs} 590nm λ_{em} 613 nm

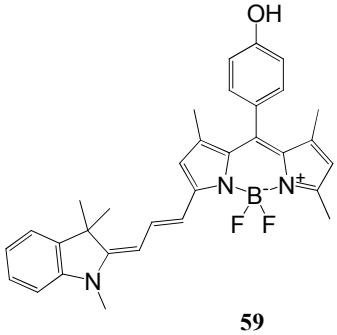

59
PBS buffer Φ N.A
λ_{abs} ca.650 nm λ_{em} 708 nm

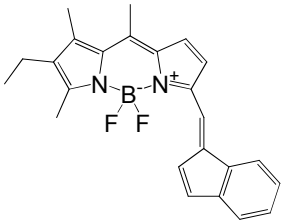

60
c–hexane Φ < 0.02
λ_{abs} 591 nm λ_{em} 596 nm
ε = 68 000 $M^{-1}cm^{-1}$

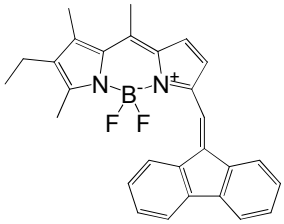

61
c–hexane Φ 0.73
λ_{abs} 589 nm λ_{em} 612 nm
ε = 56 000 $M^{-1}cm^{-1}$

rich imidazole and pyrrole rings through an ethenyl linker at the 3-position to form **57** and **58** results in a bathochromic shift which can be further fine-tuned by modifying the electron donating properties of the aryl group.[231,232] The merocyanine conjugated dye **59** displays a further large bathochromic shift to ca. 650 nm due to the extension of the π-conjugation system.[233] Unfortunately, the basic optical properties of this dye, such as the Φ_F value and the absorption and emission spectroscopy have not

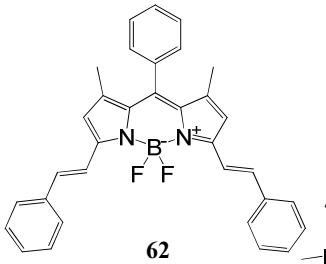

62
Toluene Φ 0.59
λ_{abs} 629 nm λ_{em} 641 nm
ε = 120 000 $M^{-1}cm^{-1}$

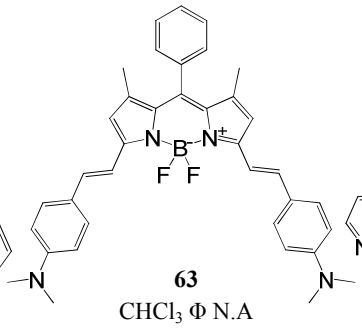

63
$CHCl_3$ Φ N.A
λ_{abs} 700 nm λ_{em} 753 nm

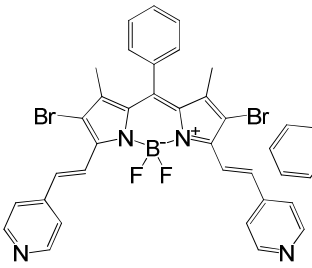

64
$CHCl_3$ Φ N.A
λ_{abs} 620 nm λ_{em} 640 nm

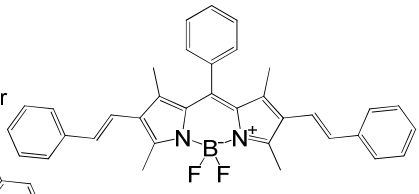

65
CH_2Cl_2 Φ 0.01
λ_{abs} 575 nm λ_{em} 633 nm
ε = 31 000 $M^{-1}cm^{-1}$

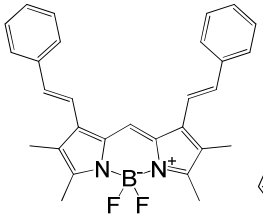

66
MeCN Φ 0.55
λ_{abs} 572 nm λ_{em} 589 nm

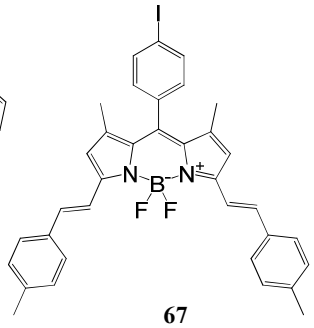

67
MTHF Φ 0.75
λ_{abs} 631 nm λ_{em} 645 nm
ε = 101 200 $M^{-1}cm^{-1}$

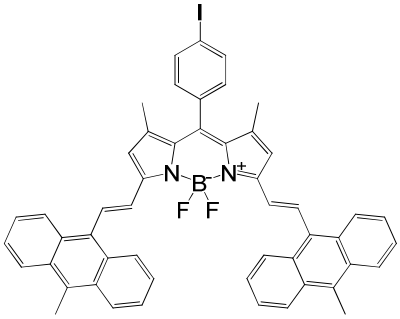

68
MTHF Φ 0.038
λ_{abs} 632 nm λ_{em} 714 nm
ε = 123 400 $M^{-1}cm^{-1}$

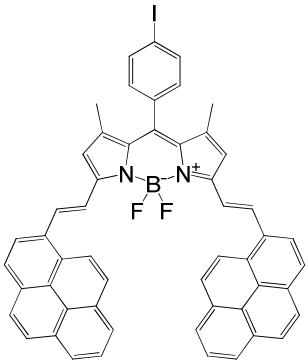

69
MTHF Φ 0.80
λ_{abs} 691 nm λ_{em} 720 nm
ε = 121 700 $M^{-1}cm^{-1}$

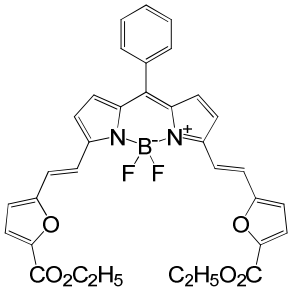

70
$CHCl_3$ Φ 0.29
λ_{abs} 671 nm λ_{em} 681 nm
ε = 80 500 $M^{-1}cm^{-1}$

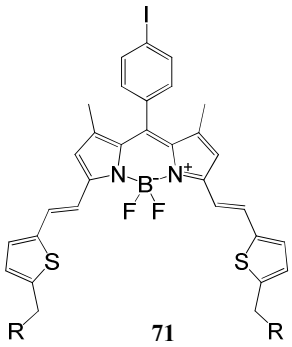

71
EtOH Φ 0.37
λ_{abs} 657 nm λ_{em} 672 nm
ε = 118 000 $M^{-1}cm^{-1}$

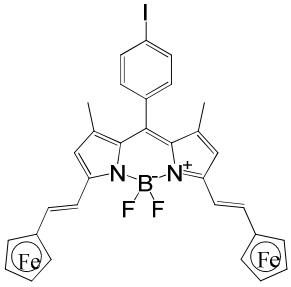

72
CH_2Cl_2 Φ N.D
λ_{abs} 700 nm

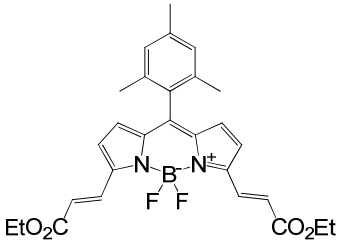

73
CH_2Cl_2 Φ 0.98
λ_{abs} 593 nm λ_{em} 602 nm
ε = 125 000 $M^{-1}cm^{-1}$

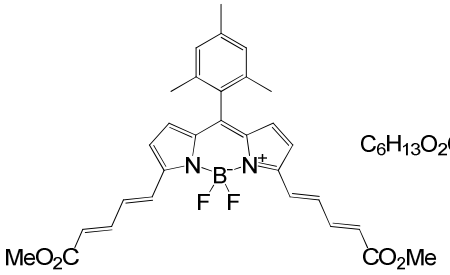

74
CH_2Cl_2 Φ 0.53
λ_{abs} 641 nm λ_{em} 651 nm
ε = 143 000 $M^{-1}cm^{-1}$

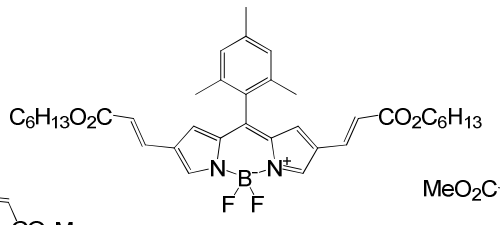

75
CH_2Cl_2 Φ 0.68
λ_{abs} 579 nm λ_{em} 606 nm
ε = 60 700 $M^{-1}cm^{-1}$

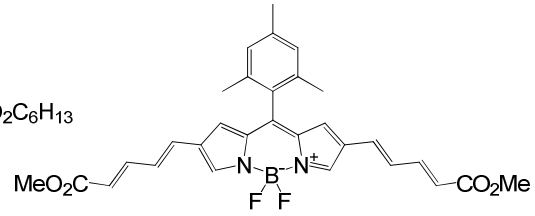

76
CH_2Cl_2 Φ 0.054
λ_{abs} 633 nm λ_{em} 662 nm
ε = 57 100 $M^{-1}cm^{-1}$

been investigated in detail. The incorporation of fluorene and indene rings with a vinyl spacer to form **60** and **61** leads to a large red-shift of the main spectral band, but the Φ_F values differ markedly.[234] The Φ_F value for **60** is very low ($\Phi < 0.02$), and no significant increase is observed in viscous solvents. This is probably due to the negative effect of nonradiative decay associated with the indene group. Theoretical calculations have confirmed that the efficient nonradiative relaxation is caused by conical intersections between the singlet excited state S_1 and the ground-state S_0.[234]

5.3.2 Distyryl-substituted BODIPYs

When two styryl substituents are introduced at the 3,5-positions to form **62**, a narrow and intense absorption band is observed with a maximum at 629 nm.[235,236] This represents a red-shift of 129 nm relative to that of **51**, which has a conventional BODIPY structure. The substitution with electron-donating dimethylamino groups at the *para*-positions of the phenyl rings of the styryl substituents to form **63** shifts the emission band into the NIR region.[237] The use of this dye for probe applications has been investigated. pH-dependent absorption and fluorescence changes have been observed at the blue end of the visible region due to the presence of two different protonation states.[237] The main absorption band of pyridyl-substituted dye **64** lies at 620 nm and is further red-shifted upon addition of TFA due to a decrease in the electron-withdrawing properties of the pyridyl groups.[237] Only moderate bathochromic shifts are observed in the spectra of **65** and **66**, the 2,6- and 1,7-distyryl-substituted BODIPYs analogues of **62**.[71,122] It is worth noting that large Stokes shifts and low Φ_F values are observed for 2,6-styryl substituted dyes. This is probably related to greater conformational flexibility of the molecular geometry in the excited state, which increases the rate of nonradiative decay.[71] The iodine atom at the *para*-position of the *meso*-phenyl group of **67** appears to have almost no effect on the photophysical properties, since the photophysical values reported are almost the same as those of **62**.[238] The optical spectra of the *bis*-anthracene derivative **68** contain broad and featureless bands and there is a low Φ_F value. The two fluorophores of **68** remain in electronic isolation but display fast intramolecular energy transfer.[238] This differs from what has been reported for BODIPY-anthracene

energy-transfer cassettes with linking alkynyl moities.[126,239] Marked red-shifts are observed for the spectral bands of **69** due to the extension of the π-conjugation system. The higher-energy absorption bands at ca. 430 nm are probably associated primarily with the pyrene moiety (Fig. 8).[238]

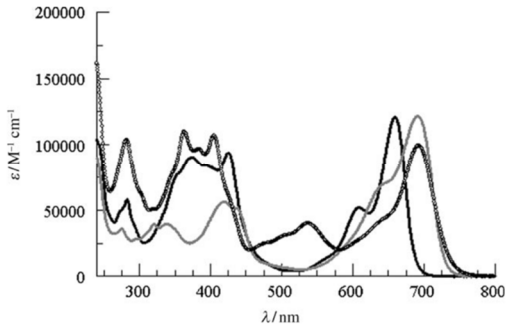

Fig 8. Absorption spectra recorded for a series pyrene-substituted BODIPY dyes in MTHF. The spectrum of **69** is shown in gray. (Reprinted with permission from ref. 238. Copyright © 2010 Wiley-VCH Verlag GmbH & Co. KGaA, Weinheim.)

When the spectral data for **70** and **71**, which have 5-membered heteroaromatic substituents at the 3,5-positions, are compared with those for **62** which has phenyl rings, it is found that the incorporation of 3,5-difuranylvinyl substituents leads to a bathochromic shift of 42 nm, while a shift of 28 nm is observed for 3,5-dithiophenevinyl substituents. This can be attributed to a narrowing of the HOMO–LUMO gap due to enhanced delocalization of the π-electrons in furan rings relative to thiophenes.[212,240] The introduction of ferrocene moieties to form **72** results in a large red-shift of 71 nm relative to the main absorption band of the phenyl substituted structure of **62**. The compound is not emissive, however, since there is substantial charge transfer from the electron-rich ferrocene moiety to the main BODIPY π-system.[241] Similarly, no fluorescence is observed for *meso*-ferrocene substituted BODIPYs.[225,242] The α-substituted structures of **73** and **74** result in spectra with typical BODIPY characteristics, such as a narrow absorption band with large molar extinction coefficients (>120 000 $M^{-1}.cm^{-1}$).[136] The emission maximum of **74** is shifted to 651 nm with a relatively high Φ_F value. In the case of β-substituted BODIPY dyes **75** and **76**, the main absorption and emission bands also exhibit substantial red-shifts, but the bandwidths become broader and there is a decrease in the molar extinction coefficients to around 60 000 $M^{-1}.cm^{-1}$. **76** has a Φ_F value of only 0.054 and thus has properties that are not as favorable for many applications as those of the corresponding α-substituted

BODIPYs. When compared to structures of dyes substituted at the 3,5-positions, the absorption band of 2,6-substituted structures of **76** are blue-shifted and the emission bands are red-shifted. This is related to the larger Stokes shifts that are observed for 2,6-substituted BODIPYs.[136]

5.3.3 Multi-π-styryl-substituted BODIPYs

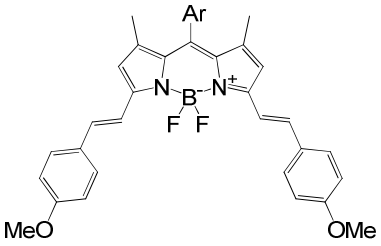

77
Ar = 3,5-didecyloxyphenyl
$CHCl_3$ Φ 0.37
λ_{abs} 645 nm , λ_{em} 660 nm
ε = 116 400 $M^{-1}cm^{-1}$

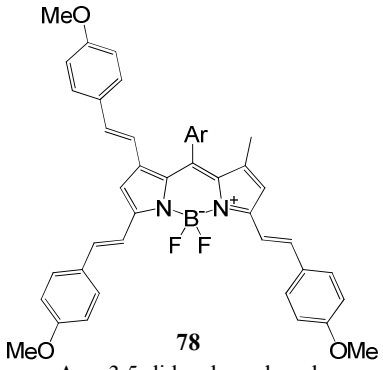

78
Ar = 3,5-didecyloxyphenyl
$CHCl_3$ Φ 0.35
λ_{abs} 665 nm , λ_{em} 682 nm
ε = 96 900 $M^{-1}cm^{-1}$

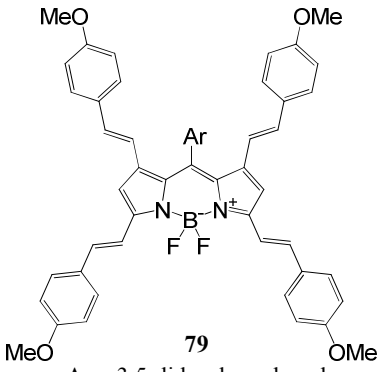

79
Ar = 3,5-didecyloxyphenyl
$CHCl_3$ Φ 0.34
λ_{abs} 689 nm , λ_{em} 710 nm
ε = 127 900 $M^{-1}cm^{-1}$

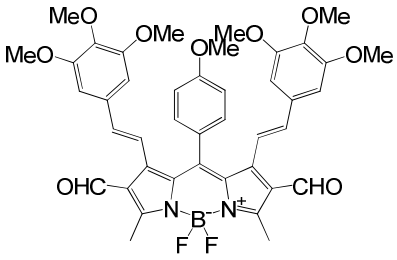

80
CH_2Cl_2 Φ 0.20
λ_{abs} 576 nm, λ_{em} 673 nm
ε = 36 900 $M^{-1}cm^{-1}$

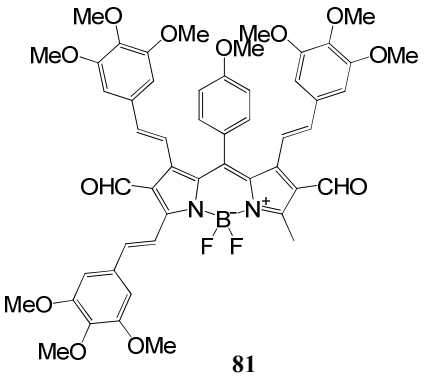

81
CH_2Cl_2 Φ 0.10
λ_{abs} 634 nm, λ_{em} 686 nm
ε = 60 600 $M^{-1}cm^{-1}$

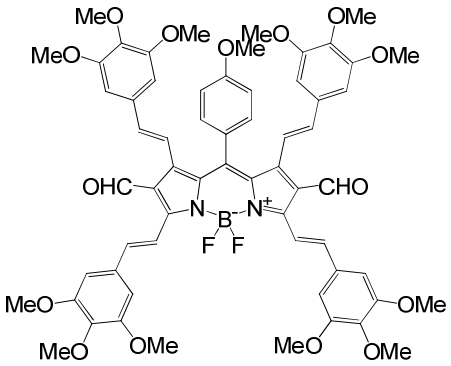

82
CH_2Cl_2 Φ 0.40
λ_{abs} 688 nm, λ_{em} 722 nm
ε = 72 700 $M^{-1}cm^{-1}$

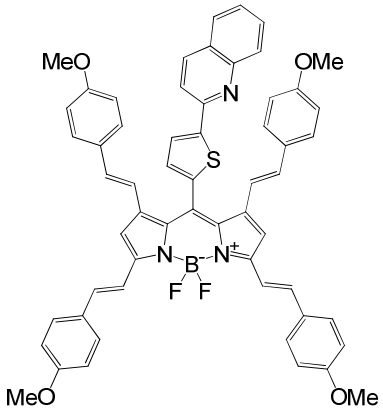

83
Dioxane Φ 0.36
λ_{abs} 708 nm, λ_{em} 732 nm
ε = 170 000 $M^{-1}cm^{-1}$

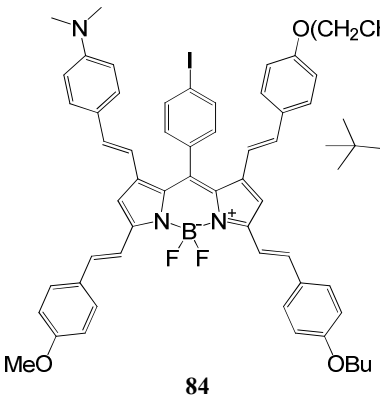

84
Dioxane Φ 0.13
λ_{abs} 700 nm, λ_{em} 714 nm
ε = 142 000 $M^{-1}cm^{-1}$

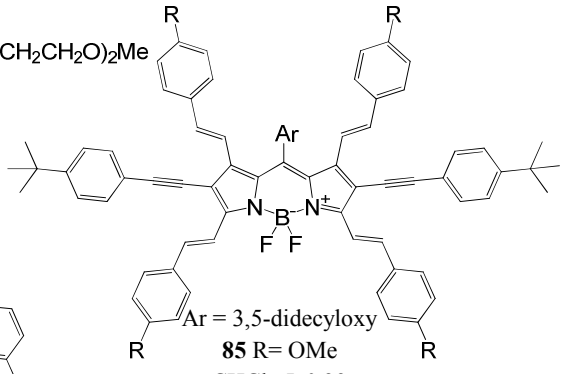

Ar = 3,5-didecyloxy
85 R= OMe
$CHCl_3$ Φ 0.23
λ_{abs} 732 nm, λ_{em} 756 nm
ε = 173 900 $M^{-1}cm^{-1}$
86 R= NMe_2
$CHCl_3$ Φ 0.05
λ_{abs} 797 nm, λ_{em} 835 nm
ε = 144 700 $M^{-1}cm^{-1}$

By fine-tuning the Knoevenagel condensation reactions of the four methyls on the BODIPY core of **51** with aromatic aldehydes, it is possible to obtain not only the monostyryl dye **52**, but also the di-, tri-, and tetrastyryl derivatives **77-79**.[138] In DFT calculations (Fig. 6), there is a marked destabilization of the HOMO of **62** (which is very similar to **77**), since the large MO coefficients at the 3,5-positions enhance the mesomeric effect of the styryl substituents (Fig 3). The absorption peak of **51** is shifted stepwise from 500 nm to 645, 665, and 689 nm in $CHCl_3$, and the emission bands are shifted to 660, 682, and 710 nm. This is especially noteworthy, since there are red-shifts of ca. 150, 172, and 200 nm relative to the emission band of **51**. These dyes have very large molar absorption coefficients rivaling those of cyanine dyes. In addition to their facile functionalization and derivatization, the moderately high Φ_F values make these styryl-BODIPYs strong candidates for use in dye applications.[138]

It is interesting to note that when electron withdrawing formyl groups are introduced at the 2,6-positions, Knoevenagel reactions can only be initiated at the 7- or 1,7-positions.[141] Steric hindrance prevents the Knoevenagel reaction from occurring at the 5- or 3,5-positions, resulting in the formation of the 2,6-diformyl-1,7-distyryl-BODIPY **80**. It should be noted that the formation of vinyl bonds at the 7-, and 1,7-positions facilitates further Knoevenagel reactions at the 3, and the 3,5-positions, to form 2,6-diformyl-1,3,7-tristyryl- and 2,6-diformyl-1,3,5,7-tetrastyryl-BODIPYs **81** and **82**. In CH_2Cl_2, BODIPYs **80-82** have intense absorption bands at 576, 634 and 688 nm, respectively with emission bands at 673, 686 and 722 nm. The significant red-shifts are caused by the extension of the π-conjugation systems. Formyl-BODIPY dyes have lower Φ_F values than conventional BODIPY dyes. This suggests that the presence of formyl groups quenches the fluorescence. The trends observed for **80-82** confirm again that the incorporation of styryl groups at the 3,5-positions has a larger effect on the wavelength of the main absorption band than incorporation at the 1,7-positions. A red-shift of 50–60 nm is observed upon the incorporation of each styryl substituent at the 3,5-positions, while a 20–30 nm shift is observed for each 1,7-position substituent.[141] The *meso*-(thiophen-2-yl)quinoline appended BODIPY **83** has an absorption maximum at 708 nm that does not shift when the solvent

polarity is increased.[243] A large pseudo-Stokes shift of up to 400 nm is observed for the energy-transfer cassette that is formed due to efficient through-bond energy transfer of up to 99%. **83** can also selectively bind Fe(III) ions in aqueous solution and in living cells, so this demonstrates the potential for developing chemosensors based on through-bond energy transfer cassettes that contain the BODIPY fluorophore as an electron acceptor.[243] The preparation of the tetrastyryl-substituted BODIPY **79** with four methoxy substituents at the *para* positions enables the synthesis of dyes with different substituents, such as **84**.[140,142] These highly colored dyes display outstanding optical properties with the absorption maxima shifting to 700 nm for **84** in dioxane, which was selected to limit aggregation effects and the rate of photodegradation. The Φ_F value of **79** is 0.34, but decreases to 0.13 for **83**, due to the presence of the dimethylaminophenyl moieties.

When a Knoevenagel reaction is carried out on a tetramethyl BODIPY derivative with 4-*t*-butylphenylethynyl substituents at the 2,6-positions, tetrastyryl BODIPYS **85** and **86** are formed.[138] BODIPYs with substituents at the 2,6-positions tend to react more readily and efficiently than those with no substituents at these positions. The absorption band maxima of **85** and **86** are shifted dramatically to the red to lie at 732 and 797 nm in $CHCl_3$, respectively, while the emission band maxima lie at 756 and 835 nm. High molar absorption coefficients similar to those of **67-69** have been reported. Although a moderate Φ_F value of 0.23 is observed for **85**, the quantum yield of **86** decreases markedly to 0.05 in $CHCl_3$, due to strong charge transfer character in the S_1 state caused by the *p*-N,N-dimethylaminostyryl moieties.[138]

5.3.4 Meso-vinyl substituted BODIPYs

Meso-vinylic BODIPYs are weakly fluorescent, particularly in polar solvents, probably due to conformational flexibility associated with the *meso*-vinyl groups. The polymethine-structure of **88** results in a red-shift of ca. 127 nm relative to the absorption band of **87**. An extension of the polymethine chain to form **89** leads to a further 100 nm red-shift of the absorption maximum.[244]

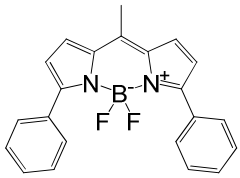

87
CH_2Cl_2 Φ 0.64
λ_{abs} 544 nm λ_{em} 577 nm
ε = 57 000M^{-1} cm^{-1}

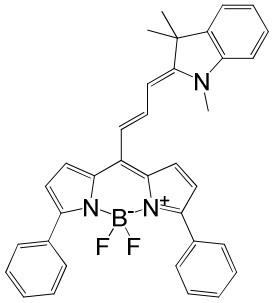

88
CH_3CN Φ < 0.1
λ_{abs} 671 nm λ_{em} 720 nm
ε = 111 000M^{-1} cm^{-1}

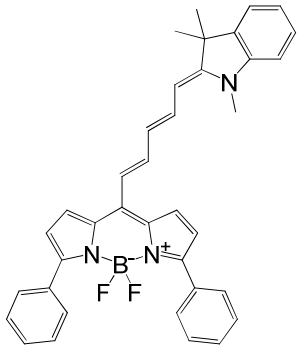

89
CH_3CN Φ N.D
λ_{abs} 771 nm
ε = 116 000M^{-1} cm^{-1}

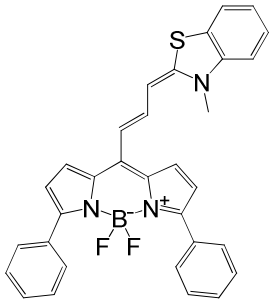

90
CH_3CN Φ < 0.1
λ_{abs} 683 nm λ_{em} 727 nm
ε = 116 000M^{-1} cm^{-1}

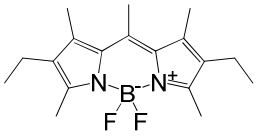

91
CH_2Cl_2 Φ 0.79
λ_{abs} 520 nm λ_{em} 534 nm
ε = 71 000 M^{-1} cm^{-1}

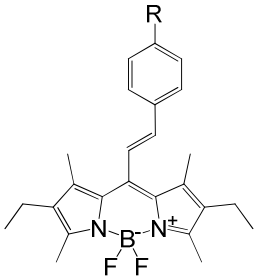

92, R = NO_2,
CH_2Cl_2 Φ < 0.01
λ_{abs} 532 nm λ_{em} 532 nm
ε = 51 000 M^{-1} cm^{-1}
93, R = OMe,
$CH2Cl_2$ Φ < 0.01
λ_{abs} 529 nm λ_{em} 542 nm
ε = 58 000 M^{-1} cm^{-1}

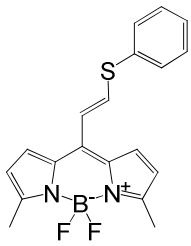

94
CH_2Cl_2 Φ N.A
λ_{abs} 528 nm λ_{em} 580 nm
ε = 20 000 M^{-1} cm^{-1}

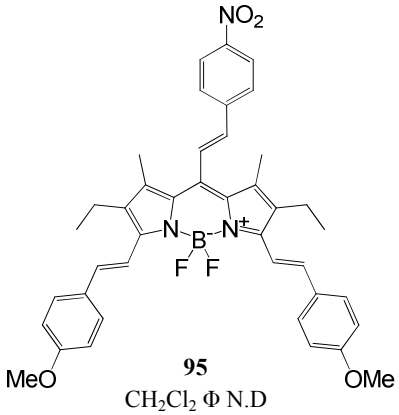

95
CH_2Cl_2 Φ N.D
λ_{abs} 666 nm
ε = 89 000 M^{-1} cm^{-1}

Interestingly, the main absorption bands of polymethine-substituted BODIPYs **88**–**90** are no longer observed upon protonation and a new peak gains intensity at shorter wavelength. No fluorescence is observed for these protonated species.[244] In contrast with what is observed upon substitution at the 3,5-positions, there is almost no shift observed in the main absorption band of *meso*-styryl dyes **92-93** and the vinylic thioether **94**.[245,246] Theoretical calculations have revealed that when **92** is further reacted with an aldehyde to form **95**, the HOMO and LUMO are mostly localized on the BODIPY and *meso*-styryl moieties respectively, in a manner that could facilitate the injection of an electron into the conduction band of TiO_2 in solar cell applications (Fig. 9).[245]

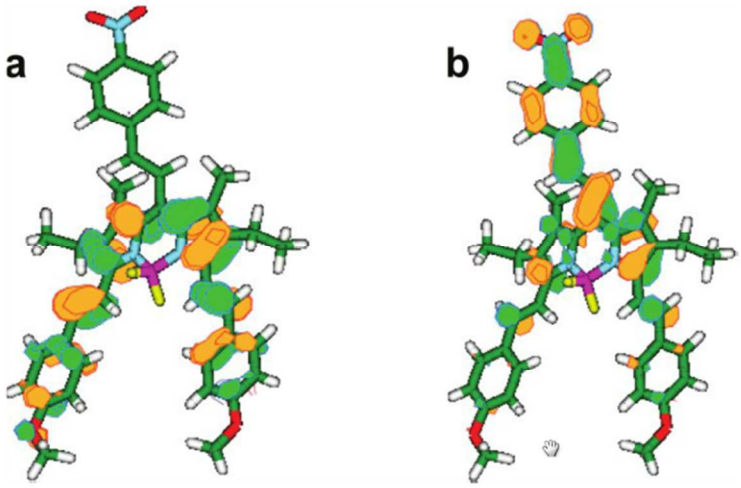

Fig 9. a) HOMO and (b) LUMO of **95** calculated by DFT. (Reprinted with permission from ref. 245. Copyright © 2011 American Chemical Society.)

5.4 Heteroatom substituted BODIPYs

The main absorption and emission bands of 3,5-position heteroatom substituted BODIPYs **96–100**, have a similar morphology to those of classic BODIPYs (Figs. 4 and 10).[104,105,109] On moving from substituents with linking oxygen atoms, to those with nitrogen, sulfur, and selenium atoms and then to those with tellurium atoms, the absorption and emission spectra display a red-shift from the green to

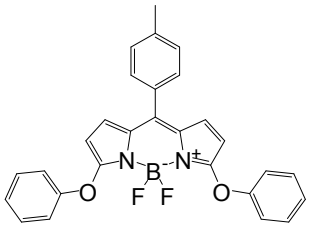

96
THF Φ 0.27
λ_{abs} 516 nm λ_{em} 533 nm
ε = 117 300 M^{-1} cm^{-1}

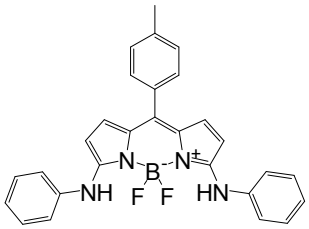

97
MeOH Φ 0.45
λ_{abs} 588 nm λ_{em} 613 nm

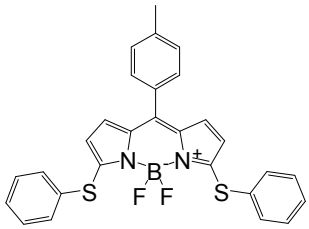

98
THF Φ 0.82
λ_{abs} 577 nm λ_{em} 599 nm
ε = 87 700 M^{-1} cm^{-1}

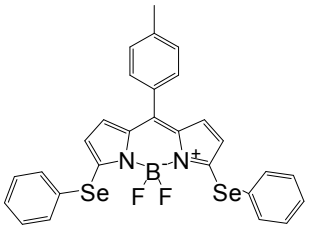

99
THF Φ 0.56
λ_{abs} 586 nm λ_{em} 609 nm
ε = 104 400 M^{-1} cm^{-1}

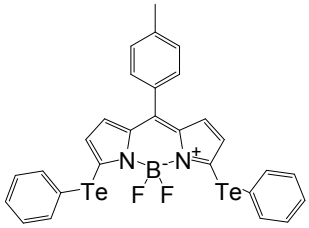

100
THF Φ 0.01
λ_{abs} 620 nm λ_{em} 659 nm
ε = 76 600 M^{-1} cm^{-1}

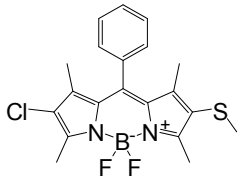

101
MeOH Φ 0.07
λ_{abs} 518 nm λ_{em} 655nm
ε = 160 000 M^{-1} cm^{-1}

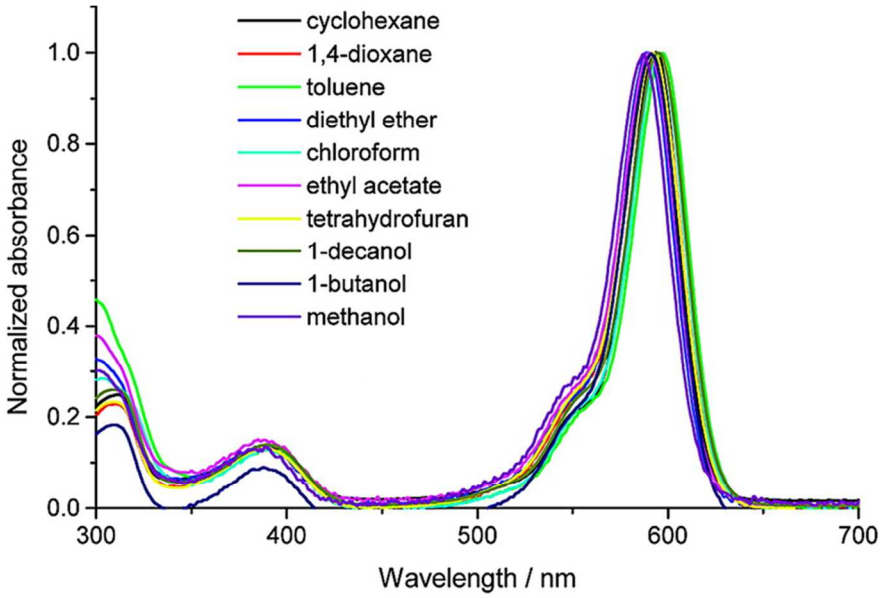

Fig 10. The absorption spectrum of **97** measured in a wide range of different solvents. (Reprinted with permission from ref. 109. Copyright © 2009 American Chemical Society.)

the NIR region. The extent of the red-shift is related to the electron donating properties of the heteroatom. The positions of the absorption and emission maxima depend to a minor extent on the solvent polarity. A red-shift of less than 10 nm observed on moving from toluene to THF. This can be attributed to the difference in solvent polarizability and a decrease of the dipole moment in the excited state with respect to the ground state. The Φ_F value of **100** is only 0.01 in THF, which is markedly smaller than those of other heteroatom-substituted BODIPYs. The main pathway responsible for this is ISC to the triplet manifold due to the heavy atom effect. Charge transfer from the electron rich Te atoms to the relatively electron deficient BODIPY core also causes fluorescence quenching in the context of Te-BODIPYs.[105] When a sulfur-atom is introduced at the 2-position to form **101**, the absorption band maximum lies in the same region as that of classic BODIPY dye **51** and there is a broad emission band in the red region with an unusually large Stokes shift of 137 nm.[247] The strong solvent dependence of this emission band indicates that the S_1 state has significant charge transfer. Oxidation of the thioether to form an electron-withdrawing sulfoxide restores the fluorescence intensity and results in a marked blue-shift in its band maximum. It has recently been reported that these spectral changes can be used as a sensor for HOCl in living cells.[247]

5.5 Fused-ring systems

Free rotation of aryl-substituents at the 3,5-positions tends to limit the extent of the red-shift of the main spectral bands. Various strategies have been adopted to achieve a greater degree of co-planarity between the π-systems of the aryl substituents by forming rigidized fused-ring systems with sp^3 hybridized carbons, heteroatoms and through B–O chelation. The properties of each of these types of BODIPY dyes will be examined in depth.

5.5.1 Fused-ring systems with sp^3 hybridized carbons

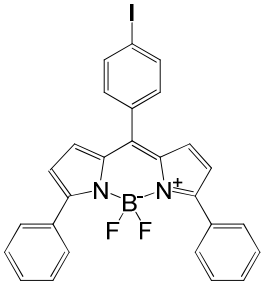

21
$CHCl_3$ Φ 0.20
λ_{abs} 555 nm λ_{em} 588 nm
ε =52 400$M^{-1}cm^{-1}$

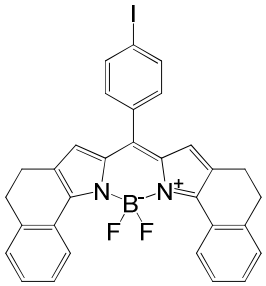

102
$CHCl_3$ Φ 0.38
λ_{abs} 634 nm λ_{em} 647 nm
ε =126 250$M^{-1}cm^{-1}$

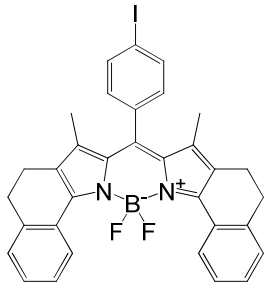

103
$CHCl_3$ Φ 0.72
λ_{abs} 619 nm λ_{em} 629
ε=145 750$M^{-1}cm^{-1}$

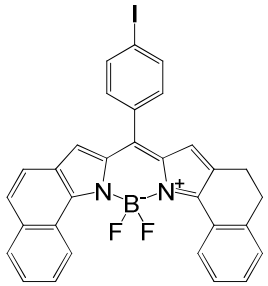

104
$CHCl_3$ Φ 0.17
λ_{abs} 634 nm λ_{em} 668 nm
ε =41 000$M^{-1}cm^{-1}$

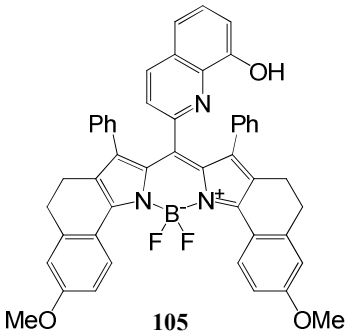

105
water/dioxane Φ N.A
λ_{abs} 660 nm λ_{em} 680 nm

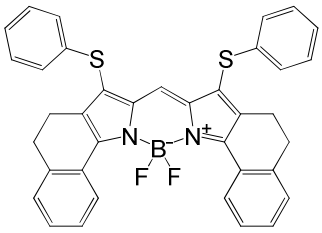

106
MeCN Φ 0.41
λ_{abs} 640 nm λ_{em} 661 nm

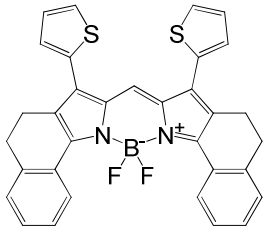

107
MeCN Φ 0.84
λ_{abs} 636 nm λ_{em} 650 nm

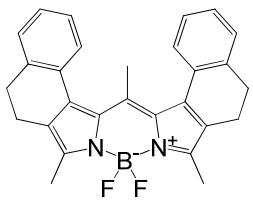

108
MeCN Φ 0.38
λ_{abs} 559 nm λ_{em} 599 nm

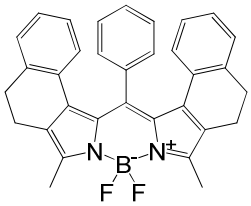

109
MeCN Φ 0.10
λ_{abs} 565 nm λ_{em} 612 nm

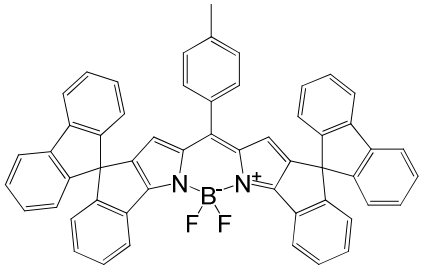

110
THF Φ 0.67
λ_{abs} 634 nm λ_{em} 642 nm
ε =167 210$M^{-1}cm^{-1}$

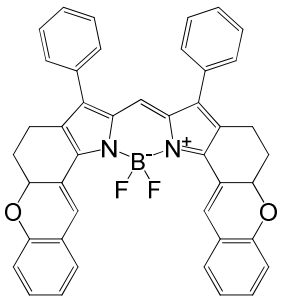

111
$CHCl_3$ Φ 0.06
λ_{abs} 732 nm λ_{em} 747 nm
ε = 29 000 $M^{-1}cm^{-1}$

When the conformational rigidization of phenyl rings substituted at the 3,5-positions is achieved by incorporating sp^3 hybridized carbons, the free rotation of the phenyl rings is eliminated. This leads to an increase in the Φ_F value and the molar extinction coefficient of the main absorption band. There is a marked red-shift of the absorption maximum, due to a narrowing of the HOMO–LUMO gap of **102** relative to that of **21** (Fig. 6), which is predicted to be caused by a relative destabilization of HOMO, since there is a larger mesomeric interaction between the phenyl groups and the BODIPY core. The presence of methyl groups at the 1,7-positions of **103** prevents the free rotation of the *meso*-aryl ring, leading to an increase in the quantum yield relative to **102**.[208,248] Surprisingly, the maximum of the absorption band of the half-oxidized BODIPY **104** is not red-shifted relative to **103**, but the fluorescence emission is red-shifted by 21 nm. The extinction coefficient and quantum yield for the main absorption band of **104** are less than half those of **103**, despite the extension of the π-conjugation system.[248]

The *meso*-hydroxyquinoline fragment of dye **105** can be used as a NIR region chemosensor for metal ions.[249] BODIPYs **106** and **107** absorb and fluoresce in the red region with a slight red-shift of the band maxima with respect to **102** and **103**, indicating a weak conjugation effect at 1,7-positions.[122] The introduction of bridged phenyl groups at the 1,7-positions, so that a fused dihydronaphthalene group is formed at the β position of the BODIPY core to form dyes **108** and **109**, leads to a blue-shift of the absorption and fluorescence emission maxima compared to the values reported for dye **102** constrained at the 3,5-positions.[250] This confirms again that the introduction of substituents at the 3,5-positions has a larger effect on the absorption maxima than the introduction of substituents at other positions. **108** and **109** could be further modified by the introduction of styryl groups at the 3,5-positions to provide NIR region chromophores that are suitable for applications.[250] Two different orientations are possible for the fused dihydronaphthalene rings with respect to the core indacene plane.[250] The rigid structure of **110** contains two spirofluorene moieties. This leads to a significant bathochromic shift of the fluorescence emission. A high Φ_F value is retained, since the spirofluorene

moieties increase the rigidity of the structure, thereby reducing the rate of nonradiative decay.[251,252] The combination of the extended π-conjugation system and the rigid conformation of **111** leads to a further red-shift, along with a decrease in the Φ_F value and the molar extinction coefficient.[253]

5.5.2 Fused-ring systems with heteroatoms

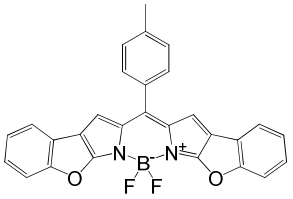

112
CH_2Cl_2 Φ 0.63
λ_{abs} 583 nm λ_{em} 597 nm

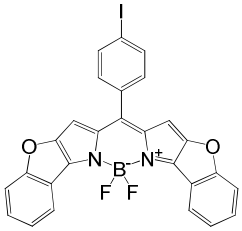

113
$CHCl_3$ Φ 0.34
λ_{abs} 637 nm λ_{em} 647 nm
ε =151 000 $M^{-1}cm^{-1}$

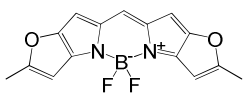

114
$CHCl_3$ Φ 0.96
λ_{abs} 579 nm λ_{em} 583 nm
ε = 202 000 $M^{-1}cm^{-1}$

115
$CHCl_3$ Φ 0.90
λ_{abs} 652 nm λ_{em} 661 nm
ε = 314 000 $M^{-1}cm^{-1}$

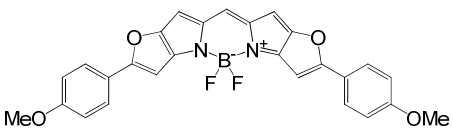

116
$CHCl_3$ Φ 0.86
λ_{abs} 673 nm λ_{em} 683 nm
ε = 288 000 $M^{-1}cm^{-1}$

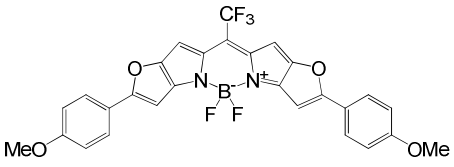

117
$CHCl_3$ Φ 0.56
λ_{abs} 723 nm λ_{em} 738 nm
ε = 253 000 $M^{-1}cm^{-1}$

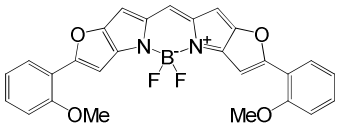

118
$CHCl_3$ Φ 0.91
λ_{abs} 671 nm λ_{em} 680 nm
ε = 313 000 $M^{-1}cm^{-1}$

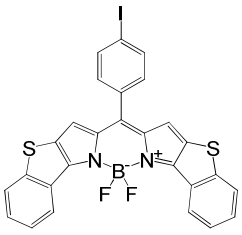

119
$CHCl_3$ Φ 0.05
λ_{abs} 658 nm λ_{em} 673 nm
ε =54 250 $M^{-1}cm^{-1}$

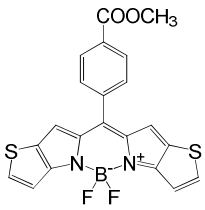

120
CH_2Cl_2 Φ 0.06
λ_{abs} 576 nm λ_{em} 604 nm
ε =122 000 $M^{-1}cm^{-1}$

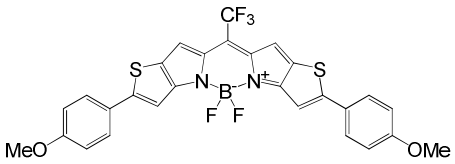

121
$CHCl_3$ Φ 0.37
λ_{abs} 731 nm λ_{em} 754 nm
ε =201 000 $M^{-1}cm^{-1}$

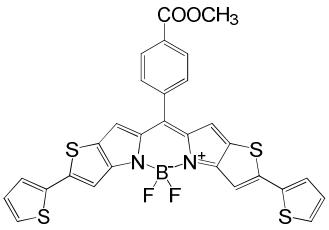

122
CH_2Cl_2 Φ 0.31
λ_{abs} 684 nm λ_{em} 716 nm
ε =203 000 $M^{-1}cm^{-1}$

Rigid conformations can also be achieved with a benzofuran moiety as is the case with **112** and **113**.[130,248] These have more intense absorption and fluorescence bands at longer wavelengths than the analogous unconstrained **21** dye. The most prominent difference between the 2,6-dioxy-benzofuran **113** and the 3,5-dioxy-benzofuran **112**, is that there is a larger red-shift of the absorption and emission bands of **113**, with bands which lie 50 nm to the red of those of **112** due to the enhanced π-conjugation of the 2,6-dioxy derivatives.

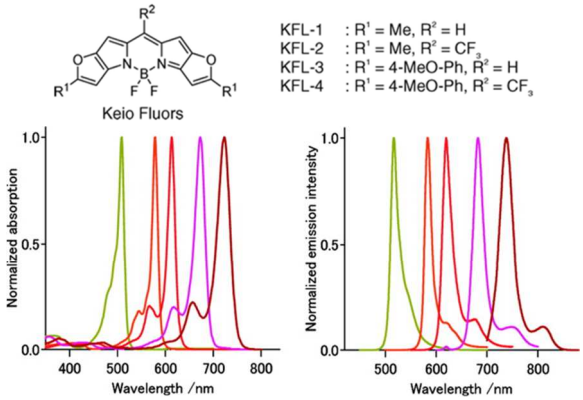

Fig. 11 The absorption and emission spectra of, from left to right, 1,3,5,7-tetramethyl-BODIPY and a series of Keio Fluors (KFL1–4) measured in $CHCl_3$. (Reprinted with permission from ref. 23. Copyright © 2008 American Chemical Society.)

Recently, a new series of analogues named Keio Fluors **114-118** were prepared with structures similar to those of classic BODIPYs but with furan ring moieties fused at the 2,6- and 3,5-positions. These dyes have extremely high molar extinction coefficients, Φ_F values, and brightness compared to other constrained systems.[23,254] In DFT calculations (Fig. 6), the energy of the HOMO of **115** is similar to that of **51**, a classic BODIPY dye, but there is a large stabilization of the LUMO due to the absence of an electron-donating aryl-substituent at the *meso*-position and/or the bonding interactions with the oxygen atom that are predicted at the points of attachments of the fused furan rings. Keio Fluors **114-118** can be viewed as being 3,5-distyryl substituted BODIPY with oxygen atom bridge linkers that hinder free rotation of the ethenyl fragments. These dyes fluoresce in the NIR region with high quantum yields (Fig. 11). The main absorption band of the methyl substituted structure of **114** is slightly blue shifted relative to that of the benzofuran **112** and there is a very small Stokes shift. Overall, the emission of **115** is red-shifted by 151 nm compared to that of **51**, the classic tetramethyl-BODIPY dye. There is a further red-shift of ca. 20 nm due to the introduction of electron-donating methoxy-substituents at the *para* or *ortho*-positions to form **116** and **118**. According to previous reports (from **22** to **23**), the presence of *ortho*-methoxyphenyl rings at the 3,5-positions of the BODIPY core tends to have a negative effect on the optical properties, since there is a shortening of the wavelength of the spectral bands, and a decrease in the molar extinction coefficients and Φ_F values. However, the *ortho*-methoxyphenyl-substituted Keio Fluors **118** exhibits similar characteristics to

other Keio Fluors type dyes, since there is no scope for hindered rotation of the phenyl ring. This means that a fine tuning of the absorption and emission band maxima can be

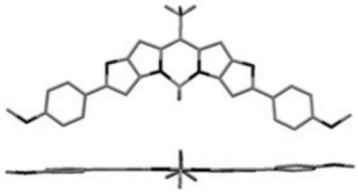

Fig. 12 The front and side views of the x-ray molecular structure of **117**. (Adapted with permission from ref. 254. Copyright © 2009 Wiley-VCH Verlag GmbH & Co. KGaA, Weinheim.)

achieved for this series of dyes by attaching substituents at various positions on the phenyl ring. The photophysical properties can be attributed to the benzofuran moiety and the phenyl rings being coplanar. This has been confirmed by single-crystal X-ray crystallography (Fig. 12).[23,254] A significant bathochromic shift of ca. 50 nm is observed for the main spectral bands of **117**, compared to those of **115** due to the presence of a *meso*-CF_3-substituent, for reasons similar to those described previously for the spectra of **21** and **31**, and for **30** and **32**.

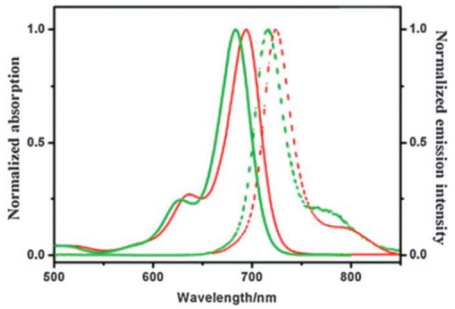

Fig. 13 Normalized absorption (solid line) and emission (dashed line) spectra of **122** (green) and a related tribromimated structure (red) in CH_2Cl_2. (Reprinted with permission from ref. 256. Copyright © 2013 Royal Society of Chemistry.)

When the conformations of BODIPY dyes are constrained by sulfur atoms, such as with dyes **119-122**,[255,256] slight red-shifts of the main spectral bands are observed and, with the exception of **119**,[248] there is a decrease in the Φ_F value, but not the molar extinction coefficient, relative to the corresponding oxygen atom constrained dyes. A further red-shift of 108 nm was observed when thienyl groups were attached to the benzothiophene rings to form **122** (Fig. 13). Bromine atoms have been incorporated into the structures of **121** and **122** to enhance the rate of ISC and hence the singlet

oxygen quantum yields, making these BODIPYs potentially suitable for use as NIR region photosensitizers.[255,256]

5.5.3 Fused-ring systems with B–O chelation

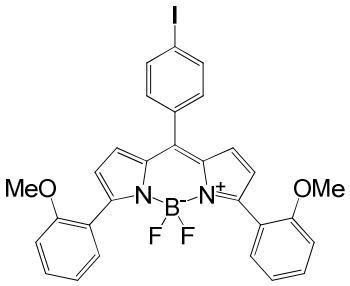

123
$CHCl_3$ Φ 0.07
λ_{abs} 550 nm λ_{em} 597 nm
ε =34 500 $M^{-1}cm^{-1}$

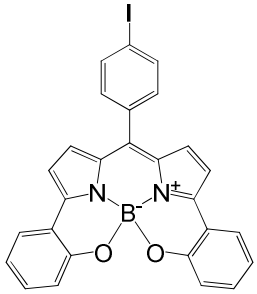

124
$CHCl_3$ Φ 0.41
λ_{abs} 630 nm λ_{em} 654 nm
ε =46 000 $M^{-1}cm^{-1}$

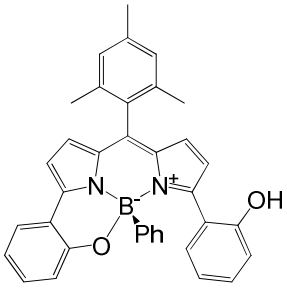

125
$CHCl_3$ Φ 0.65
λ_{abs} 588 nm λ_{em} 614 nm

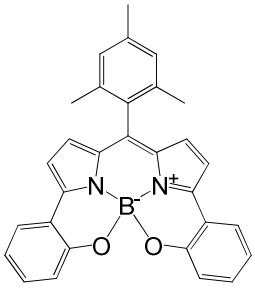

126
$CHCl_3$ Φ 0.72
λ_{abs} 626 nm λ_{em} 645 nm

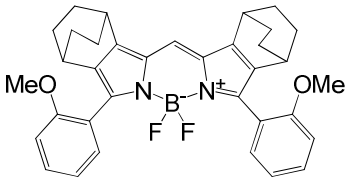

127
CH_2Cl_2 Φ 0.77
λ_{abs} 550 nm λ_{em} 583 nm
ε =61 600 $M^{-1}cm^{-1}$

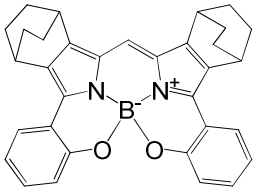

128
CH_2Cl_2 Φ 0.99
λ_{abs} 626 nm λ_{em} 645 nm
ε =63 000 $M^{-1}cm^{-1}$

The absorption bands of O-chelated BODIPYs exhibit a significant red-shift of ca. 65–80 nm. Narrow emission band are observed and there is an increase in the Φ_F values relative to the corresponding precursor dye (i.e. **123** and **124**, or **127** and **128**). This is probably due to a decrease in the dihedral angle between the phenyl rings and the BODIPY core. When the MO energies of **124** are compared to those of **21** (Fig. 6), which has freely rotating phenyl rings, it is clear that the narrowing of the HOMO–LUMO gap is mainly due to a destabilization of the HOMO when the aryl substituents are constrained to lie almost co-planar with the BODIPY core.[257,258] The chiral boron center in the mono O-linked structure of **125** could be used in chiral recognition applications or to provide circularly polarized luminescence.[259,260] The bicyclo[2.2.2]octadiene-fused (BCOD-fused) and O-chelated dye **128** exhibits unusually strong fluorescence with a Φ_F value of 0.99. This can be attributed to the

BCOD rings blocking the quenching associated with π-π stacking of the BODIPY core stacking, the absence of rotation of a *meso*-phenyl group and the B–O chelation of the phenyl rings at the 3,5-positions.[258]

5.6 Fused-ring-expansion systems

Another strategy that has proven to be useful in forming NIR BODIPY dyes is the fused-ring-expansion of the π-system. Fusion can be achieved at either the β-positions of the pyrrole ring or at the α-position, and BODIPY moieties have also be fused with porphyrin macrocycles.

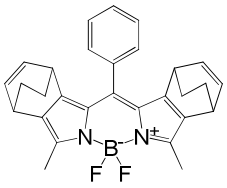

129
MeCN Φ 0.81
λ_{abs} 526 nm λ_{em} 543 nm
ε =45 700 $M^{-1}cm^{-1}$

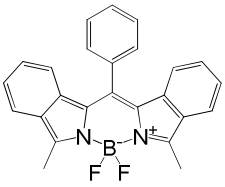

130
MeCN Φ 0.87
λ_{abs} 597 nm λ_{em} 606 nm
ε =112 000 $M^{-1}cm^{-1}$

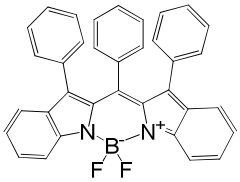

131
CH_2Cl_2 Φ N. D
λ_{abs} 568nm
ε =36 000 $M^{-1}cm^{-1}$

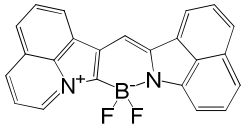

132
DMSO Φ N. A
λ_{abs} 622 nm λ_{em} N. A
ε =92 500 $M^{-1}cm^{-1}$

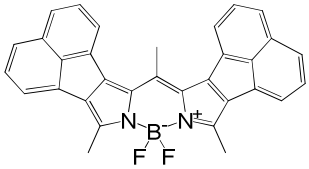

133
$CHCl_3$ Φ N.A
λ_{abs} 657 nm λ_{em} N.A.
ε =141 200 $M^{-1}cm^{-1}$

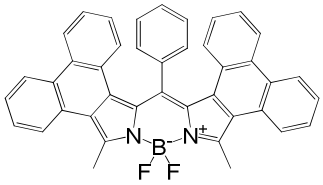

134
Hexane Φ 0.94
λ_{abs} 630 nm λ_{em} 647 nm
ε =117 500 $M^{-1}cm^{-1}$

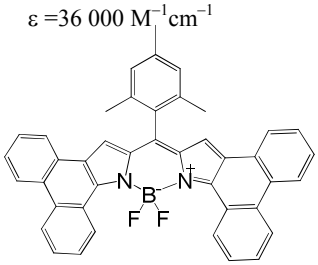

135
CH_2Cl_2 Φ 0.51
λ_{abs} 673 nm λ_{em} 692 nm
ε =140 000 $M^{-1}cm^{-1}$

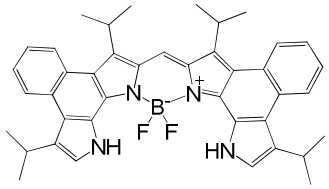

136
$CHCl_3$ Φ 0.63
λ_{abs} 727 nm λ_{em} 744 nm
ε =337 000 $M^{-1}cm^{-1}$

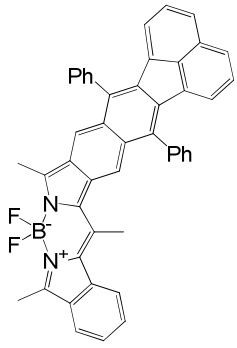

137
CH_2Cl_2 Φ 0.36
λ_{abs} 681 nm λ_{em} 697 nm
ε =91 200 $M^{-1}cm^{-1}$

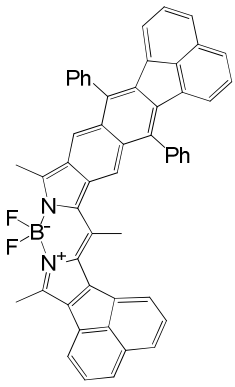

138
CH_2Cl_2 Φ 0.70
λ_{abs} 658 nm λ_{em} 695 nm
ε =79 400 $M^{-1}cm^{-1}$

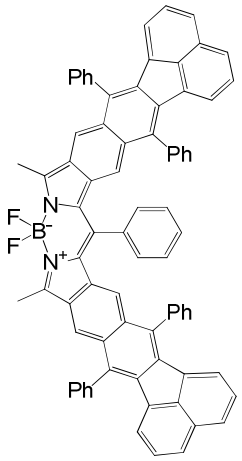

139
CH_2Cl_2 Φ 0.32
λ_{abs} 765 nm λ_{em} 783 nm
ε =199 500 $M^{-1}cm^{-1}$

5.6.1 Fused-ring-expansion at the α, and β-positions

BODIPY **129** contains two fused BCOD moieties at the β positions and has a spectrum similar to that of tetramethyl-BODIPY **51** with a high Φ_F values of 0.81.[261,262] Fused-ring-expansion of the BODIPY structure to form BODIPYs **129-139** results in spectral bands that are bathochromically shifted into the red end of the visible region and in some cases into the NIR region. For example, the absorption bands of **130-133** exhibit large bathochromic shifts of 71, 42, 96, and 131 nm, respectively, relative to the main absorption band of **129**. In DFT calculations (Fig. 6), there is a marked destabilization of the HOMO of **130** relative to that of **51**, a classic BODIPY dye, due to the antibonding nature of the interactions with the fused benzo groups at the points of attachments on the β-carbons of the pyrrole moieties. The absorption and emission spectra of the benzo[β]-fused BODIPY **130** exhibit similar band morphologies to those of classic BODIPY dyes (e.g. narrow bandwidths, mirror-symmetry with the emission band) and retain high Φ_F values.[262] However, the benzo[α]-fused BODIPY **131** lacks these typical BODIPY properties. A broad absorption band (500–700 nm) is observed and there is no emission intensity, probably due to conformational flexibility associated with the steric hindrance between the aryl substituents.[263]

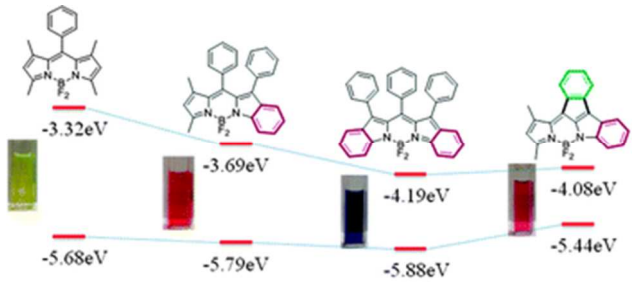

Fig. 14 The effect of fusion of a benzene ring at the α-position on the energies of the frontier π-MOs of **131**. (Reprinted with permission from ref. 263. Copyright © 2013 Royal Society of Chemistry.)

Interestingly, DFT calculations and electrochemical analyses indicate that the fusion of a benzene ring at the α-position results in a stabilization of the LUMO but has a smaller effect on the energy of the HOMO (Fig. 14). In contrast, benzo-fusion at the β-position destabilizes the HOMO, but has a smaller impact on the energy of the LUMO (Fig. 14). These results can be conceptualized by viewing the BODIPY structure as a combination of an electron-donating pyrrole and an electron-accepting

azafulvene moiety. The benzo[α]-fused structure enhances the azafulvene character resulting in a stabilization of the LUMO energy level, while the fusion of a benzene ring at the β-position enhances the pyrrole character, resulting in a destabilization of the HOMO.[263,264] In the 1980s, the benz[*c*,*d*]indole **132** was reported to have an absorption band at 622 nm, but the emission spectrum is not available and no quantum yield values are available.[265] There is a particularly large red-shift of the spectral bands when acenaphtho groups are fused at the β-carbons of the pyrrole moieties to form **133**.[266] There is a significant stabilization of the LUMO (Fig. 6), since there is a bonding interaction at the points of attachment on the β-carbons of the pyrrole moieties. There is also a destabilization of the HOMO, since there is an antibonding interaction at the points of attachment of the acenaphtho rings.

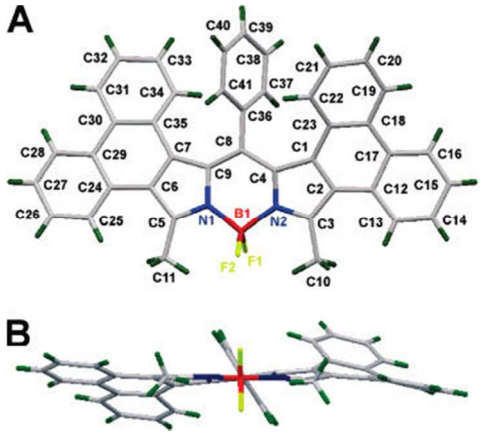

Fig. 15 Crystal structure of **134** viewed from the top (A) and along the B(1)-C(8) axis (B). (Reprinted with permission from ref. 267. Copyright © 2008 American Chemical Society.)

The phenanthro-fused BODIPY **134** has an intense absorption band at 630 nm with a high molar absorption coefficient (ε ≥ 100,000) and a Φ_F value that is near unity.[267] This suggests that the fusion of the larger phenanthrene moieties induce a 'propeller-like' distortion of the BODIPY structure (Fig. 15), which facilitates a stronger electronic influence by the *meso*-substituent while retaining the advantages of the virtually decoupled architecture of *meso*-aryl-substituted BODIPYs with large torsion angles between the phenyl ring and the BODIPY core. There is a smaller stabilization of the LUMO of **134** than for **133** (Fig. 6), possibly due to there being a weaker bonding interaction at the points of attachment of the peripheral fused rings on the β-carbons of the pyrrole moieties. The decrease in the HOMO–LUMO gap causes a slight blue shift of the main absorption band, so

incorporating acenaphtho groups appears to be the better strategy for achieving a red shift of the main spectral bands. It should be noted, however, that the absorption band of **134** lies in the output range (ca. 635 nm) of the most commonly used red light excitation sources (HeNe and diode lasers). The properties of the chromophore can be fine-tuned through further structural modifications. Styryl groups can be introduced at the 3,5-positions, leading to significant red-shifts of the main spectral bands.[267] BODIPY **135** has a more intense and red-shifted absorption band (673 nm) than that of **134**. There is a higher relative stabilization of the LUMO of **135** (Fig. 6), due to the different points of attachments on the pyrrole moieties. The Φ_F value is relatively high, despite the narrow HOMO–LUMO gap. The molecular structure of **135** is planar due to the absence of a steric interaction with a *meso*-aryl-substituent. Strong π-π interactions through the peripheral phenanthrene moieties leads to fluorescence quenching in the solid state.[268] The naphthobipyrrole derived BODIPY **136** has markedly red shifted absorption (727 nm) and emission band maxima (744 nm).[269] The absorption band has a very high molar extinction coefficient (ε = 327000 M^{-1} cm^{-1}) and there is a reasonably high Φ_F value. The dye was also found to have reasonably good photostability. The emission peaks for dyes **137** and **138**, which contain a single fluorantho[8,9-*f*]isoindole moiety and either a benzo or acenaphtho fused ring, are observed at similar wavelengths, while the absorption bands lie at 681 and 658 nm, respectively.[270] When two fluorantho[8,9-*f*]isoindole moieties are incorporated to form **139** the main spectral bands lie in the NIR region beyond 750 nm and there is a relatively low Φ_F value of ca. 0.3. **139** is unstable in air, probably due to a large destabilization of the HOMO energy level, which leads to a marked decrease in the first oxidation potential.[270]

5.6.2 Meso-, β- and porphyrin-fused-BODIPYs

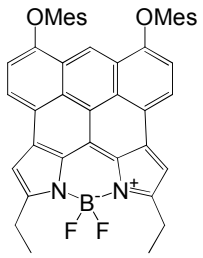

140
toluene Φ < 0.008
λ_{abs} 658, 784, 867 nm λ_{em} 924 nm
ε = 11300 $M^{-1}cm^{-1}$ (658)
5800 $M^{-1}cm^{-1}$ (784), 6200 $M^{-1}cm^{-1}$ (867)

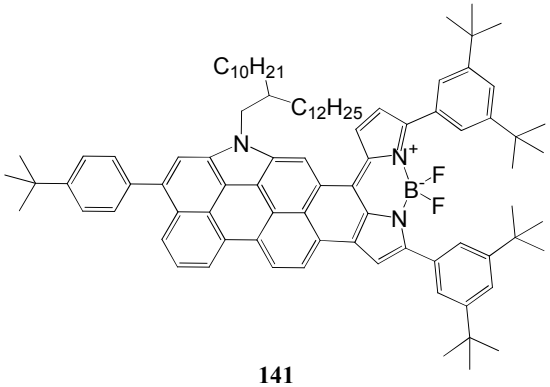

141
toluene Φ 0.008
λ_{abs} 670, 780 nm λ_{em} 742, 830 nm
ε = 91 000 $M^{-1}cm^{-1}$ (670nm)

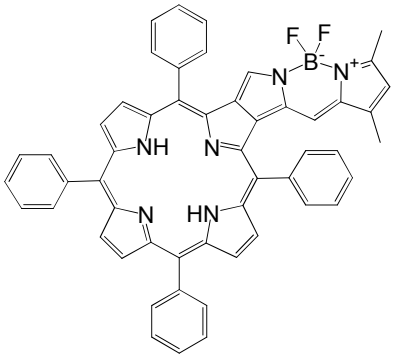

142
CH_2Cl_2, Φ 0.04
λ_{abs} 388, 413, 531, 640 nm λ_{em} 693 nm
ε = 51500 $M^{-1}cm^{-1}$ (380), 44500 $M^{-1}cm^{-1}$ (413),
65000 $M^{-1}cm^{-1}$ (531), 58250 $M^{-1}cm^{-1}$ (640)

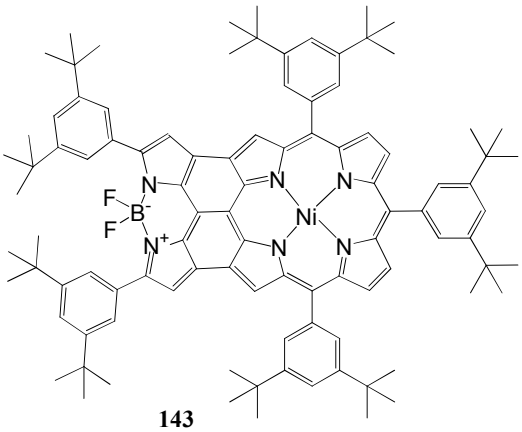

143
toluene N.D
λ_{abs} 890 nm,
ε = 49 000 $M^{-1}cm^{-1}$

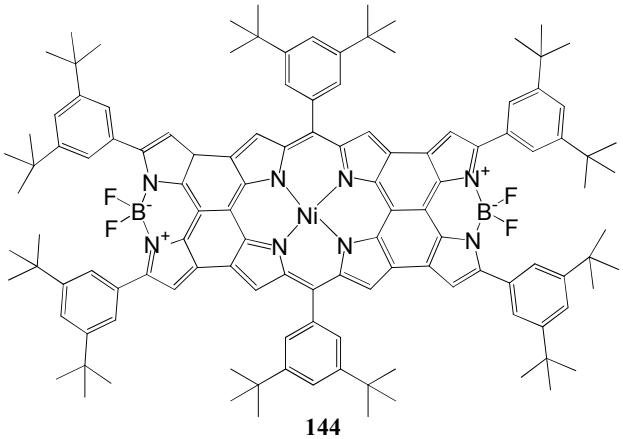

144
toluene N.D
λ_{abs} 1040 nm,
ε = 68 000 $M^{-1}cm^{-1}$

Another strategy for achieving a bathochromic shift of the main BODIPY absorption band is the fusion of the BODIPY π-system to the *meso*-carbon and/or the β-pyrrole carbons of a porphyrin ring. This results in a marked expansion of the π-conjugation system and a shift of the absorption and emission bands to the far-red of the visible region or the NIR region. In contrast to classic BODIPYs, **140** exhibits a broad envelope of absorption intensity between 500 and 930 nm with maxima at 658 nm, 784 nm and 867 nm.[271] When an anthracene moiety is fused to the β-positions of the BODIPY core, there is a remarkable bathochromic shift of the absorption and emission (924 nm) bands, but the Φ_F value is under 0.008.[271] In a similar manner, the β-fused structure of BODIPY **141** results in a red-shift of the main absorption band to 670 nm together (ε = 91 000 $M^{-1}.cm^{-1}$) with a shoulder at ca. 780 nm. Two distinct emission bands are observed in a wide range of solvents at 742 and 830 nm. A

relatively low Φ_F value of 0.008 was reported in toluene.[272] Although this is mainly attributable to the effect of aggregation in solution, other factors such as changes in conformation and the charge transfer character of the S_1 state (from the electron-donating N-annulated perylene moiety to the electron-accepting BODIPY core) may also contribute to the decrease in the Φ_F value.[272]

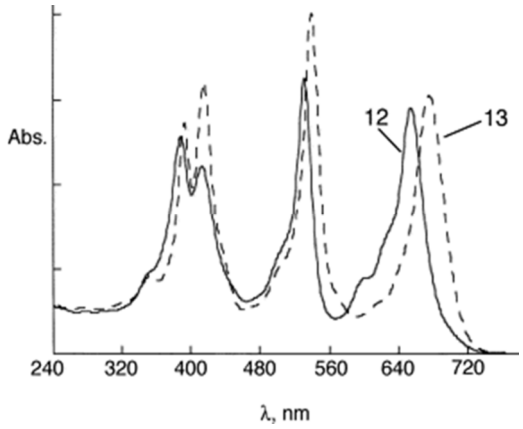

Fig. 16 The absorption spectra of **142** (solid line) and its Zn(II) complex (dashed line) in CH_2Cl_2 at room temperature. (Adapted with permission from ref. 273. Copyright © 2004 Elsevier.)

In compounds **142-144**,[273,274] BODIPY moieties are fused to porphyrin rings. These dyes have intense absorption bands in the NIR region due to the extension of the π-conjugation system. The absorption spectrum of **142**, which has a BODIPY moiety fused at the β-pyrrole carbons of a tetraphenylporphyrin ring, contains four moderately intense bands in the 300–750 nm region, at 388, 413, 531, and 640 nm in CH_2Cl_2 (Fig. 16). The emission maximum shifts dramatically to 693 nm and there is a low Φ_F value of around 0.04. In **143**, a BODIPY moiety is fused to a *meso*-carbon and two neighboring β-pyrrole carbons of a Ni tetraarylporphyrin resulting in an even greater extension of the π-system and a larger bathochromic shift to 890 nm (Fig. 17). When a second BODIPY moiety is fused to form **144** there is a further shift of the absorption band to beyond 1000 nm, the longest wavelength to be reported for the absorption maximum of a BODIPY derivative (Fig. 17). Although the fusion of the BODIPY chromophore to a porphyrin ring is an effective method for obtaining a bathochromic shift of the main absorption band, a major drawback in the context of **143** and **144** is

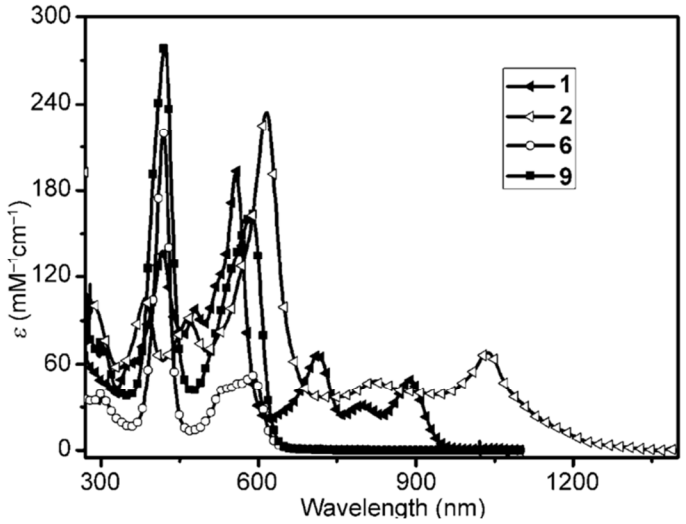

Fig. 17 The absorption spectrum of **143** (1) and **144** (2) and their corresponding *meso*-substituted porphyrins (6 and 9) in toluene. (Reprinted with permission from ref. 274. Copyright © 2011 Wiley-VCH Verlag GmbH & Co. KGaA, Weinheim.)

that the dyes do not fluoresce. This is the norm for Ni(II) porphyrins, however, due to the presence of low-lying ligand-to-metal charge transfer bands.[274]

5.7 β-aromatic ring-fused and α-substituted BODIPYs

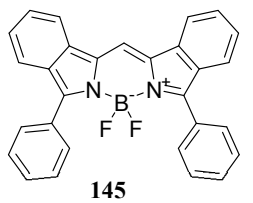

145
CH_2Cl_2 Φ 0.88
λ_{abs} 634 nm λ_{em} 658 nm
ε = 108 400 $M^{-1}cm^{-1}$

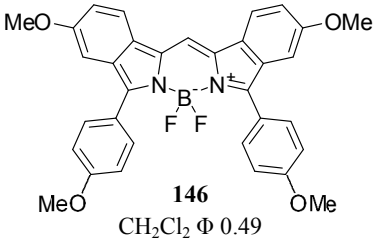

146
CH_2Cl_2 Φ 0.49
λ_{abs} 673 nm λ_{em} 704 nm
ε = 118 600 $M^{-1}cm^{-1}$

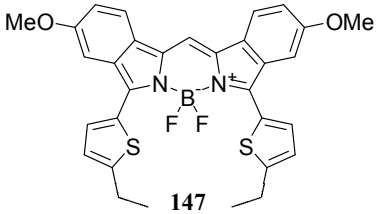

147
CH_2Cl_2 Φ 0.20
λ_{abs} 727 nm λ_{em} 780 nm
ε = 100 000 $M^{-1}cm^{-1}$

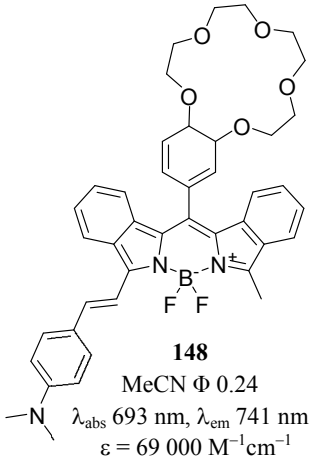

148
MeCN Φ 0.24
λ_{abs} 693 nm, λ_{em} 741 nm
ε = 69 000 $M^{-1}cm^{-1}$

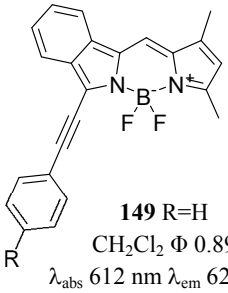

149 R=H
CH_2Cl_2 Φ 0.89
λ_{abs} 612 nm λ_{em} 629 nm
ε = 49 000 $M^{-1}cm^{-1}$
150 R=OMe
CH_2Cl_2 Φ 0.63
λ_{abs} 616 nm λ_{em} 633 nm
ε = 34 000 $M^{-1}cm^{-1}$

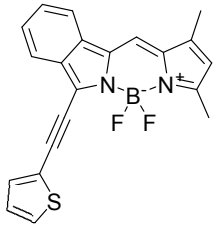

151
CH_2Cl_2 Φ 0.44
λ_{abs} 618 nm, λ_{em} 631 nm
ε = 14 000 $M^{-1}cm^{-1}$

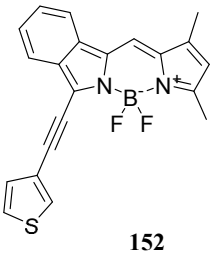

152
CH_2Cl_2 Φ 0.80
λ_{abs} 612 nm, λ_{em} 628 nm
ε = 93 300 $M^{-1}cm^{-1}$

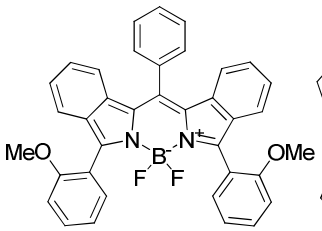

153
CH_2Cl_2 Φ 0.91
λ_{abs} 617 nm, λ_{em} 652 nm
ε = 102 330 $M^{-1}cm^{-1}$

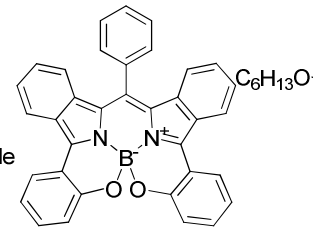

154
CH_2Cl_2 Φ 0.58
λ_{abs} 711 nm, λ_{em} 733 nm
ε = 91 200 $M^{-1}cm^{-1}$

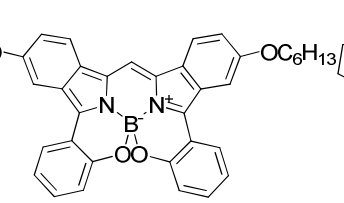

155
THF Φ N.A
λ_{abs} 748 nm, λ_{em} N.A
ε = 83 400 $M^{-1}cm^{-1}$

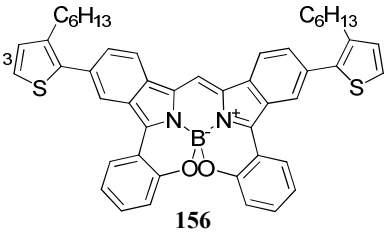

156
THF Φ N.A
λ_{abs} 733 nm, λ_{em} N.A
ε = 135 000 $M^{-1}cm^{-1}$

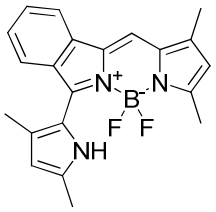

157
CH_2Cl_2 Φ 0.61
λ_{abs} 609 nm, λ_{em} 631

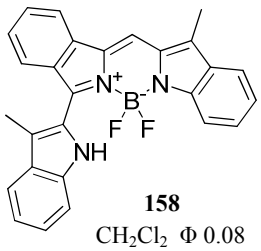

158
CH_2Cl_2 Φ 0.08
λ_{abs} 611 nm, λ_{em} 648nm

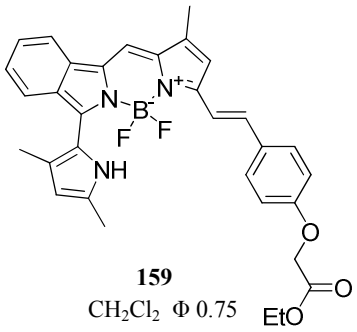

159
CH_2Cl_2 Φ 0.75
λ_{abs} 680nm, λ_{em} 705nm

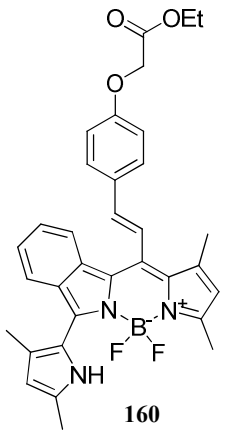

160
CH_2Cl_2 Φ 0.01
λ_{abs} 608 nm, λ_{em} 687nm

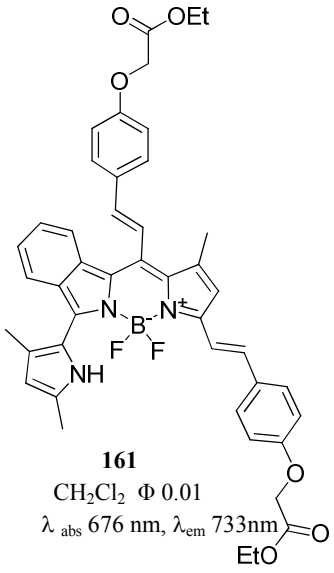

161
CH_2Cl_2 Φ 0.01
λ_{abs} 676 nm, λ_{em} 733nm

Since β-aromatic ring fusion has been proven to be an efficient way to shift the absorption and emission bands to longer wavelength, structural modification at the α-positions provides an opportunity to obtain a further bathochromic shift. For example, when a phenyl group is introduced to form **145**, a very intense absorption band is observed at 634 nm in CH_2Cl_2.[275] This represents a red-shift of ca. 40 nm compared to **130**. The Φ_F value of 0.88 is similar to that of **130** (Φ_F = 0.87**)**. When four electron-donating OMe substituents are introduced to form **146**, there is a further ca. 40 nm red shift of the main absorption band maximum,[275] while the introduction of ethylthiophene groups results

in a bathochromic shift of 54 nm. **146** and **147** emit at exceptionally long wavelengths beyond 700 nm. The thiophene moiety plays a key role in extending the π-conjugation system. The Φ_F value decreases in the same order as the red-shifts of the spectral band, from 0.88 to 0.49, to only 0.20, due in part to an increase in ISC caused by the heavy atom effect of the sulfur atoms.[275,276]

The main absorption and emission bands of the benzo-fused and styryl-substituted **148** dye are shifted into the NIR region.[139] The incorporation of a $-NMe_2$ group onto the styryl group provides a sensor for pH. Interestingly, **148** displays low fluorescence anisotropy. Many NIR dyes with long polymethine chains, such as styryl dyes, have rather high anisotropies. Low anisotropies can be useful when molecules are used as markers for biological superstructures, since the anisotropy can be modified considerably upon incorporation of the marker into the restricted environment of a biomolecule.[139] A series of asymmetric benzo-fused BODIPYs with alkynyl groups at the α-positions, **149-152**, were recently prepared to provide linkers to other aromatic groups.[277] The introduction of the alkynyl group was achieved with a Sonogashira coupling reaction. In CH_2Cl_2, these dyes exhibit typical BODIPY absorption and emission properties, with bands centered at 612–618 and 625–633 nm, respectively. No significant solvatochromic shifts are observed**.** Although high Φ_F values of between 0.6–0.9 have been reported for **147**, **150** and **152**, a lower value of $\Phi_F = 0.44$ has been reported for **151**. This can be attributed to the presence of a low-lying charge separated S_1 state, since there is an electron-rich 2-ethynylthiophene moiety and the BODIPY core is electron deficient.

When an anisole substituent is added to form **153**, the main absorption band lies at 617 nm in THF, which represents a blue-shift of 17 nm relative to that of **145**. This is related to the lack of co-planarity between the two π-systems due to the steric hindrance caused by the *o*-methoxy groups on the phenyl substituents. In the crystal structure of **153**, the average dihedral angles between the plane of the *o*-methoxyphenyl group and the indacene plane is 85.7°, which is much larger than the 57° angle in the structure of **145**. The Φ_F value of 0.91 is similar to that of **145**.[258] Demethylation of **153** with BBr_3 and simultaneous cyclization to form a spirobi[1,3,2]oxazaborine moiety affords a structurally

constrained dye **154** in high yield.[258] The absorption and emission bands lie at 711 and 733 nm, respectively, and are red shifted by 94 and 81 nm relative to the spectra of **153**. The Φ_F value decreases to 0.58. Further modifications of the substituents on the β-fused benzo ring leads to significant bathochromic shifts of the main spectral bands. As a result, the absorption bands of **155** and **156** are red shifted from 711 nm to 748 and 733 nm, respectively, in THF. No Φ_F values have been reported. Surprisingly, when films are prepared on a glass plate, the film for **155** exhibits an intense absorption band that stretches out to 1060 nm with a maximum of 922 nm, due to aggregation effects. It should be noted that **156** can be used as a photosensitizer in polymeric solar cells, since the incorporation of the 3-hexylthiophene-substituent improves the photovoltaic performance.[278,279]

Recently, dyes **157** and **158** have been reported which have pyrrole and indole substituents at the 3-position and a benzene ring fused at the β-positions of the same pyrrole moiety.[280] The absorption (λ_{max}=609 nm) and emission (λ_{em} = 631 nm) bands of **157** exhibit significant red-shifts of 106 and 110 nm, relative to those of **20**, and there is a high Φ_F value of 0.61 in CH_2Cl_2. As the number of alkyl substituents on the other pyrrole moiety is increased, the absorption and emission bands are steadily shifted to longer wavelengths. When an additional fused benzo group is added at the α-positions of the other pyrrole moiety to form **158**, there is a marked decrease in the quantum yield to only 0.08.

Further red-shifts of this class of BODIPY dye can be achieved by grafting styryl groups onto the BODIPY core to form dyes **159-161**.[280] These structures demonstrate that a *meso*-methyl group can not only undergo a Knoevenagel reaction, but can compete with the 3,5-position methyl groups in this regard. BODIPY **159** is green in color under ambient conditions (λ_{max} = 680 nm) and exhibits strong fluorescence emission in the NIR region (λ_{em} = 705 nm) with a quantum yield of 0.75 in CH_2Cl_2. There are significant red-shifts of the absorption and emission bands of 71 and 74 nm, respectively, relative to the spectra of **157**. In contrast, the *meso*-substituted **160** dye absorbs at 608 nm and emits at 687 nm, and has the largest Stokes shift (1891 cm^{-1}) reported for this series of dyes. The absorption and emission bands of **161** and **159** have been reported to lie at similar wavelengths. This

demonstrates that the *meso*-styryl substituent does not have a significant effect on the π-conjugation system of the BODIPY core. There is a 49° torsion angle between the plane of the BODIPY core and that of the *meso*-styryl ring. In a similar manner to **92-95**,[245] the *meso*-styryl-substituted **160** dye fluoresces only weakly with a quantum yield of less than 0.01.

5.8 Aza-BODIPYs

One of the most significant strategies for shifting the spectral bands of the BODIPY to the red is the incorporation of a nitrogen atom at *meso*-position to form an aza-BODIPY dye. This strategy can readily combined with other structural modifications involving the substitution or fused-ring-expansion of the pyrrole moieties. The properties of tetra-aryl, conformationally restricted, and β-aromatic-fused and α-substituted aza-BODIPY structures will be examined in depth.

5.8.1 Tetra-aryl systems

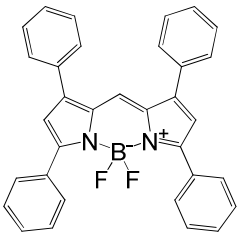

35
THF Φ 0.92
λ_{abs} 571 nm λ_{em} 601 nm
ε = 74 100 $M^{-1}cm^{-1}$

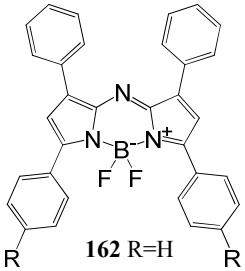

162 R=H
$CHCl_3$ Φ 0.34
λ_{abs} 650 nm λ_{em} 672 nm
ε = 79 000 $M^{-1}cm^{-1}$
163 R=OMe
$CHCl_3$ Φ 0.36
λ_{abs} 688 nm λ_{em} 715 nm
ε = 85 000 $M^{-1}cm^{-1}$
164 R=NMe_2 $CHCl_3$Φ N.A
λ_{abs} 799 nm λ_{em} 823 nm
ε = 87 000 $M^{-1}cm^{-1}$

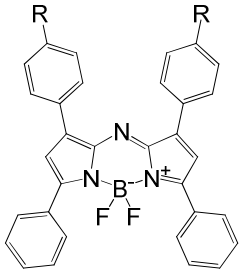

165 R=OMe
$CHCl_3$ Φ 0.23
λ_{abs} 664 nm λ_{em} 695 nm
ε = 78 000 $M^{-1}cm^{-1}$
166 R=NMe_2
Toluene Φ N.A
λ_{abs} 763 nm λ_{em} 822 nm

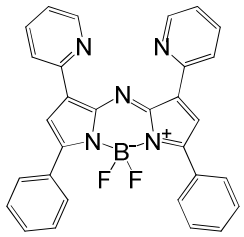

167
MeCN Φ 0.19
λ_{abs} 655 nm λ_{em} 682 nm

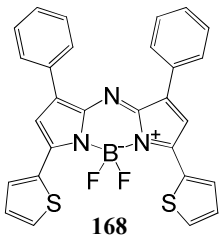

168
CH_2Cl_2 Φ 0.44
λ_{abs} 718 nm λ_{em} 740 nm
ε = 120 500 $M^{-1}cm^{-1}$

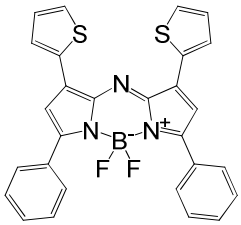

169
CH_2Cl_2 Φ 0.10
λ_{abs} 683 nm λ_{em} 725 nm
ε =78 000 $M^{-1}cm^{-1}$

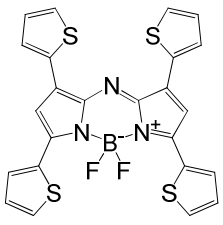

170
CH_2Cl_2 Φ 0.11
λ_{abs} 742 nm λ_{em} 764 nm
ε = 110 000 $M^{-1}cm^{-1}$

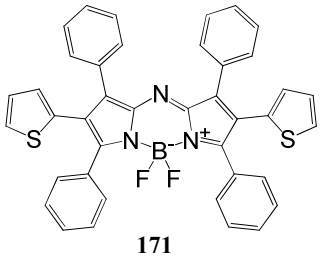

171
CH_2Cl_2 Φ N.D
λ_{abs} 650 nm
ε = 40 000 $M^{-1}cm^{-1}$

In aza-BODIPY dyes such as **162**,[188] the *meso*-carbon is replaced by an aza-nitrogen atom. There is a bathochromic shift of approximately 80 nm compared to the analogous tetrasubstituted BODIPY analogue **35** (Fig. 6), since there is a marked stabilization of the LUMO due to there being a large MO coefficient at the *meso*-position where the electronegative nitrogen atom is introduced. The introduction of electron-donating –OMe and $–NMe_2$ *para*-substituents onto the phenyl substituents at the 3,5-positions to form **163** and **164** results in additional red-shifts of the absorption maximum from 650 nm to 688 and 799 nm, respectively.[188,281] There is a destabilization of both the LUMOs and the HOMOs of **163** and **164** due to the inductive effects associated with the *para*-substituents. The large MO coefficients at the 3,5-positions result in a relative destabilization of the HOMO due to the mesomeric interaction between the aryl substituents and the BODIPY chromophore. The incorporation of electron-donating substituents at the *para*-positions of 1,7-position phenyl substituents results in a smaller red-shift effect relative to the corresponding 3,5-position analogues, since there are smaller MO coefficients at these positions in the HOMO (Fig. 3). For example, the absorption bands of **165**[189] and **166**[282], the 1,7-substituted analogues of **163** and **164**, lie at 664 and 763 nm, a blue-shift of 24 and 36 nm, respectively. The absorption and fluorescence spectra of the amino-substituted structures of **164** and **166** exhibit a strong pH-dependence across a broad pH range.

When 2-pyridyl substituents are incorporated at the 1,7-positions to form **167** a well-defined coordination pocket is formed which can be used to carry out a ratiometric sensing of Hg^{2+} in the NIR region.[283] The absorption band maximum can be red-shifted by 92 nm into the red region by replacing the phenyl rings at the 1,3,5,7-positions of **162** with thiophenes to form **170**. There are two possible explanations for this. Firstly, the introduction of electron-rich thiophenes has a similar effect to that of an electron-donating substituent leading to a relative destabilization of the HOMO due primarily to the larger MO coefficients at the 3,5-positions (Fig. 3). Secondly, there are smaller torsion angles between the thienyl rings and the BODIPY core than is the case with phenyl rings.[284,285] A greater red-shift is observed for the 3,5-thiophene substituted aza-BODIPY structure of **168 (**68 nm**)** relative to **162**, than for the 1,7-thiophene substituted structure of **169 (**33 nm**)**. The molar extinction

coefficients observed for **168-170** differ markedly based on the substitution pattern (120 500 $mol^{-1}.cm^{-1}$ for **168**, 110 000 $mol^{-1}.cm^{-1}$ for **169**, and 78 000 $mol^{-1}.cm^{-1}$ for **170**). The absorption and emission spectra of these compounds are not sensitive to solvent polarity, which suggests that they could be used in biotechnology applications.[284,285] Thiophene-substitution at the 2,6-positions to form **171** results in a broadened and hypsochromic absorption band at 650 nm with a relatively low ε_{max} value. This value is the same as for **162** and indicates that the thiophene moieties at the 2,6-positions do not have any influence on the wavelengths of the main absorption bands of **171**. DFT geometry optimizations predict a propeller-like structure of the peripheral (het)aryl-rings in **171** with dihedral angles of between 56–60°. In contrast, the thiophene moieties of compounds **168-170** have smaller dihedral angles of between 14–19° and the phenyl rings of **168** and **169** result in angles of between 28–36°. This confirms the diminished influence of thiophene substituents when they are introduced at the 2.6-positions due to steric hindrance.[284]

5.8.2 Conformationally restricted systems

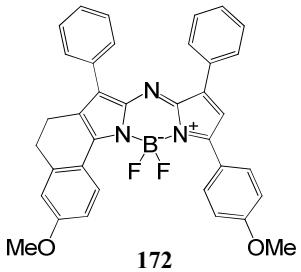

172
$CHCl_3$ Φ 0.38
λ_{abs} 708 nm λ_{em} 732 nm
ε = 96 200 $M^{-1}cm^{-1}$

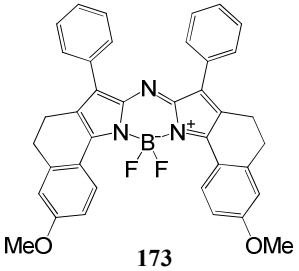

173
$CHCl_3$ Φ 0.28
λ_{abs} 740 nm λ_{em} 752 nm
ε = 159 000 $M^{-1}cm^{-1}$

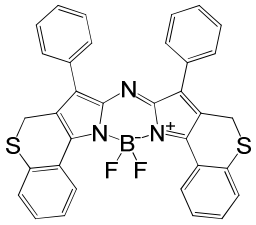

174
$CHCl_3$ Φ 0.11
λ_{abs} 706 nm λ_{em} 730 nm
ε = 115 000 $M^{-1}cm^{-1}$

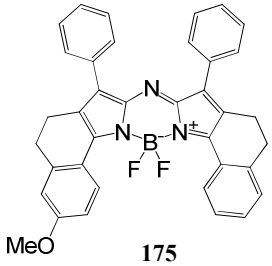

175
$CHCl_3$ Φ 0.32
λ_{abs} 723 nm λ_{em} 734 nm
ε = 157 000 $M^{-1}cm^{-1}$

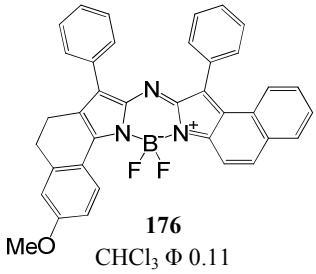

176
$CHCl_3$ Φ 0.11
λ_{abs} 715 nm λ_{em} 730 nm
ε = 141 000 $M^{-1}cm^{-1}$

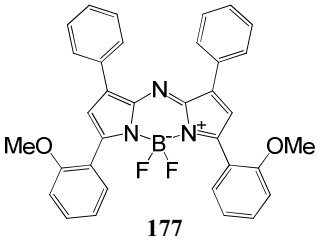

177
Toluene Φ 0.07
λ_{abs} 640 nm λ_{em} 688 nm
ε = 73850 $M^{-1}cm^{-1}$

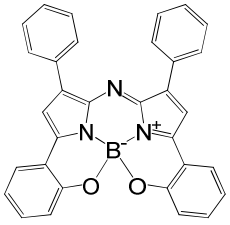

178
Toluene Φ 0.51
λ_{abs} 728 nm λ_{em} 746 nm

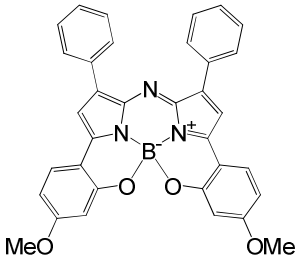

179
$CHCl_3$ Φ 0.18
λ_{abs} 765 nm λ_{em} 782 nm

Conformationally restricted aza-BODIPY dyes have markedly red-shifted absorption bands with high molar extinction coefficients. When the free rotation of aryl substituents is restricted at both the 3- and 5-positions by forming **173** a very high ε value of 159 000 $mol^{-1}.cm^{-1}$ is obtained for the main absorption band. The band lies at 740 nm, a red-shift of 52 nm, relative to the spectrum of **163**. **173** possesses a moderate Φ_F value in the NIR region, making it potentially suitable for a wide range of applications. In the structure of **172**, only one side is restricted. The spectral bands lie at shorter wavelength than those of **173** and there are much lower molar extinction coefficients, since the phenyl ring is no longer forced into a co-planar conformation with the BODIPY core. The heterocyclic restricted structure of **174** results in a lower fluorescence quantum yield due to ISC to the triplet manifold resulting from the heavy atom effect associated with the sulfur atoms. The non-symmetric structure of **175** results in a slightly higher Φ_F value relative to **173**. The absorption band lies at shorter wavelength because of the absence of one of the electron donating methoxy substituents. BODIPY **176** also has a lower Φ_F value. This is consistent with the trends observed for the BODIPYs in the previous section, since the oxidation of a carbocyclic restricted ring system increases the conformational flexibility of the molecule.[286,287]

The structure of **178** contains B–O bonds which link the central boron atom to the *ortho*-positions of phenyl rings substituted at the 3,5-positions.[289] The absorption and emission maxima are red shifted by 88 and 58 nm and there is a 7-fold increase in the quantum yield relative to the unconstrained structure of **177**.[288] A further red-shift of 37 nm is observed upon the introduction of electron-donating methoxy substituents to form **179**. The significant red-shift observed in the spectral bands of the conformationally restricted molecules can be ascribed to the enhanced coplanarity between the π-systems of the BODIPY core and the aryl groups at the 3,5-positions.[289]

5.8.3 β-aromatic-fused and α-substituted aza-BODIPYs

There is a marked red-shift of the absorption and emission bands of benzo-fused aza-BODIPYs **180-183** relative to the spectra of the analogous 1,3,5,7-tetraaryl aza-BODIPYs. For example, fused-ring-

expansion with benzene rings to form **180** results in a 62 nm red-shift of the absorption band compared to that of **162**.[196,197] In DFT calculations (Fig. 6), there is a narrowing of the HOMO–LUMO gap of **180** relative to **162** due to as the destabilization of the HOMO is greater than that of the LUMO because of the relative large MO coefficient of the HOMO on the benzo fragment.

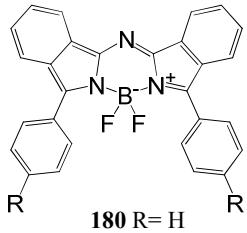

180 R= H
CH_2Cl_2 Φ 0.14
λ_{abs} 712 nm λ_{em} 736 nm
ε = 95 000 $M^{-1}cm^{-1}$
181 R= F
CH_2Cl_2 Φ 0.16
λ_{abs} 713 nm λ_{em} 724 nm
ε =63 000 $M^{-1}cm^{-1}$
182 R= $N(CH_3)_2$
CH_2Cl_2 Φ 0.01
λ_{abs} 794 nm λ_{em} 830 nm
ε =174 000 $M^{-1}cm^{-1}$

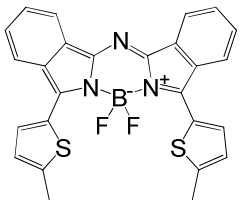

183
CH_2Cl_2 Φ N.A
λ_{abs} 793 nm λ_{em} 841 nm
ε = 95 000 $M^{-1}cm^{-1}$

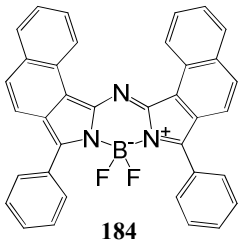

184
CH_2Cl_2 Φ 0.14
λ_{abs} 737 nm λ_{em} 753 nm
ε =71 000 $M^{-1}cm^{-1}$

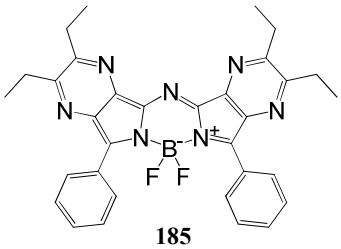

185
THF Φ N.A
λ_{abs} 685 nm λ_{em} 721 nm

In a similar manner to that described earlier for **21** and **30**, **31** and **32**, **52** and **61**, **105** and **106**, and **162**, **168** and **170**, substitution with thiophene rings to form **183**,or the incorporation of electron-donating groups at the *para*-position of phenyl rings at the 3,5-positions to form **182**, results in a marked red-shift of the main spectral bands to longer wavelength, with significant emission intensity observed in the NIR region.[198] There is a large relative destabilization of the HOMO of **183** (Fig. 6), due to a strong mesomeric interaction between the thiophene substituents and the core BODIPY chromophore. Although smaller extinction coefficients have been reported when electron-withdrawing fluorine atoms are added at the *para*-positions to form **181**, the absorption and emission band maxima and the Φ_F value remain almost unchanged.[196] When dimethylamino substituents are introduced at the *para*-position of the phenyl rings of **182**, the Φ_F value exhibits a marked solvent dependence with values of 0.10 and 0.01 in hexane and acetonitrile, respectively, and there is a significant red-shift of the main spectral bands. The fluorescence quenching in polar solvents can be attributed to the formation of a low-lying charge-separated S_1 state resulting in efficient nonradiative

relaxation through conical intersections formed between the potential-energy surfaces of the ground and excited states. BODIPY **182** can be used as a ratiometric 'turn-on' NIR fluorescent sensor for changes in pH.[186] The incorporation of 1,2-naphtho-fused rings to form **184** results in a 25 nm red-shift of the absorption band relative to that of **180**, along with a small change in the other spectroscopic properties.[186] The pyrazine-fused aza-BODIPY **185** has an intense absorption band at 685 nm, which lies 24 nm to the blue of that of **180**. The blue-shift is probably due to the higher electronegativity of the pyrazine nitrogen atoms, which causes an increase in the HOMO–LUMO band gap (Fig. 18). **185** may find applications as a colorimetric and fluorometric sensor for the NH_4^+ ion.[290]

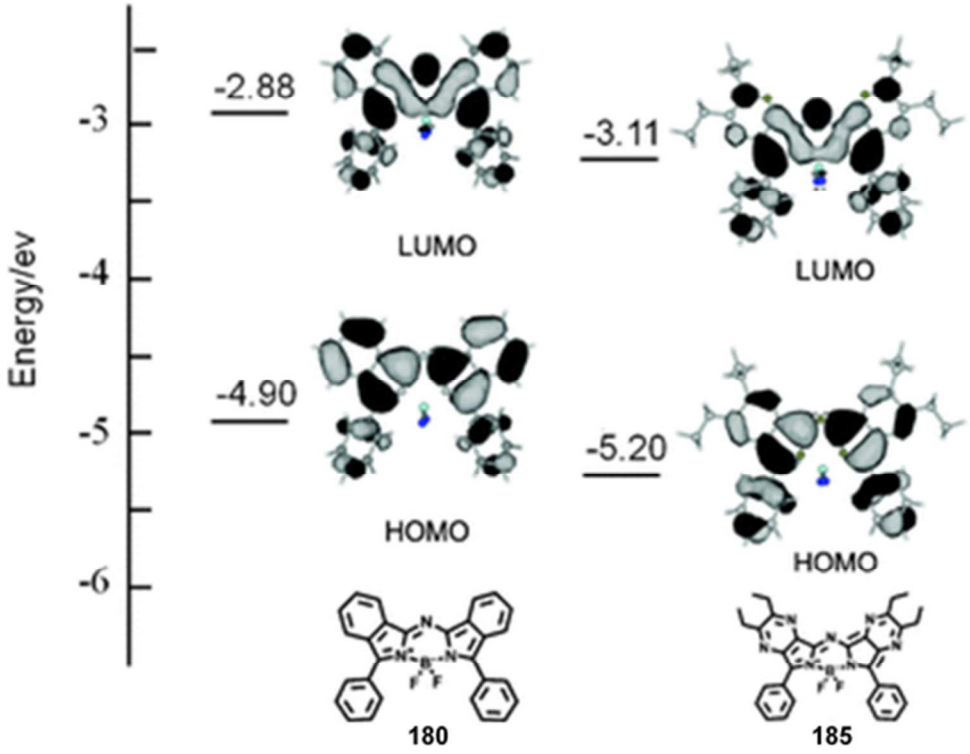

Fig. 18 Energy-level diagram for the frontier π-MOs of **180** and **185**. The nodal patterns of each MO are shown at an isosurface value of 0.02 a.u. (Reprinted with permission from ref. 290. Copyright © 2011 Royal Society of Chemistry.)

5.9 *Bis*-BODIPYs

Red shifts of the absorption bands can also be obtained by forming BODIPY dimer. The properties of directly linked dimers and coplanar fused dimers will be examined in depth.

5.9.1 Directly linked bis-BODIPYs

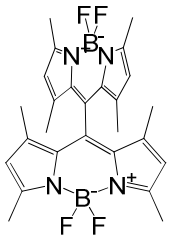

186
$CHCl_3$ Φ 0.31
λ_{abs} 515 nm λ_{em} 588 nm

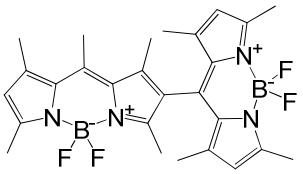

187
$CHCl_3$ Φ 0.03
λ_{abs} 516 nm λ_{em} 527 nm

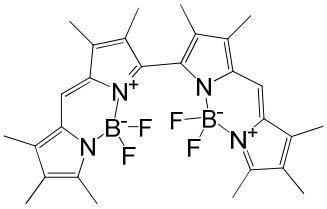

188
CH_2Cl_2 Φ 0.70
λ_{abs} 489 562 nm λ_{em} 650 nm
ε = 64 400 $M^{-1}cm^{-1}$ (489)
73 600 $M^{-1}cm^{-1}$(562)

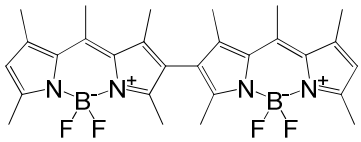

189
CH_2Cl_2 Φ 0.66
λ_{abs} 526 nm λ_{em} 563 nm
ε = 150 000 $M^{-1}cm^{-1}$

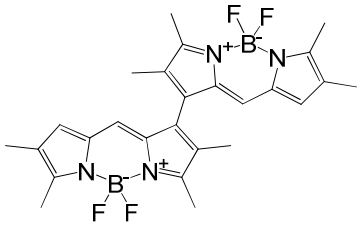

190
CH_2Cl_2 Φ 0.05
λ_{abs} 557 nm λ_{em} 598 nm
ε = 80 000 $M^{-1}cm^{-1}$

Slight red-shifts of the main spectral band wavelengths are usually observed for directly linked *bis*-BODIPYs **186-190** relative to the corresponding monomers. For example, there is almost no red shift of the absorption maxima of the *meso-meso* and *meso*-β linked dyes **186** and **187** relative to the corresponding tetramethyl-BODIPY, but a large Stokes shift is observed for the *meso-meso* linked dye **186**. **186** and **187** are potentially useful for photodynamic therapy applications due to the interactions between the two BODIPY chromophores in the excited state.[291-293] The absorption spectrum of the α-α linked dye **188** is characterized by two major bands at 489 and 562 nm, which is consistent with an exciton splitting effect. The fluorescence emission spectrum of **188** contains a broad emission band at 650 nm with a Stokes shift of 88 nm with respect to the lowest-energy absorption band.[294-296] The β-β linked BODIPY **189** has a typical cyanine-type absorption spectrum. Although there is an increase in

the width of the main spectral band relative to the corresponding monomer, the molar extinction coefficient of ca. 150 000 M is three times greater than that of the monomer.[297-300] The absorption and emission profiles of the 1,1'-linked dimer **190** resemble those of the monomer with a set of vibronic bands at higher and lower energies. This demonstrates that there is minimal ground-state interaction or excitonic coupling between the two chromophores. The fluorescence quantum yield of **190** is significantly lower, however, and exhibits a strong dependence on solvent polarity with Φ_F values ranging from 0.67 in toluene to 0.05 in dichloromethane and 0.00 in DMSO. This is consistent with the formation of a nonemissive S_1 state with strong charge-transfer character. The possibility that dimer **190** can undergo symmetry-breaking internal charge transfer has been confirmed by cyclic voltammetry.[121]

5.9.2 Aromatic-fused bis-BODIPYs and analogues

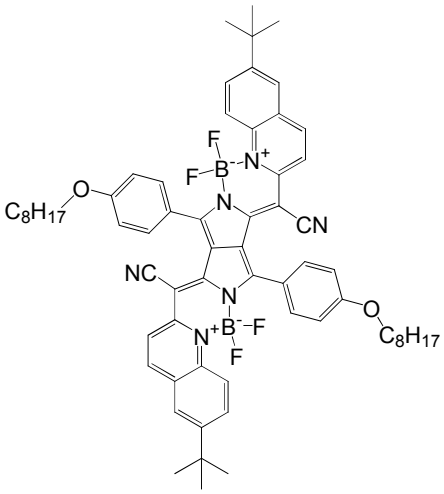

191
$CHCl_3$ Φ 0.59
λ_{abs} 754 nm λ_{em} 773 nm
ε = 205 000 $M^{-1}cm^{-1}$

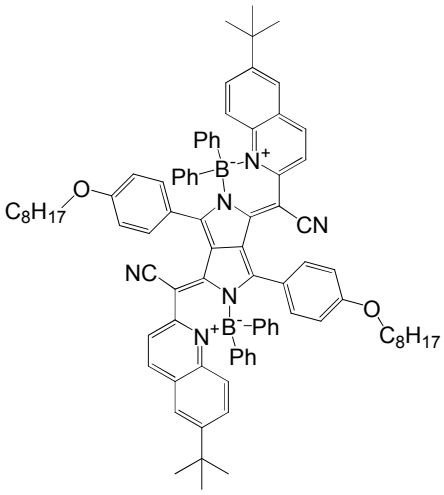

192
$CHCl_3$ Φ 0.53
λ_{abs} 819 nm λ_{em} 831 nm
ε = 256 000 $M^{-1}cm^{-1}$

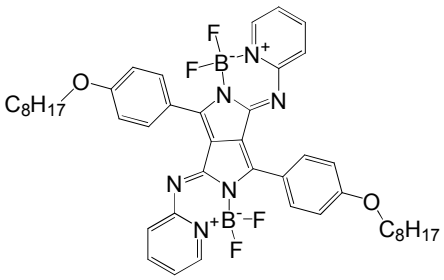

193
$CHCl_3$ Φ 0.87
λ_{abs} 638 nm λ_{em} 661 nm
ε = 78 000 $M^{-1}cm^{-1}$

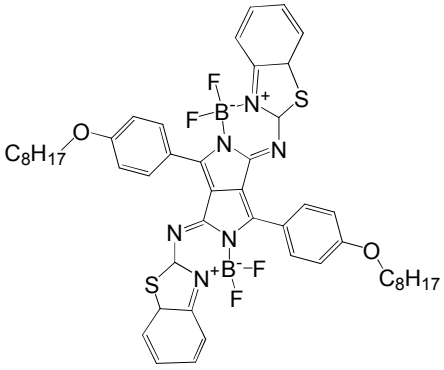

194
$CHCl_3$ Φ 0.81
λ_{abs} 655 nm λ_{em} 676 nm
ε = 110 000 $M^{-1}cm^{-1}$

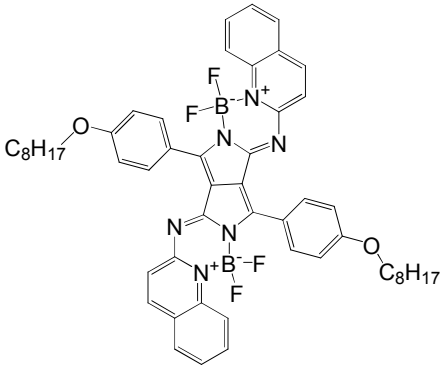

195
$CHCl_3$ Φ 0.83
λ_{abs} 671 nm λ_{em} 692 nm
ε = 100 000 $M^{-1}cm^{-1}$

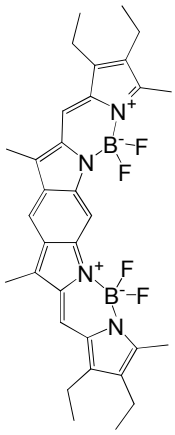

196
$CHCl_3$ Φ 0.72
λ_{abs} 692 nm λ_{em} 703 nm
ε = 232 000 $M^{-1}cm^{-1}$

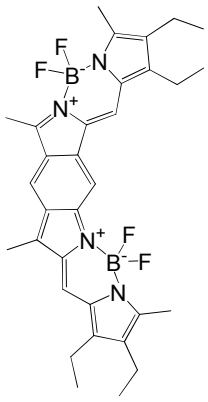

197
$CHCl_3$ Φ 0.32
λ_{abs} 758 nm λ_{em} 774 nm
ε = 190 000 $M^{-1}cm^{-1}$

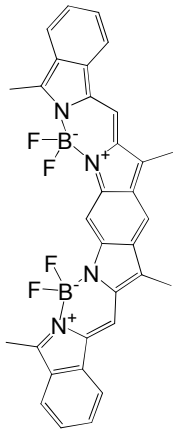

198
$CHCl_3$ Φ 0.36
λ_{abs} 775 nm λ_{em} 781 nm
ε = 141 000 $M^{-1}cm^{-1}$

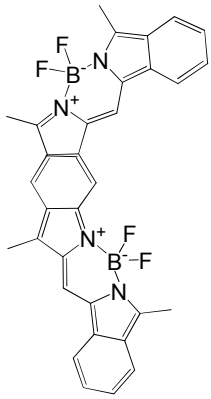

199
$CHCl_3$ Φ 0.04
λ_{abs} 848 nm λ_{em} 868 nm
ε = 204 000 $M^{-1}cm^{-1}$

Typically, π-fused *bis*-BODIPYs exhibit narrow and intense absorption and emission bands in the red/NIR region with high molar absorption coefficients (> 100 000 $M^{-1}.cm^{-1}$) and moderate Φ_F values (> 0.3). This makes these dyes promising candidates for applications in the NIR region. *Bis*-BODIPY **191** contains a pyrrolopyrrole (PPCy) moiety and provides a good example of the effects of forming a more rigid chromophore. There is a narrowing of the vibronic bands ($\Delta\nu \approx 500$ cm^{-1}) and an increase in the ε_{00} values, since there is a shift of the Franck-Condon factors in favor of the main electronic transition. The large bathochromic shift observed on moving from **191** to **192** is probably related to the differing σ-inductive effects of the BF_2 and BPh_2 moieties. The ε_{max} value of **192**, the BPh_2 complex is higher, since there is a decrease in width of the main spectral bands and an increase in the strength of the main electronic 0-0 band. Although the Φ_F value decreases slightly as the polarity of the solvent increases, it remains remarkably high in DMSO. Therefore, PPCy derivatives are likely to form excellent NIR fluorophores in aqueous environments, once appropriate substituents are introduced.[301,302] PPCy dyes can be synthesized through the condensation reaction of diketopyrrolopyrrole with different aromatic acetonitrile groups. They have potentially useful spectroscopic properties such as very intense and narrow absorption bands and strong emission in the NIR region (with absorption bands ranging from 684 to 864 nm), high photostability, and low chemical reactivity.[301-306]

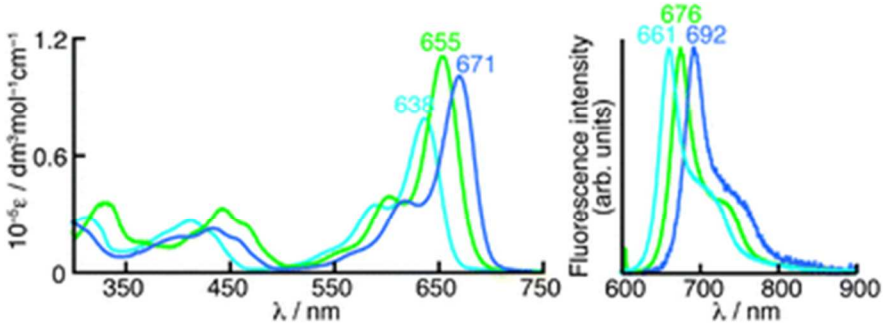

Fig. 19 UV-visible absorption (left) and fluorescence (right) spectra of **193** (light blue), **194** (green), and **195** (blue) in $CHCl_3$. (Reprinted with permission from ref. 307. Copyright © 2013 Royal Society of Chemistry.)

Pyrrolopyrrole *bis*-aza-BODIPYs **193-195** have high Φ_F values (> 0.8) and intense absorption bands with maxima ranging in descending energy from that of **193** (638 nm) to **194** (655 nm) and then to **195**

(671 nm) due to changes in the fused-ring moieties.[307] The fluorescence emission spectra are red-shifted in the same order from 661 nm for **193** to 692 nm for **195** (Fig. 19). The absorption maximum of the C_{2v} symmetry benzene-fused *bis*-BODIPY syn-**196** lies at 692 nm, while the absorption maximum of the C_{2h} symmetry anti-**197** isomer lies at 758 nm. These *bis*-BODIPYs emit strongly at 703 and 774 nm, respectively.[308] When benzoBODIPY chromophores are fused with a shared bridging benzene, the absorption and emission maxima of the C_{2v} and C_{2h} isomers **198** and **199** lie in

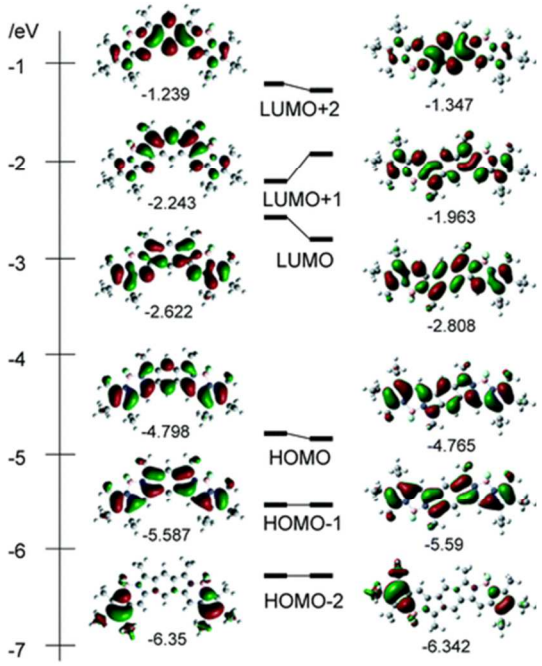

Fig. 20 The calculated frontier π-MOs of syn-**196** (left) and anti-**197** (right). (Reprinted with permission from ref. 308. Copyright © 2012 Royal Society of Chemistry.)

the NIR region. The absorption and emission bands of **199** at 848 nm and 868 nm are more highly red-shifted than those of **198** at 775 nm and 781 nm. However, the benzene-fused *bis*-benzoBODIPYs are labile in aerobic conditions and readily decompose when dissolved in solution.[308] The difference between the syn and anti isomers can be explained using the results of TD-DFT calculations.[308] The energies of the HOMOs are similar, but the LUMO energy of the anti isomer is lower than that of the syn isomer, leading to a much smaller HOMO–LUMO gap (Fig. 20). The extra stabilization of the LUMO of the anti isomer results from the delocalization of the LUMO through the benzo bridge, since there are significant MO coefficients on the middle set of carbons of the benzo bridge. In contrast,

there is a nodal plane through these atoms in the context of the syn isomer, which means there is no interaction between the two BODIPY moieties.[308]

5.10 BODIPY analogues

Although BODIPY dyes are potentially useful in a wide variety of different applications, the solid-state emission properties of most BODIPY derivatives have been found to be relatively poor with low Φ_F values being reported. Recently, borate complexes with N–B–O, N–B–N and N–B–C coordinate patterns have been developed by using the boron atom as a structuring template for forming rigid and near-planar cyanine structures.[309-330, 376-377] Although these compounds usually display large Stokes shifts and significant solid-state emission, only a few of these molecular systems have absorption and emission bands in the red/NIR region. In this section, a typical set of these BODIPY analogues have been selected to explore the strategies that can be used to shift the absorption and emission bands to longer wavelengths. Low symmetry BODIPY analogues provide a way to make the potential energy surfaces of the ground and excited states more distinct energetically, leading to large Stokes shifts relative to BODIPY dyes. The growing diversity of such analogues is sure to further enrich BODIPY chemistry in the years ahead.

5.10.1 N–B–O analogues

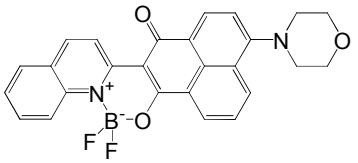

200
CH_2Cl_2 Φ 0.50
λ_{abs} 427 nm λ_{em} 588 nm
ε =16 600 $M^{-1}cm^{-1}$

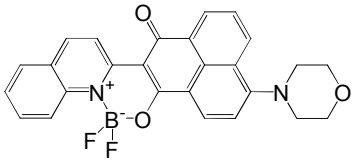

201
CH_2Cl_2 Φ 0.53
λ_{abs} 468 nm λ_{em} 544 nm
ε =14 500 $M^{-1}cm^{-1}$

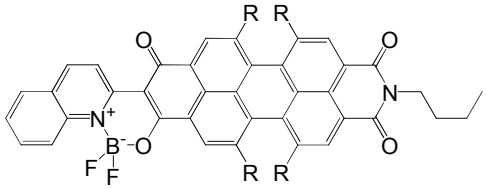

202 R= *p*-tert-butylphenol
CH_2Cl_2 Φ 0.50
λ_{abs} 616 nm λ_{em} 655 nm

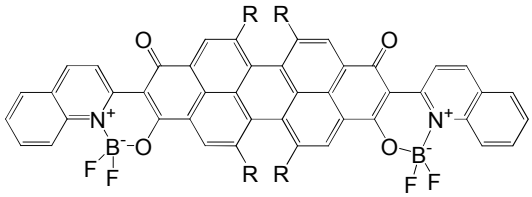

203 R= *p*-tert-butylphenol
CH_2Cl_2 Φ 0.35
λ_{abs} 650 nm λ_{em} 689 nm

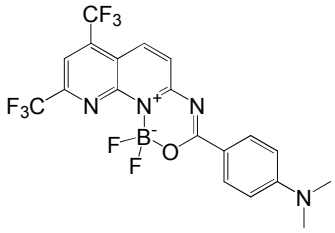

204
CH_2Cl_2 Φ < 0.01
λ_{abs} 480 nm λ_{em} 642 nm
ε =41 000 $M^{-1}cm^{-1}$

Large Stokes shifts are observed for N–B–O dye **200** and the emission spectra are strongly solvent dependent. The emission maxima vary from 620 nm in acetonitrile to 564 nm in methanol.[331] In contrast with **200**, the emission maxima of **201** differ only slightly as the solvent polarity is increased and exhibit smaller Stokes shifts. DFT calculations have confirmed that there is less charge transfer character between the electron-donating phenalene moiety and the main π-conjugation system in the S_1 state of **201** (Fig. 21). Both dyes exhibit strong fluorescence with a narrow emission band and a large Stokes shift, due to there being weak π-π packing interactions in the solid-state.[331] The absorption maxima of **202** and **203** lie at 616 and 650 nm, respectively, and the main emission band is red-shifted by 45 nm on moving from **202** to **203**.[332] The red-shift can be attributed to the expansion of the π-conjugation system due to the coordination of an additional boron atom. The dyes have strong electron withdrawing properties and are promising candidates for use as n-type organic semiconductors. The BODIPY analogue **204** exhibits an emission band at 642 nm with a relatively low Φ_F value due to the strong charge transfer character associated with the $S_0 \rightarrow S_1$ transition. There are large solvatochromic shifts due to the push-pull structure.[333]

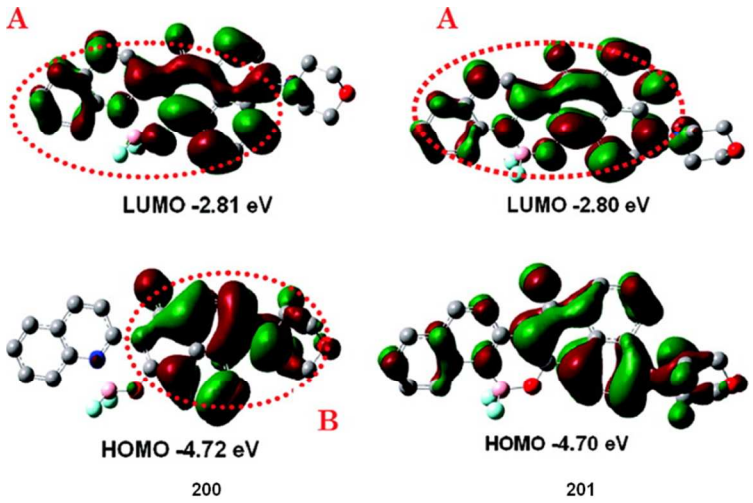

Fig. 21 The HOMO and LUMOs of **200** and **201**. The electron density in the LUMOs is mainly distributed over part A. For **200**, the electron density in the HOMO is localized on part B. A more effective ICT excited-state is suggested in **200**, which is consistent with the results of the spectral studies. (Reprinted with permission from ref. 331. Copyright © 2008 American Chemical Society.)

5.10.2 N–B–N analogues

Broad absorption and fluorescence bands are observed in the spectra of **205** with large Stokes shifts observed both in solution and in the solid state. There is a low-lying LUMO, which makes this compound suitable for use as electron-transport materials in electroluminescent devices.[334] Broad envelopes of intense bands are observed in the UV regions of the absorption spectra of boron-pyridyl-imino-isoindoline BODIPY analogues **206-209** (Fig. 22).[335] The spectra are, therefore more similar to those of pyrene derivatives than to those of BODIPY dyes. In CH_2Cl_2, **206** has a major absorption peak at 361 nm with a shoulder at 379 nm and display a blue shift of 34 nm compared to that of boron-pyridyl-isoindoline analogues **205**. DFT calculations predict an increase of the HOMO–LUMO gap of

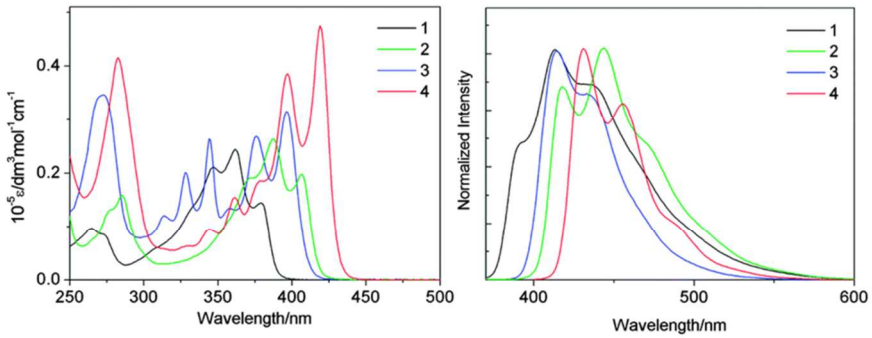

Fig. 22 The absorption and emission spectra of **206-209** in CH_2Cl_2. (Reprinted with permission from ref. 335. Copyright © 2014 Royal Society of Chemistry.)

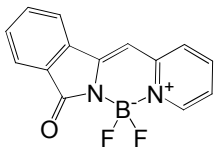

205
CH_2Cl_2 Φ 0.47
λ_{abs} 395 415(sh) nm
λ_{em} 454 nm

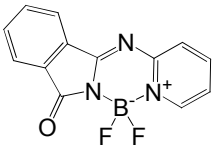

206
CH_2Cl_2 Φ 0.33
λ_{abs} 361 379(sh) nm
λ_{em} 391(sh) 413 nm
ε = 24 400 $M^{-1}cm^{-1}$

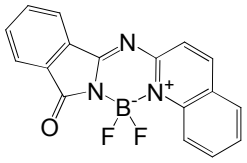

207
CH_2Cl_2 Φ 0.74
λ_{abs} 387 406(sh) nm
λ_{em} 417 (sh) 444 nm
ε = 26 700 $M^{-1}cm^{-1}$

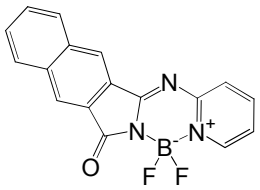

208
CH_2Cl_2 Φ 0.86
λ_{abs} 396 nm λ_{em} 414 nm
ε = 31 700 $M^{-1}cm^{-1}$

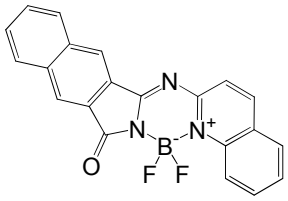

209
CH_2Cl_2 Φ 0.93
λ_{abs} 419 nm λ_{em} 430 nm
ε = 47 500 $M^{-1}cm^{-1}$

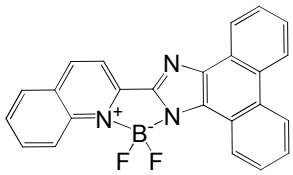

210
CH_2Cl_2 Φ 0.90
λ_{abs} 476 nm λ_{em} 585 nm
ε = 36 300 $M^{-1}cm^{-1}$

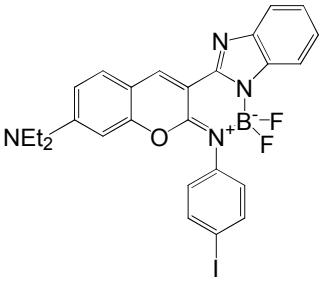

211
CH_2Cl_2 Φ 0.81
λ_{abs} 496 nm λ_{em} 545 nm
ε = 47 000 $M^{-1}cm^{-1}$

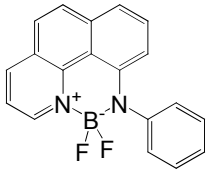

212
CH_2Cl_2 Φ 0.60
λ_{abs} 465 nm λ_{em} 584 nm
ε = 9 114 $M^{-1}cm^{-1}$

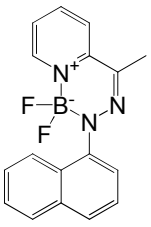

213
CH_2Cl_2 Φ 0.07
λ_{abs} 432 nm λ_{em} 538 nm

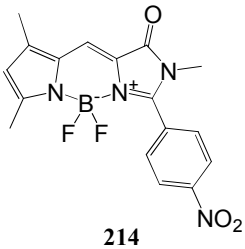

214
Hexane Φ 0.53
λ_{abs} 498 nm λ_{em} 587 nm

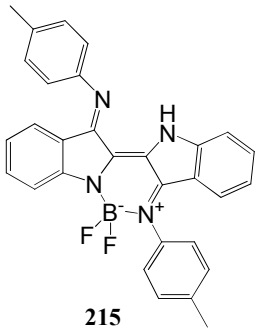

215
CH_2Cl_2 Φ N.A
λ_{abs} 649 nm λ_{em} 756 nm
ε = 29 900 $M^{-1}cm^{-1}$

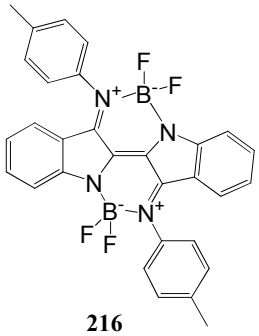

216
CH_2Cl_2 Φ N.A
λ_{abs} 743 nm λ_{em} 808 nm
ε = 34 200 $M^{-1}cm^{-1}$

206 relative to **205** due to a stabilization of the HOMO. This can be readily explained based on the large MO coefficient on the aza-nitrogen and the presence of a nodal plane at this position in the HOMO (Fig. 23). Fused-ring-expansion with benzene rings on the pyridyl (**207**) and indoline (**208**) moieties results in 26 nm and 35 nm red shifts of the main absorption bands relative to that of **206**. Upon further fused-ring-expansion to form **209**, which has fused benzene rings on both the pyridyl and

indoline moieties, there is a 58 nm red shift to 419 nm. The extinction coefficient increases from 24400 M^{-1} cm^{-1} for **206** to a maximum of 47 500 M^{-1} cm^{-1} for **209**, due to the extension of π-conjugation system. **206-209** display strong emission with fluorescence quantum yields of 0.33 (**206**), 0.74 (**207**), 0.86 (**208**) and 0.90 (**209**). Importantly, intense solid-state fluorescence is observed, with quantum yields of 0.22, 0.09, 0.10, and 0.12 for **206-209**, respectively. This suggests that the asymmetrical structures significantly enhance the solid-state emission properties.[335]

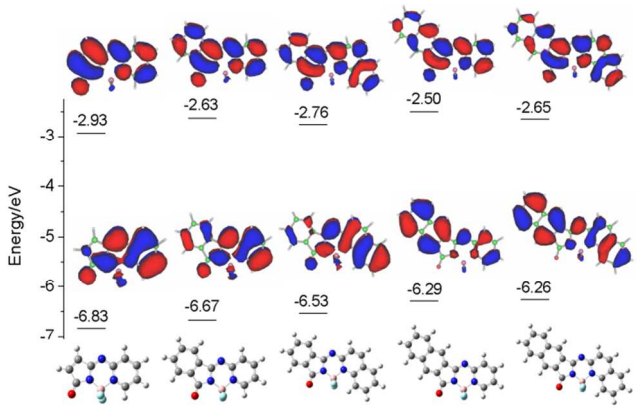

Fig. 23 The energy level diagram from left to right for the frontier π-MOs of a boron-pyridyl-imino-pyrrole model compound and **206-209** using the B3LYP functional with 6-31G(d) basis sets. The angular nodal patterns are shown at an isosurface value of 0.02 a.u. (Reprinted with permission from ref. 335. Copyright © 2014 Royal Society of Chemistry.)

210, a phenanthro[9,10-*d*]imidazole-quinoline substituted dye, has a large Stokes shift of 109 nm in CH_2Cl_2 and red fluorescence is observed in the solid state.[336] The optical properties for dye **211** are affected only slightly by the solvent polarity and there is a relatively small Stokes shifts. This is consistent with the presence of a conventional S_0–S_1 transition with no significant charge transfer character.[337] In contrast, large Stokes shifts of over 110 nm are observed for **212** and **213** due to aggregation-induced emission.[338,339] **212** and its derivatives exhibit exceptional photostability and are competitively membrane-specific.[338] Dye **214** is synthesized by coordinating boron to the green fluorescent protein (GFP) and is usually referred to as GFP-chromophore. The compounds are neutral, uncharged, and highly fluorescent and can be readily sulfonated and modified to include a point of attachment for biomolecules.[340] The mono-BF_2 compound **215** has an intense absorption band at 649 nm. The incorporation of a second BF_2 moiety to form **216** results in a further red-shift of the

absorption maximum to 743 nm. **216** is unstable and gradually decomposes to the mono-BF_2 structure of **215**. Both **215** and **216** exhibit weak emission in the NIR region. No Φ_F values have been reported.[341]

6 Conclusions and perspectives

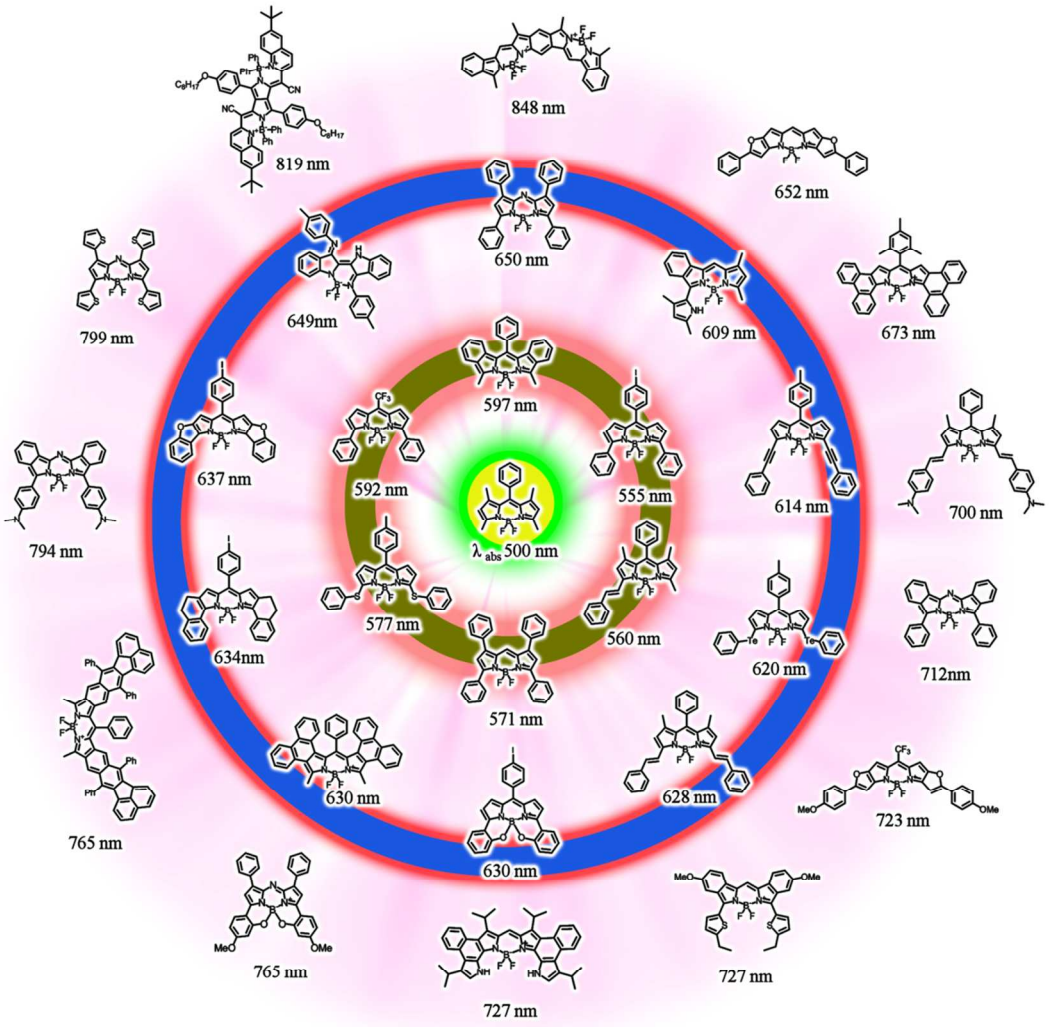

Fig 24. Selected structurally-modified BODIPYs that absorb at different wavelength ranges from 500 to 850 nm.

Various structural modification strategies (Fig. 24) can be used to shift the wavelengths of the main BODIPY bands into the red/NIR region. When tetramethyl-BODIPY **51** is used as a reference point for the parent dipyrrin chromophore, the following trends are observed:

- **aryl substitution**: a red shift of ca. 55 nm for phenyl groups at the 3,5-positions (**21**) and 38 nm at 1,7-positions (**33**).

- **ethynylphenyl substitution**: a red shift of ca. 114 nm for ethynylphenyl groups at the 3,5-positions (**46**) and 70 nm at the 1,7-positions (**41**).
- **styryl substitution**: a red shift of 129 nm for styryl substituents at the 3,5 positions (**62**) and 72 nm for substitution at the 1,7-positions (**66**), there is a further red-shift of 44 nm when there are styryl substituents at 1,3,5,7-positions (**77** to **79**).
- **heteroatoms**: the presence of heteroatoms at the 3,5-positions such as Se (**99**), Te (**100**), result in red-shifts of 86 and 120 nm, respectively.
- **aza-BODIPYs with aryl substituents**: a red shift of ca. 80 nm when the *meso*-carbon is replaced by a nitrogen atom (**35** to **162**, **145** to **180**).
- **Aromatic ring fusion**: phenyl ring fusion at the β-position (**130**) leads to a red-shift of 97 nm, this strategy enables the extension of the π-conjugation system of the indacene plane along with the attachment of functional groups at 3,5-position, such styryls or ethnylphenyl. This strategy has the potential to yield intense NIR region chromophores while maintaining the ability to incorporate all of the other functionalization possibilities. Phenanthro-fused BODIPYs (**134**) absorb and emit in the red region with intense and narrow emission bands (Φ_F = 1.0 is sometimes achieved) while retaining the possibility of further modification at the 3,5-positions. Taking into account the trends observed for 3,5-dimethylaminostyryl substituents, it appears that it may be possible to synthesize BODIPY dyes that absorb beyond 850 nm.
- **Rigidization**: a red-shift of 52–94 nm upon rigidization of two 3,5-phenyl groups (**21** to **102**, **123** to **124**, **127** to **128**, **153** to **154**, **163** to **173**, **177** to **178**), which can be viewed as involving the fusion of two dihydronaphthalene groups to the BODIPY core. This leads to an increase in the Φ_F value. Rigidization of two 3,5-styryl groups with oxygen and sulfur atom bridge linkers (**62** to **115, 71** to **122**), results in red-shifts of 23 nm and 27 nm,

respectively, and leads to other beneficial spectroscopic properties such as high extinction coefficients and Φ_F values.

- **Electron-donating *para*-position substituents**: a red-shift of 28–41 and 70–127 nm after the introduction of electron donating methoxy and dimethylamino groups, at the *para*-position of the 3,5-diphenyl rings (**39** to **40**, **62** to **63**, **162** to **163** to **164**).
- **Combinations of the above**: for example, the incorporation of a dimethylamino group at the *para*-positions of the 3,5-diaryl rings of a benzo-fused aza-BODIPY **182** results in a markedly red-shifted absorption band, which lies at 794 nm.
- **Positions where substituents are introduced**: Modification at the 3,5-positions results in greater red-shifts of the absorption and emission maxima than those observed when substituents are introduced at the 2,6- and 1,7-positions. The Stokes shifts observed for BODIPYs with substituents at the 2,6-positions are usually larger than those for dyes with substituents at the 1,7- or 3,5-positions, since there is more flexibility in the molecular geometry upon photoexcitation.
- **Five-membered heterocyclic substituents**: thiophenes and pyrroles play a similar role to electron-donating phenyl substituents in causing a red shift ca. 80 nm (**21** to **30**, **31** to **32**, **162** to **168** to **170**, **180** to **183**). These results can be ascribed to the smaller torsion angles and their stronger electron donating properties.

Other strategies, which have also proven to have a beneficial effect on the spectroscopic properties, can be summarized as follows:

- Inhibiting the rotation of *meso*-substituents increases the Φ_F value. For example, methyl substituents at the 1,7-positions result in an increase in the Φ_F value from 0.38 (**102**) to 0.72 (**103**). Another good example is provided by the increase of the Φ_F value from 0.41 (**124**) to 0.72 (**126**) when the protons at the *ortho*-positions of the *meso* aryl substituents are replaced with methyl groups.

- Although modifications at the *meso*-position often have only a minor influence on the absorption and emission maxima, the incorporation of a strongly electron-withdrawing *meso*-CF_3-substituent group results in a bathochromic shift of ca. 40 nm in the spectral bands relative to *meso*-aryl-BODIPYs (**21** to **31**, **30** to **32**, **116** to **117**).

The versatility of the structural modifications that can be made to the BODIPY core has led to the preparation of a wide range of BODIPYs, with spectral bands in the 650–850 nm 'biological window". Despite the considerable progress that has been made in the synthesis of NIR region BODIPY derivatives, theoretical calculations have not fully been utilized to the extent they could have been during the analysis of the structure-property relationships.[41,71,342-345] For example, very few calculations have been carried out to address why substituents have markedly differing effects depending on substitution position, despite the likelihood that an MO theory approach would provide new insights in this regard. The considerable progress has been made in this regard in porphyrinoid chemistry in recent years suggests that this approach would greatly facilitate the rational design of red/NIR absorbing BODIPY dyes for applications.[346-350] This review has attempted to address this issue.

To effectively use NIR region BODIPY dyes for labeling during biological analyses, or as biomarkers in biomedical applications such as imaging diagnosis, hydrophilic character is usually required. The range of synthetic methodologies that are available for the preparation of water-soluble dyes is limited, however. This represents a bottleneck that impedes further progress in biomedical analysis. To date, although a few water-soluble BODIPY derivatives have been prepared by introducing oligo-(ethyleneglycol) chains,[351-355] nucleotides,[356] sulfonated peptides,[357-359] carboxylates,[360-367] sulfonates,[363-370] phosphonate[371] or betaine moieties,[372] there has been only limited progress where the preparation of π-extended dyes emitting in the 650–850 nm window is concerned. In most cases, solubility is achieved by linking a polar group such as a negatively charged sulfonate to the dye. The negative charge is potentially problematic, however, since it may hinder the binding of negatively charged bioanalytes.[31,373]

In addition to the hydrophobicity problem, aggregation in aqueous solution is another major drawback faced with NIR region BODIPY dyes, since it results in a quenching of the fluorescence intensity. Recently, Ziessel and co-workers reported a promising structural modification strategy in this regard.[374] A bulky polar substituent can be introduced at the boron center, in a manner that hinders aggregation in aqueous media, thereby leading to bright fluorophores with moderate fluorescence quantum yields. Although there is a significant demand in biotechnology fields for water-soluble NIR region dyes, suitable NIR emitting BODIPY that could meet this demand have yet to emerge.

For most NIR region BODIPY dyes, the absorption and emission bands overlap significantly, leading to an interaction between the excitation beam and the emission signal. Fluorescence resonance energy transfer cassettes, which can separate the emission and excitation bands more effectively, could prove useful for applications, especially water-soluble multiplex cassettes.[22] Alternatively, upconversion luminescence is a process where NIR light is converted to higher energy light through the sequential absorption of multiple photons or energy transfers. The design of new NIR region BODIPY dyes, with spectra which are compatible with rare-earth upconversion nanophosphors, or with sensitized triplet-triplet annihilation, has yet to be explored.[13,375] Future research on NIR region BODIPY dyes is likely to revolve around applications in biotechnology such as genomics and diagnostics. Nanotechnology can provide a wide range of different platforms for the formation of conjugates and this could provide a viable platform for the delivery of BODIPY dyes.

7 Glossary of abbreviations

BODIPY	difluoroboron dipyrromethene or 4,4-difluoro-4-bora-3a,4a-diaza-s-indacene
DDQ	2,3-dichloro-5,6-dicyano-p-benzoquinone
MO	molecular orbital
HOMO	highest occupied molecular orbital
LUMO	lowest unoccupied molecular orbital
DFT	density functional theory

TD-DFT	time-dependent density functional theory
NIR	near-infrared
PET	photoinduced electron transfer
ICT	intramolecular charge transfer
CT	charge transfer
THF	tetrahydrofuran
MTHF	methyltetrahydrofuran
EtOH	ethanol
MeOH	methanol
MeCN	acetonitrile
DMSO	dimethyl sulfoxide
PBS	buffer phosphate-buffered saline pH 7.4
GFP	green fluorescent protein
ε	molar absorption coefficient
Φ	fluorescence quantum yield
λ_{abs}	wavelength of maximal absorbance
λ_{em}	wavelength of maximal fluorescence emission spectral radiant power
N.A.	not available
N.D.	not detected
sh	shoulder

Acknowledgements

This research was supported by NSFC (21371090 & 21101049), the Major State Basic Research Development Program of China (Grant Nos. 2011CB808704 & 2013CB922101). The theoretical calculations were carried out at the Centre for High Performance Computing in Cape Town, South Africa.

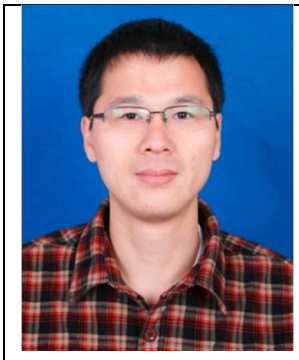

Dr Hua Lu received his PhD degree from Nanjing University (2010) under the supervision of Professor Zhen Shen. He is an associate professor at the Key Laboratory of Organosilicon Chemistry and Material Technology of the Chinese Ministry of Education at Hangzhou Normal University. His research focuses on dyes and pigments with the photophysics, DFT calculations and biological imaging of BODIPYs being of particularly strong interest.

Dr Yongchao Yang received his PhD degree on the design and synthesis of novel near-infrared BODIPYs for bioimaging and photodynamic therapy from Nanjing University (2013) under the supervision of Professor Zhen Shen.

Dr John Mack obtained a BSc (Hons) degree with first class honours from Aberdeen University (1988) and received a PhD at the University of Western Ontario (1994) for research on phthalocyanine anion radicals under the supervision of Professor Martin J. Stillman. He subsequently carried out spectroscopic research on porphyrins, phthalocyanines and BODIPYs at the University of Western Ontario and Tohoku University. He works as a senior researcher in the Department of Chemistry at Rhodes University in South Africa. There contines to be a strong focus on porphyrinoids and BODIPYs within his research.

Prof Zhen Shen received a PhD degree from Nanjing University (2000) under the supervision of Professor Xiao-Zeng You. After postdoctoral research for one year with Prof. Jörg Daub at Regensburg University, Germany and for two years with Prof. Noboru Ono at Ehime University, Japan on a fellowship from JSPS, she joined the State Key Laboratory of Coordination Chemistry, Nanjing University in 2003. She became a full professor in 2007 and received an SPP/JPP Young Investigator Award for her research in porphyrin chemistry in 2010. Her research interests are mainly focused on the synthesis, spectroscopic properties and biological applications of BODIPYs and porphyrins.

Reference

1 A. Gomez-Hens and M. P. Aguilar-Caballos, *Trends. Anal. Chem.*, 2004, **23**, 127–136.

2 R. Raghavachari, (ed.). 2001. *Near-Infrared Applications in Biotechnology*., Practical Spectroscopy Series. Vol. 25. Marcel Dekker, Inc.

3 E. Terpetschnig, O. S. Wolfbeis in *Near-Infrared Dyes for High Technology Applications* (Eds.: S. DIhne, U. Resch–Genger, O. S. Wolfbeis), Kluwer Academic, Dordrecht, 1998, pp. 161.

4 L. Yuan, W. Lin, K. Zheng, L. He and W. Huang, *Chem. Soc. Rev.*, 2013, **42**, 622–661.

5 T. Vo-Dinh, *Biomedical Photonics Handbook*. Taylor & Francis, Inc. ISBN 0-8493-1116-0, 2002.

6 S. A. Hilderbrand and R. Weissleder, *Curr. Opin. Chem. Biol.*, 2010, **14**, 71–78.

7 J. V. Frangioni, *Curr. Opin. Chem. Biol.,* 2003, **7**, 626–634.

8 Z. Cheng, Z. Wu, Z. Xiong, S. S. Gambhir and X. Chen, *Bioconjug. Chem.,* 2005, **16**, 1433–1441.

9 R. Weissleder, *Nat. Biotechnol.,* 2001, **19**, 316–317.

10 V. Ntziachristos, J. Ripoll, L. H. V. Wang and R. Weissleder, *Nat. Biotechnol*., 2005, **23**, 313–320.

11 A. Becker, C. Hessenius, K. Licha, B. Ebert, U. Sukowski, W. Semmler, B. Wiedenmann and C. Grotzinger, *Nat. Biotechnol*., 2001, **19**, 327–331.

12 C. L. Amiot, S. Xu, S. Liang, L. Pan, J. Xiao and J. Zhao. *Sensors,* 2008, **8**, 3082–3105.

13 J. Zhou, Z. Liu and F. Li, *Chem. Soc. Rev.*, 2012, **41**, 1323–1349.

14 W. Wu, L. Yao, T. Yang, R. Yin, F. Li and Y. Yu, *J. Am. Chem. Soc.,* 2011, **133**, 15810–15813.

15 J. O. Escobedo, O. Rusin, S. Lim and R. M. Strongin, *Curr. Opin. Chem. Biol.*, 2010, **14**, 64–70.

16 C. D. Geddes (ed.), Reviews in Fluorescence 2009, DOI 10.1007/978-1-4419-9672-5_4, Springer Science+Business Media, LLC 2011

17 M. Fu, Y. Xiao, X. Qian, D, Zhao and Y. Xu, *Chem. Commun.*, 2008, 1780–1782.

18 Y. Koide, Y. Urano, K. Hanaoka, T. Terai and T. Nagano, *J. Am. Chem. Soc.*, 2011, **133**, 5680–5682.

19 Y. Koide, Y. Urano, K. Hanaoka, T. Terai and T, Nagano, *ACS Chem. Biol.*, 2011, **6**, 600–608.

20 P. Ceroni, *Chem. Eur. J.*, 2011, **17**, 9560–9564.

21 G. Qian and Z. Y. Wang, *Chem. Asian J.*, 2010, **5**, 1006–1029.

22 J. Fan, M. Hu, P. Zhan and X. Peng, *Chem. Soc. Rev.*, 2013, **42**, 29–43.

23 K. Umezawa, Y. Nakamura, H. Makino, D. Citterio and K. Suzuki, *J. Am. Chem. Soc.*, 2008, **130**, 1550–1551.

24, N. Tyutyulkov, J. Fabian, A. Mehlhorn, F. Dietz and A. Tadjer, *Polymethine Dyes*, St. Kliment Ohridski University Press, Sofia, 1991, pp. 128–137.

25 S. A. Soper and Q. L. Mattingly, *J. Am. Chem. Soc.*, 1994, **116**, 3744–3752.

26 J. E. H. Buston, J. R. Young and H. L. Anderson, *Chem. Commun.*, 2000, 905–906.

27 R. C. Benson and H. A. Kues, *J. Chem. Eng. Data*, 1977, **22**, 379 –383.

28 M. Sczepan, W. Rettig, Y. L. Bricks, Y. L. Slominski and A. I. Tolmachev, *J. Photochem. Photobiol. A,* 1999, **124**, 75–84.

29 K. H. Drexhage, *J. Res. Natl. Bur. Stand. Sect. A* , 1976, **80**, 421–428.

30 M. Vogel, W. Rettig, R. Sens and K. H. Drexhage, *Chem. Phys. Lett.*, 1988, **147**, 452–460.

31 K. Kolmakov, V. N. Belov, J. Bierwagen, C. Ringemann, V. Müller, C. Eggeling and S. W. Hell, *Chem. Eur. J.*, 2010, **16**, 158–166.

32 A. Loudet and K. Burgess, *Chem. Rev.*, 2007, **107**, 4891–4932.

33 G. Ulrich, R. Ziessel and A. Harriman, *Angew. Chem., Int. Ed.*, 2008, **47**, 1184–1201.

34 K. M. Kadish, K. M. Smith and R. Guilard, *Handbook of Porphyrin Science, With Applications to Chemistry, Physics, Materials Science, Engineering, Biology and Medicine.*, 2010, pp 1–153.

35 N. Boens, V. Leen and W. Dehaen, *Chem. Soc. Rev.*, 2012, **41**, 1130–1172.

36 R. Ziessel, G. Ulricha and A. Harriman, *New J. Chem.*, 2007, **31**, 496–501.

37 A. Kamkaew, S. H. Lim, H. B. Lee, L. V. Kiew, L. Y. Chung and K. Burgess, *Chem. Soc. Rev.,* 2013, **42**, 77–88.

38 S. Xiao, Q. Cao and F. Dan, *Curr. Org. Chem.,* 2012, **16**, 2970–2981.

39 S. G. Awuah and Y. You, *RSC. Adv.*, 2012, **2**, 11169–11183.

40 A. B. Nepomnyashchii and A. J. Bard, *Acc. Chem. Res.*, 2012, **45**, 1844–1853.

41, S. Chibani, B. L. Guennic, A. Charaf-Eddin, A. D. Laurenta and D. Jacquemin, *Chem. Sci.*, 2013, **4**, 1950–1963.

42 A. Treibs and F. H. Kreuzer, *Justus Liebigs Ann. Chem.*, 1968, **718**, 208–223.

43 M. Shah, K. Thangraj, M. L. Soong, L. Wolford, J. H. Boyer, I. R. Politzer and T. G. Pavlopoulos, *Heteroat. Chem.*, 1990, **1**, 389–399.

44 S. C. Guggenheimer, J. H. Boyer, K. Thangaraj, M. Shah, M. L. Soong and T. G. Pavlopoulos, *Appl. Opt.*, 1993, **32**, 3942-3943.

45 Robert E. Hermes, Toomas H. Allik, Suresh Chandra and J. Andrew Hutchinson, *Appl. Phys. Lett.*, 1993, **63**, 877–879.

46 J. H. Boyer, A. M. Haag, G. Sathyomoorthi, M. L. Soong, and K. Thangaraj, *Heteroat. Chem.*, 1993, **4**, 39–49.

47 G. Sathyamoorthi, J. H. Boyer, T. H. Allik and S. Chandra, *Heteroat. Chem.*, 1994, **5**, 403–407.

48 A. Maslyukov, S. Sokolov, M. Kaivola, K. Nyholm, and S. Popov, *Applied Optics.*, 1995, **34**, 1516–1518.

49 T. López Arbeloa, F. López Arbeloa, I. López Arbeloa, I García-Moreno, A Costela, R Sastre and F Amat-Guerri, *Chem. Phys. Lett.,* 1999, **299**, 315–321.

50 A. B. Descalzo,*H. J. Xu, Z, Shen and K. Rurack, *Ann. N.Y. Acad. Sci.*, 2008, **1130**, 164–171.

51. H. Lu, Z. Xue, J. Mack, Z. Shen, X.Y ou and N. Kobayashi, *Chem. Commun*., 2010, **46**, 3565–3567.

52. G. Sathyamoorthi, M. L. Soong, T. W. Ross and J. H. Boyer, *Heteroat. Chem.*, 1993, **4**, 593–608.

53 H. Lu, L. Xiong, H. Liu, M. Yu, Z. Shen, F. Li and X. You, *Org. Biomol. Chem*., 2009, **7**, 2554–2558.

54 Y. H. Yu, Z. Shen, H. Y. Xu, Y. W. Wang, T. Okujima, N. Ono, Y. Z. Li and X. Z. You, *J. Mol. Struct.*, 2007, **827**, 130–136.

55 A. C. Benniston and G. Copley, *Phys. Chem. Chem. Phys.*, 2009, **11**, 4124–4131.

56 M. Benstead, G. H. Mehl and R. W. Boyle, *Tetrahedron*, 2011, **67**, 3573–3601.

57 T. K. Khana, M. Bröingb, S. Mathura and M. Ravikanthc, *Coord. Chem. Rev.*, 2013, **257**, 2348–2387.

58 G. Ulrich, C. Goze, M. Guardigli, A. Roda and R Ziessel, *Angew. Chem. Int. Ed.*, 2005, **44**, 3694–3698.

59 C. Goze, G. Ulrich and R. Ziessel, *Org. Lett.*, 2006, **8**, 4445–4448.

60 G. Ulrich, C. Goze, S. Goeb, P. Retailleau and R. Ziessel, *New J. Chem.*, 2006, **30**, 982–986.

61 A. Haefele, G. Ulrich, P. Retailleau and R. Ziessel, *Tetrahedron. Lett.*, 2008, **49**, 3716–3721.

62 A. Harriman, L. J. Mallon, B. Stewart, G. Ulrich and R. Ziessel, *Eur. J. Org. Chem.*, 2007, **19**, 3191–3198.

63 F. Camerel, G. Ulrich, P. Retailleau and R. Ziessel, *Angew. Chem. Int. Ed.*, 2008, **47**, 8876–8880.

64 K. K. Jagtap, N. Shivran, S. Mula, D. B. Naik, S. K. Sarkar, T. Mukherjee, D. K. Maity and A. K. Ray, *Chem. Eur. J.*, 2013, **19**, 702–708.

65 X. D. Jiang, J. Zhang, T. Furuyama and W. Zhao, *Org. Lett.*, 2012, **14**, 248–251.

66 H. L. Wong, W. T. Wong and V. W. W. Yam, *Org. Lett.*, 2012, **14**, 1862–1865.

67 X. D. Jiang, Y. Fu, T. Zhang and W. Zhao, *Tetrahedron. Lett.*, 2012, **53**, 5703–5706.

68 T. Lundrigan and A. Thompson, *J. Org. Chem.*, 2012, **78**, 757–761.

69 B. R. Groves, S. M. Crawford, T. Lundrigan, C. F. Matta, S. Sowlati-Hashjinb and A. Thompson, *Chem. Commun.*, 2013, **49**, 816–818.

70 J. Lu, So. B. Ko, N. R. Walters and S. Wang, *Org. Lett.*, 2012, **14**, 5660–5663.

71 L. Gai, J. Mack, H. Lu, H. Yamada, G. Lai, Z. Li and Z. Shen, *Chem. Eur. J*., 2014, **20**, 1091–1102**.**

72 J. Michl, *J. Am. Chem. Soc.*, 1978, **100**, 6801–6811.

73 J. Michl, *Pure Appl. Chem.*, 1980, **52**, 1549–1563;

74 J. Michl, *Tetrahedron.*, 1984, **40**, 3845–3934.

75 M. Kollmannsberger, K. Rurack, U. Resch-Genger and J. Daub, *J. Phys. Chem. A*, 1998, **102**, 10211–10220.

76 W. Qin, M. Baruah, M. V. Auweraer, F. C. De Schryver and N. Boens, *J. Phys. Chem. A*, 2005, **109**, 7371–7384.

77 I. V. Sazanovich, C. Kirmaier, E. Hindin, L. Yu, D. F. Bocian, J. S. Lindsey and D. Holten, *J. Am. Chem. Soc.*, 2004, **126**, 2664–2665.

78 H. L. Kee, C. Kirmaier, L. Yu, P. Thamyongkit, W. J. Youngblood, M. E. Calder, L. Ramos, B. C. Noll, D. F. Bocian, W. R. Scheidt, R. R. Birge, J. S. Lindsey and D. Holten, *J. Phys. Chem. B*, 2005, **109**, 20433–20443.

79 F. Li, S. I. Yang, Y. Ciringh, J. Seth, C. H. Martin, D. L. Singh, D. Kim, R. R. Birge, D. F. Bocian, D. Holten and J. S. Lindsey, *J. Am. Chem. Soc.*, 1998, **120**, 10001–10017.

80 H. Röhr, C. Trieflinger, K. Rurack and J. Daub, *Chem. Eur. J.*, 2006, **12**, 689–700.

81 M. Hecht, T. Fischer, P. Dietrich, W. Kraus, A. B. Descalzo, W. E. S. Unger and K. Rurack, *ChemistryOpen*, 2013, **2**, 25–38.

82 W. Qin, M. Baruah, A. Stefan, M. Van der Auweraer and N. Boens, *ChemPhysChem*, 2005, **6**, 2343–2351.

83 J. Karolin, L. B.-A. Johansson, J. Strandberg and T. NyZ, *J. Am. Chem. Soc.,* 1994, **116**, 7801–7806.

84 G. Jones II, S. Kumar, O. Klueva and D. Pacheco, *J. Phys. Chem. A,* 2003, **107**, 8429–8434.

85 Z.R. Grabowski, K. Rotkiewicz and W. Rettig, *Chem. Rev.,* 2003, **103**, 3899–4031.

86 W. Rettig, *Electron Transfer*, 1994, 253–299.

87 L. Gai, J. Mack, H. Liu, Z. Xu, H. Lu and Z. Li, *Sensors Actuators B-Chem.*, 2013, **182**, 1–6.

88 K. Tanaka, T. Miura, N. Umezawa, Y Urano, K. Kikuchi, T. Higuchi and T Nagano, *J. Am. Chem. Soc.,* 2001, **123**, 2530–2536.

89 T. Miura, Y. Urano, K. Tanaka, T. Nagano, K. Ohkubo and S. Fukuzumi, *J. Am. Chem. Soc.,* 2003, **125**, 8666–8671.

90 Y. Urano, M. Kamiya, K. Kanda, T. Ueno, K. Hirose and T. Nagano, *J.Am. Chem. Soc.,* 2005, **127**, 4888–4894.

91 M. A. Fox, *Photochem. Photobio*., 1990, **52**, 617–627.

92 K. Rurack and U. Resch-Genger, *Chem. Soc. Rev., 2002,* **31**, 116–127.

93 J. Banñuelos, F. L. Arbeloa, T. Arbeloa, S. Salleres, F. Amat-Guerri, M. Liras and I. L. Arbeloa, *J. Phys. Chem. A,* 2008, **112**, 10816–10822.

94 M. E. McCarroll, Y. Shi, S. Harris, S. Puli, I. Kimaru, R. S. Xu, L. C. Wang and D. Dyer, *J. Phys. Chem. B,* 2006, **110**, 22991–22994.

95 D. P. Kennedy, C. M. Kormos and S. C. Burdette, *J. Am. Chem. Soc.,* 2009, **131**, 8578–8586.

96 H. Lu, S. Zhang, H. Liu, Y. Wang, Z. Shen, C. Liu and X. You, *J. Phys. Chem. A*, 2009, **113**, 14081–14086.

97 R. A. Marcus, *Angew. Chem., Int. Ed. Engl.,* 1993, **32**, 1111–1121.

98 A. Weller, *Pure Appl. Chem.,* 1968, **16**, 115–123.

99 L. J. Fan, Y. Zhang, C. B. Murphy, S. E. Angell, M. F. L. Parker, B. R. Flynn and W. E. Jones, *Coord. Chem. Rev.,* 2009, **253**, 410–422.

100 A. P. De Silva, H. Q. N. Gunaratne, T. Gunnlaugsson, A. J. M. Huxley, C. P. McCoy, J. T. Rademacher and T. E. Rice, *Chem. Rev.,* 1997, **97**, 1515–1566.

101 M. Kasha, *Discuss. Faraday. Soc.*, 1950, **9**, 14–19.

102 M. Baruah, W. Qin, N. Basarić, W. M. De Borggraeve and N. Boens, *J. Org. Chem.*, 2005, **70**, 4152–4157.

103 M. Baruah, W. Qin, R. A. L. Vallée, D. Beljonne, T. Rohand, W. Dehaen and N. Boens, *Org. Lett.*, 2005, **7**, 4377–4380.

104 T. Rohand, M. Baruah, W. Qin, N. Boens and W. Dehaen, *Chem. Commun.*, 2006, 266–268.

105 E. Fron, E. Coutiño-Gonzalez, L. Pandey, M. Sliwa, M. Van der Auweraer, F. C. De Schryver, J. Thomas, Z. Dong, V. Leen, M. Smet, W. Dehaen and T. Vosch, *New J. Chem.*, 2009, **33**, 1490–1496.

106 W. Qin, T. Rohand,M. Baruah, A. Stefan, M. Van der Auweraer, W. Dehaen and N. Boens, *Chem. Phys. Lett.*, 2006, **420**, 562–568.

107 T. Rohand, J. Lycoops, S. Smout, E. Braeken, M. Sliwa, M. Van der Auweraer, W. Dehaen, W. M. De Borggraeve and N. Boens, *Photochem. Photobiol. Sci.*, 2007, **6**, 1061–1066.

108 W. Qin, T. Rohand, W. Dehaen, J. N. Clifford, K. Driessen, D. Beljonne, B. Van Averbeke, M. Van der Auweraer and N. Boens, *J. Phys. Chem. A*, 2007, **111**, 8588–8597.

109 W. Qin, V. Leen, W. Dehaen, J. Cui, C. Xu, X. Tang, W. Liu, T. Rohand, D. Beljonne, B. Van Averbeke, J. Clifford, K. Driesen, K. Binnemans, M. Van der Auweraer and N. Boens, J. *Phys. Chem. C*, 2009, **113**, 11731–11740.

110 L. Li, B. Nguyen and K. Burgess, *Bioorg. Med. Chem. Lett.*, 2008, **18**, 3112–3116.

111 C. Zhao, X. Wang, J. Cao, P. Feng, J. Zhang, Y. Zhang ,Y. Yang and Z. Yang, *Dyes. Pigms.*, 2013, **96**, 328-332.

112 J. C. C. Er, M. K. Tang, C. G. Chia, H. M. Liew, M. Vendrell and Y. T. Chang, *Chem. Sci.*, 2013, **4**, 2168-2176.

113 V. Leen, E. Braeken, K. Luckermans, C. Jackers, M. Van der Auweraer, N. Boens and W. Dehaen, *Chem. Commun.*, 2009, 4515–4517.

114 T. Rohand, W. Qin, N. Boens and W. Dehaen, *Eur. J. Org. Chem.*, 2006, 4658–4663.

115 S. Yin, V. Leen, S. V. Snick, N. Boensa and W. Dehaen, *Chem. Commun.,* 2010, **46**, 6329–6331.

116 L. Jiao, C. Yu, T. Uppal, M. Liu, Y. Li, Y. Zhou, E. Hao, X. Hu and M. G. H. Vicente, *Org. Biomol. Chem.*, 2010, **8**, 2517–2519.

117 L. Jiao, W. Pang, J. Zhou, Y. Wei, X. Mu, G. Bai and E. Hao, *J. Org. Chem.*, 2011, **76**, 9988–9996.

118 V. Leen, T. Leemans, N. Boens and W. Dehaen, *Eur. J. Org. Chem.*, 2011, **23**, 4386– 4396.

119 J. Han, O. Gonzalez, A. Aguilar-Aguilar, E. Peña-Cabrera and K. Burgess, *Org. Biomol. Chem.*, 2009, **7**, 34–36.

120 V. Lakshmi and M. Ravikanth, *Dyes. Pigms.,* 2013, **96**, 665–671.

121 A. Poirel, A. De Nicola, P. Retailleau and R. Ziessel, *J. Org. Chem.*, 2012, **77**, 7512–7525.

122 V. Leen, D. Miscoria, S. Yin, A. Filarowski, J. M. Ngongo, M. Van der Auweraer, N. Boens and W. Dehaen, *J. Org. Chem.*, 2011, **76**, 8168–8176.

123 Y. Chen, J. Zhao, H. Guo and L. Xie, *J. Org. Chem.*, 2012, **77**, 2192–2206

124 D. Zhang, Y. Wen, Y. Xiao, G. Yu, Y. Liu and X. Qian, *Chem. Commun.*, 2008, **39**, 4777–4779.

125 L. Bonardi, G. Ulrich and R. Ziessel, *Org. Lett.*, 2008, **10**, 2183–2186.

126 P. G. Van Patten, A. P. Shreve, J. S. Lindsey, R. J. Donohoe, T. G Kim, M. R. Topp, R. M. Hochstrasser and K. Burgess, *Chem. Eur. J.*, 2003, **9**, 4430–4441.

127 V. Leen, V. Zaragozí Gonzalvo, W. M. De Borggraeve, N. Boens and W. Dehaen, *Chem. Commun.*, 2010, **46**, 4908–4910.

128 M. Zhang, E. Hao, J. Zhou, C. Yu, G. Bai, F. Wang and L. Jiao, *Org. Biomol. Chem.*, 2012, **10**, 2139–2145.

129 V. Leen, M. Van der Auweraer, N. Boens and W. Dehaen, *Org. Lett.*, 2011, **13**, 1470–1473.

130 V. Leen, W. Qin, W. Yang, J. Cui, C. Xu, X. Tang, W. Liu, K. Robeyns, L. Van Meervelt, D. Beljonne, R. Lazzaroni, C. Tonnelé, N. Boens and W. Dehaen, *Chem. Asian. J.*, 2010, **5**, 2016–2026.

131 M. Zhang, E. Hao, Y. Xu, S. Zhang, H. Zhu, Q. Wang, C. Yu and L. Jiao, *RSC Adv.*, 2012, **2**, 11215–11218

132 R. K. Gupta, R. Pandey, S. Sharma and D. S. Pandey, *Dalton. Trans.*, 2012, **41**, 8556–8266.

133 M. R. Rao, M. D. Tiwari, J. R. Bellare and M. Ravikanth, *J. Org. Chem.*, 2011, **76**, 7263–7268.

134 C. Thivierge, R. Bandichhor and K. Burgess, *Org. Lett.,* 2007, **9**, 2135–2138.

135 B. Verbelen, V. Leen, L. Wang, N. Boens and W. Dehaen, *Chem. Commun.*, 2012, **48**, 9129–9131.

136. J. Chen, M. Mizumura, H. Shinokubo amd A. Osuka, *Chem.Eur. J.*, 2009, **15**, 5942–5949.

137 K. Rurack, M. Kollmannsberger and J. Daub, *Angew.Chem., Int. Ed.*, 2001, **40**, 385–387.

138 O. Buyukcakir, O. A. Bozdemir,S. Kolemen, S. Erbas and E. U. Akkaya, *Org. Lett.*, 2009. **11**, 4644–4647.

139 Y. H. Yu, A. B. Descalzo, Z. Shen, Q. Liu, Y. W. Wang, M. Spieles, Y. Z. Li, K. Rurack and X. Z. You, *Chem. Asian J.,* 2006, **1**, 176–187.

140 T. Bura, D. Hablot and R. Ziessel, *Tetrahedron. Lett.*, 2011, **52**, 2370-2374.

141 S. Zhu, J. Zhang, G. Vegesna, A. Tiwari, F. T. Luo, M. Zeller, R. Luck, H. Li, S. Green and H. Liu, *RSC Adv.*, 2012, **2**, 404–407.

142 T. Bura, P. Retailleau, G. Ulrich and R. Ziessel, *J. Org. Chem.*, 2011, **76**, 1109–1117.

143 J. Lee, N. Kang, Y. K. Kim, A. Samanta, S. Feng, H. K. Kim, M. Vendrell, J. H. Park and Y. T. Chang, *J. Am. Chem. Soc.*, 2009, **131**, 10077–10082.

144 P. Didier, G. Ulrich, Y. Mély and R. Ziessel, *Org. Biomol. Chem.*, 2009, **7**, 3639–3642.

145 Q. Zheng, G. Xu and P. N. Prasad, *Chem. Eur. J.*, 2008, **14**, 5812 – 5819.

146 X. Zhang, Y. Xiao, J. Qi, J. Qu, B. Kim, X. Yue and K. D. Belfield, *J. Org. Chem.*, 2013, **78**, 9153−9160.

147 T. Bura, P. Retailleau and R. Ziessel, *Angew. Chem. Int. Ed.,* 2010, **49**, 6659 – 6663.

148 T. Rousseau, A. Cravino, T. Bura, G. Ulrich, R. Ziessel and J. Roncali, *Chem. Commun.*, 2009, 1673–1675.

149 T. Rousseau, A. Cravino, E. Ripaud, P. Leriche, S. Rihn, A. De Nicola, R. Ziessel and J. Roncali, *Chem. Commun.*, 2010, **46**, 5082–5084.

150 Y. Zhao, Y. Zhang, X. Lv, Y. Liu, M. Chen, P. Wang, J. Liu and Wei Guo, *J. Mater. Chem.*, 2011, **21**, 13168 – 13171.

151 D. Kumaresan, R. P. Thummel, T. Bura, G. Ulrich and R. Ziessel, *Chem. Eur. J.,* 2009, **15**, 6335 – 6339.

152 T. Bura, N. Leclerc, S. Fall, P. Lévêque, T. Heiser and R. Ziessel, *Org. Lett.,* 2011, **13**, 6030 – 6033.

153 S. Kolemen, Y. Cakmak, S. Erten-Ela, Y. Altay, J. Brendel, M. Thelakkat and E. U. Akkaya, *Org. Lett.,* 2012, **12**, 3812 –3815.

154 A. Harriman, M. A. H. Alamiry, J. P. Hagon, D. Hablot and R. Ziessel, *Angew. Chem. Int. Ed.*, 2013, **52**, 1–6.

155 R. Ziessel, A. Nano, E. Heyer, T. Bura and P. Retailleau, *Chem. Eur. J.*, 2013, **19**, 2582–2588.

156 Y. Ooyama, Y. Hagiwara, T. Mizumo, Y. Harima and J. Ohshita, *New J. Chem.*, 2013, **37**, 2479–2485.

157 R. Ziessel, G. Ulrich, A. Haefele and A. Harriman, *J. Am. Chem. Soc*., 2013, **135**, 11330–11344.

158 Y. Rio, W. Seitz, A. Gouloumis, P. Vázquez, J. L. Sessler, D. M. Guldi and T. Torres, *Chem. Eur. J.*, 2010, **16**, 1929–1940.

159 J. Y. Liu, M. E. El-Knhouly, S. Fukuzumi, D. K. P. Ng, *Chem. Eur. J.*, 2011, **17**, 1605–1613.

160 F. D'Souza, P. M. Smith, M. E. Zandler, A. L. McCarty, M. Itou, Y. Araki and O. Ito, *J. Am. Chem. Soc.*, 2004, **126**, 7898–7907.

161 V. Engelhardt, S. Kuhri, J. Fleischhauer, M. García-Iglesias, D. González-Rodríguez, G. Bottari, T.s Torres, D. M. Guldi and R. Faust, *Chem. Sci.*, 2013, **4**, 3888–3893.

162 S. Atilgan, Z. Ekmekci, A. L. Dogan, D. Gucb and E. U. Akkaya, *Chem. Commun.*, 2006, 4398–4400.

163 S. Ozlem, and E. U. Akkaya. *J. Am. Chem. Soc*., 2009, **131**, 48–49.

164 A. Bozdemir, R. Guliyev, O. Buyukcakir, S. Selcuk, S. Kolemen, G. Gulseren, T. Nalbantoglu, H. Boyaci and E. U. Akkaya, *J. Am. Chem. Soc.*, 2010, **132**, 8029–8036.

165 R. Guliyev, S. Ozturk, Z. Kostereli and E. U. Akkaya, *Angew. Chem. Int. Ed.,* 2011, **50**, 9826-9831.

166 S. Erbas-Cakmak and E. U. Akkaya, *Angew. Chem. Int. Ed.,* 2013, **52**, 11364–11368.

167 R. Gotor, A. M. Costero, S. Gil, M. Parra, P. Gaviña and K. Rurack, *Chem. Commun.*, 2013, **49**, 11056–11058.

168 B. Wang, P. Li, F. Yu, J. Chen, Z. Qu and K. Han, *Chem. Commun.*, 2013, **49**, 5790–5792.

169 D. Zhai, S. C. Lee, S. W. Yunb and Y. T. Chang, *Chem. Commun.*, 2013,**49**, 7207–7209.

170 S. Zhu, Zhang, J. Janjanam, G. Vegesna, F. T. Luo, A. Tiwari and H. Liu, *J. Mater. Chem. B*, 2013, **1**, 1722–1728.

171 X. Li, S. Zhang, J. Cao, N. Xie, T. Liu, B. Yang, Q. He and Y. Hu, *Chem. Commun.*, 2013, **49**, 8656–8658.

172 I. García-Moreno, D. Zhang, Á. Costela, V. Martín, R. Sastre and Y. Xiao, *J. Appl. Phys.*, 2010, **107**, 073105–073107.

173 D. Zhang, V. Martín, I. García-Moreno, A. Costela, M. E. Pérez-Ojedab and Y. Xiao, *Phys. Chem. Chem. Phys.*, 2011, **13**, 13026–13033.

174 Y. Yang, Z. Liao, Y. Zhou, Y. Cui, and G. Qian, *Opt. Lett.*, 2013, **38**, 1627–1629.

175 D. H. R. Barton, J. Kerbagore and S. Zard, *Tetrahedron,* 1990, **46**, 7587–7598.

176 N. Ono, H. Kawamura and M. Bougauchi, *Tetrahedron,* 1990, **46**, 7483–7496.

177 J. L. Sessler, A. Mozattari and M. Johnson, *Org. Synth. Coll.*,1991, **10**, 68–77.

178 A. H Corwin, *Heterocyclic Compounds*, Vol. 1, Wiley, NY, 1950, Chapter 6.

179 R. A. Jones and G. P. Bean, *The Chemistry of Pyrroles*, Academic Press, London, 1977, 51–57, 74–79.

180 R. W. Wagner and J. S. Lindsey,. *Pure Appl. Chem.,* 1996, **68**, 1373–1380.

181 Z. Li, E. Mintzer and R. Bittman, *J. Org. Chem.,* 2006, **71**, 1718–1721.

182 C. Tahtaoui, C. Thomas, F. Rohmer, P. Klotz, G. Duportail, Y. Mely, D. Bonnet and M Hibert, *J. Org. Chem.*, 2007, **72**, 269–272.

183 L. Wu and K. Burgess, *Chem. Commun.*, 2008, 4933–4935.

184 M. Rogers, *J. Chem. Soc.*, 1943, 590–596.

185 W. Davies and M. Rogers, *J. Chem. Soc.*, 1944, 126–131.

186 E. Knott, *J. Chem. Soc*., 1947, 1196–1201.

187 T. H. Allik, R. E. Hermes, G. Sathyamoorthi and J. H. Boyer, *Proc. SPIE-Int. Soc. Opt. Eng.*, 1994, **2115**, 240–248.

188 J. Killoran, L. Allen, J. Gallagher, W. Gallagher and D. F. O'Shea, *Chem. Commun.*, 2002, 1862–1863.

189 A. Gorman, J. Killoran, C. O'Shea, T. Kenna, W. M. Gallagher and D. F. O'Shea, *J. Am. Chem. Soc.*, 2004, **126**, 10619–10631.

190 W. M. Gallagher, L. T. Allen, C. O'Shea, T. Kenna, M. Hall, A. Gorman, J. Killoran and D. F. O'Shea, *Br. J. Cancer.*, 2005, **92**, 1702–1710.

191 S. O. McDonnell, M. J. Hall, L. T. Allen, A. Byrne, W. M. Gallagher and D. F. O'Shea, *J. Am. Chem. Soc.*, 2005, **127**, 16360–16361.

192 M. J. Hall, L. T. Allen and D. F. O'Shea, *Org. Biomol. Chem.*, 2006, **4**, 776–780.

193 J. Killoran and D. F. O'Shea, *Chem. Commun.*, 2006, 1503–1505.

194 A. Palma, M. Tasior, D. O. Frimannsson, T. Truc Vu, R. Méallet-Renault and D. F. O'Shea, *Org. Lett.*, 2009, **11**, 3638–3641.

195 H. Bredereck and H. W. Vollmann, *Chem. Ber.*, 1972, **105**, 2271–2283.

196 H. Lu, S. Shimizu, J. Mack, Z. Shen and N. Kobayashi, *Chem. Asian. J*., 2011, **6**, 1026–1037.

197 V. F. Donyagina, S. Shimizu, N. Kobayashi and E. A. Lukyanets, *Tetrahedron Lett.*, 2008, **49**, 6152–6154.

198 R. Gresser, M. Hummert, H. Hartmann, K. Leo and M. Riede, *Chem. Eur. J.*, 2011, **17**, 2939–2947.

199 Gaussian 09, Revision D.01, M. J. Frisch, G. W. Trucks, H. B. Schlegel, G. E. Scuseria, M. A. Robb, J. R. Cheeseman, G. Scalmani, V. Barone, B. Mennucci, G. A. Petersson, H. Nakatsuji, M. Caricato, X. Li, H. P. Hratchian, A. F. Izmaylov, J. Bloino, G. Zheng, J. L. Sonnenberg, M. Hada, M. Ehara, K. Toyota, R. Fukuda, J.

Hasegawa, M. Ishida, T. Nakajima, Y. Honda, O. Kitao, H. Nakai, T. Vreven, J. A. Montgomery, Jr., J. E. Peralta, F. Ogliaro, M. Bearpark, J. J. Heyd, E. Brothers, K. N. Kudin, V. N. Staroverov, R. Kobayashi, J. Normand, K. Raghavachari, A. Rendell, J. C. Burant, S. S. Iyengar, J. Tomasi, M. Cossi, N. Rega, J. M. Millam, M. Klene, J. E. Knox, J. B. Cross, V. Bakken, C. Adamo, J. Jaramillo, R. Gomperts, R. E. Stratmann, O. Yazyev, A. J. Austin, R. Cammi, C. Pomelli, J. W. Ochterski, R. L. Martin, K. Morokuma, V. G. Zakrzewski, G. A. Voth, P. Salvador, J. J. Dannenberg, S. Dapprich, A. D. Daniels, Ö. Farkas, J. B. Foresman, J. V. Ortiz, J. Cioslowski, and D. J. Fox, Gaussian, Inc., Wallingford CT, 2009.

200 C. Lee, W. Yang and R. G. Parr, *Phys. Rev. B*, 1988, **37**, 785–789.

201 A. D. Becke, *J. Chem. Phys.*, 1993, **98**, 5648–5652

202 A. D. Becke; *Phys. Rev. A*, 1988, **38**, 3098–3100.

203 P. J. Stephens, F. J. Devlin, C. F. Chabalowski and M. J. Frisch, *J. Phys. Chem.*, 1994, **98**, 11623–11627.

204 S. H. Vosko, L. Wilk and M. Nusair, *Can. J. Phys.*, 1980, ***58***, *1200–1211*.

205 T. H. Dunning Jr and P. J. Hay, in *Modern Theoretical Chemistry*, Ed. H. F. Schaefer III, Vol. 3 (Plenum, New York, 1976) 1–28.

206 R. W**.** Wagner and J. S**.** Lindsey, *Pure. Appl. Chem*., 1996, **68**, 1373–1380.

207 L. H. Thoresen, H. Kim, M. B. Welch, A. Burghart and K. Burgess, *Synlett*, 1998, 1276–1278.

208 A. Burghurt, H. Kim, M. B. Welch, L. H. Thoresen, J. Reibenspies, K. Burgess, F. Bergstrém and L. Johansson, *J. Org. Chem.*, 1999, **64**, 7813–7819.

209 E. Y. Schmidt, N.V. Zorina, M. Y. Dvorko, N. I. Protsuk, K. V. Belyaeva, G. Clavier, R. Méallet-Renault, T. T. Vu, A. I. Mikhaleva and B. A. Trofimov, *Chem Eur. J*, 2011, **17**, 3069–3073.

210 E. Yu. Schmidt, B. A. Trofimov, A. I. Mikhaleva, N. V. Zorina, N. I. Protzuk, K. B. Petrushenko, I. A. Ushakov, M. Yu. Dvorko, R. Méallet-Renault, G. Clavier, T. T. Vu, H. T. T. Tran and R. B. Pansu, *Chem. Eur. J.* 2009, **15**, 5823–5830.

211 Y. M. Poronik, V. P. Yakubovskyi, M. P. Shandura, Y. G. Vlasenko, A. N. Chernega and Y. P. Kovtun, *Eur. J. Org. Chem.* 2010, 2746–2752.

212 S. Rihn, P. Retailleau, N. Bugsaliewicz, A. D. Nicola and R. Ziessel, *Tetrahedron. Lett.*, 2009, **50**, 7008–7013.

213 L. N. Sobenina, A. M. Vasil'tsov, O. V. Petrova, K. B. Petrushenko, I. A. Ushakov, G. Clavier, R. Méallet-Renault, A. I. Mikhaleva and B. A. Trofimov, *Org. Lett.*, 2011, **13**, 2524–2527.

214 D. V. Roberts, B. P. Wittmershaus, Y. Z. Zhang, S. Swan and M. P. Klinosky, *J. Lumin.*, 1998, **79**, 225–231.

215 B. P. Wittmershaus, J. J. Skibicki, J. B. McLafferty, Y. Z. Zhang and S. Swan, *J. Fluoresc.*, 2001, **11**, 119–128.

216 B. P. Wittmershaus, T. T. Baseler, G. T. Beaumont and Y. Z. Zhang, *J. Lumin.*, 2002, **96**, 107–118.

217 A. Wakamiya, N. Sugita and S. Yamaguchi. *Chem. Lett.*, 2008, **37**, 1094–1095.

218 V. Lakshmi and M. Ravikanth, *J. Org. Chem.*, 2011, **76**, 8466–8471.

219 V. Lakshmi and M. Ravikanth, *Dyes. Pigms.*, 2013, **96**, 665-671.

220 D. Zhang, Y. Wang, Y. Xiao, S. Qian and X. Qian, *Tetrahedron*, 2009, **65** ,8099–8103.

221 Y. Xiao, D. Zhang, X. Qian, A. Costela, I. Garcia-Moreno, V. Martin, M. E. Perez-Ojeda, J. Bauelos, L. Gartziad and I. López Arbeload, *Chem. Commun.*, 2011, **47**, 11513–11515.

222 G. L. Fu, H. Pan, Y. H. Zhao and C. H. Zhao, *Org. Biomol. Chem.*, 2011, **9**, 8141–8146.

223 H. Sun, X. Dong, S. Liu, Q. Zhao, X. Mou, H. Y. Yang and W. Huang, *J. Phys. Chem. C*, 2011, **115**, 19947–19954.

224 H. Lu, Q. Wang, L. Gai, Z. Li, Y. Deng, X. Xiao, G. Lai and Z. Shen, *Chem. Eur. J.*, 2012, **18** , 7852–7861.

225 M. R. Rao, K.V. P. Kumar and M. Ravikanth, *J. Organomet. Chem.*, 2010, **695** , 863–869.

226 M. Kollmannsberger, T. Gareis, S. Heinl, J. Breu and J. Daub, *Angew. Chem. Int. Ed.*, 1997, **36**, 1333–1335.

227 K. Rurack, M. Kollmannsberger and J. Daub, *Angew. Chem. Int. Ed.*, 2001, **40**, 385–387.

228 J. Shao, H. Guo, S. Ji and J. Zhao, *Biosensors and Bioelectronics*, 2011, **26**, 3012–3017.

229 B. R. Ziessel and T. Bura, J. Olivier, *Synlett*, 2010, **15**, 2304–2310.

230 R. Ziessel, S. Rihn, and A. Harriman, *Chem. Eur. J.*, 2010, **16**, 11942–11953.

231 N. Boens, W. Qin, M. Baruah, W. M. De Borggraeve, A. Filarowski , N. Smisdom, M. Ameloot, L. Crovetto, E. M. Talavera and J. M. Alvarez-Pez, *Chem. Eur. J.*, 2011, **17**, 10924–10934.

232 Y. Lv, J. Xu, Y. Guo and S. Shao, *J. Incl. Phenom. Macrocycl. Chem.*, 2012, **72**, 95–101.

233 X. Cao, W. Lin, K. Zheng and L. He, *Chem.Commun.*, 2012, **48**, 10529–10531.

234 J. Bañelos-Prieto, A. R. Agarrabeitia, I. Garcia-Moreno, I. Lopez-Arbeloa, A. Costela, L. Infantes, M. E. Perez-Ojeda, M. Palacios-Cuesta and M. J. Ortiz, *Chem. Eur. J.*, 2010, **16**, 14094–14105.

235 K. Rurack, M. Kollmannsberger and J. Daub, *New J. Chem.*, 2001, **25**, 289–292.

236 L. Huang, X. Yu, W. Wu and J. Zhao, *Org. Lett.,* 2012, **14**, 2594–2597.

237 E. Deniz, G. C. Isbasar, Ö. A. Bozdemir, L. T. Yildirim, A. Siemiarczuk and E. U. Akkaya, *Org. Lett.*, 2008, **10**, 3401–3403.

238 R. Ziessel, S. Rihn, and A. Harriman, *Chem. Eur. J.*, 2010, **16**, 11942–11953.

239 G. S. Jiao, L. H. Thoresen, T. G. Kim, W. C. Haaland, F. Gao, M. R. Topp, R. M. Hochstrasser, M. L. Metzker and K. Burgess, *Chem. Eur. J.*, 2006, **12**, 7816 – 7826.

240 S. Kim, T. Y. Ohulchanskyy, A. Baev and P. N. Prasad, *J. Mater. Chem.*, 2009, **19**, 3181–3188.

241 X. Yin, Y. Li, Y. Li, Y. Zhu, X. Tang, H. Zheng and D. Zhu, *Tetrahedron*, 2009, **65**, 8373–8377.

242 S. Chen, W. Chen, W. Shi and H. Ma*, Chem. Eur. J.*, 2012, **18**, 925–930.

243 X. Y. Qu, Q. Liu, X. N. Ji, H. C. Chen, Z. K. Zhou, Z. Shen, *Chem. Commun.*, 2012, **48**, 4600-4602.

244 V. P. Yakubovskyi, M. P. Shandura and Y. P. Kovtun, *Eur. J. Org. Chem.,* 2009, **19**, 3237–3243.

245 N. Shivran, S. Mula, T. K. Ghanty and S. Chattopadhyay, *Org. Lett.*, 2011, **13**, 5870–5873.

246 T. V. Goud, A. Tutar and J. Biellmann, *Tetrahedron*, 2006, **62**, 5084–5091.

247 T. Kim, S. Park, Y. Choi and Y. Kim, *Chem. Asian J.*, 2011, **6**, 1358–1361.

248 J. Chen, A. Burghart, A. Derecskei-Kovacs and K. Burgess, *J. Org. Chem.,* 2000, **65***,* 2900–2906.

249 Y. Mei, P. A. Bentley and W. Wang, *Tetrahedron Lett.*, 2006, **47**, 2447–2449.

250 Y. W. Wang, A. B. Descalzo, Z. Shen, X. Z. You and K. Rurack, *Chem. Eur. J.*, 2010, **16**, 2887–2903.

251 T. Kowada, S. Yamaguchi and K. Ohe, *Org. Lett.*, 2010, **12**, 296–299.

252 T. Kowada, S. Yamaguchi, H. Fujinaga and K. Ohe, *Tetrahedron*, 2011, **67**, 3105–3110.

253 X. D. Jiang, R. Gao, Y. Yue, G. T. Sun and W. Zhao, *Org. Biomol. Chem.*, 2012, **10**, 6861–6865.

254 K. Umezawa, A. Matsui, Y. Nakamura, D. Citterio and K. Suzuki, *Chem. Eur. J.*, 2009, **15**, 1096–1106.

255 S. G. Awuah, J. Polreis, V. Biradar and Y. You, *Org. Lett.*, 2011, **13**, 3884–3887.

256 Y. Yang, Q. Guo, H. Chen, Z. Zhou, Z. Guo and Z. Shen, *Chem. Commun.*, 2013, **49**, 3940–3942.

257 H. Kim, A. Burghart, M. B. Welch, J. Reibenspies and K. Burgess, *Chem. Commun.*, 1999, 1889–1890.

258 Y. Tomimori, T. Okujima, T. Yano, S. Mori, N. Ono, H. Yamada and H. Uno, *Tetrahedron*, 2011, **67**, 3187–3193.

259 C. Ikeda, T. Maruyama and T. Nabeshima, *Tetrahedron Lett.*, 2009, **50**, 3349–3351.

260 C. Ikeda, S. Ueda and T. Nabeshima, *Chem. Commun.*, 2009, 2544–2546.

261 M. Wada, S. Ito, H. Uno, T. Murashima, N. Ono, T. Urano and Y. Urano, *Tetrahedron Lett.*, 2001, **42**, 6711–6713.

262 Z. Shen, H. Röhr, K. Rurack, H. Uno, M. Spieles, B. Schulz, G. Reck and N. Ono, *Chem. Eur. J.*, 2004, **10**, 4853–4871.

263 Y. Ni, W. Zeng, K. W. Huang and J. Wu, *Chem. Commun.,* 2013, **49**, 1217–1219.

264 A. Wakamiya, T. Murakamib and S. Yamaguchi, *Chem. Sci.*, 2013, **4**, 1002–1007.

265 N. P. Vasilenko, F. A. Mikhailenko and J. I. Rozhinsky, *Dyes. Pigms.*, 1981, **2**, 231–237.

266 N. Ono, T. Yamamoto, N. Shimada, K. Kuroki, M. Wada, R. Utsunomiya, T. Yano, H. Uno and T. Murashima, *Heterocycles*, 2003, **61**, 433–447.

267 A. B. Descalzo, H. J. Xu, Z. L. Xue, K. Hoffmann, Z. Shen, M. G. Weller, X. Z. You and K. Rurack, *Org. Lett.*, 2008, **10**, 1581–1584.

268 Y. Matsuo, A. Saeki, S. Seki, Y. Kureishi, S. Saito, S. Yamaguchi and H. Shinokubo, *Org. Lett.*, 2012, **14**, 866–869.

269 T. Sarma, P. K. Panda and J. Setsune, *Chem. Commun*., 2013, **49**, 9806-9808.

270 T. Okujima, Y. Tomimori, J. Nakamura, H. Yamada, H. Uno and N. Ono, *Tetrahedron*, 2010, **66**, 6895–6900.

271 L. Zeng, C. Jiao, X. Huang, K. W. Huang, W. S. Chin, and J. Wu, *Org. Lett.*, 2011, **13**, 6026–6029.

272 C. Jiao, K. W. Huang, and J. Wu, *Org. Lett.*, 2011, **13**, 632–635.

273 K. Tan, L. Jaquinod, R. Paolesse, S. Nardis, C. D. Natale, A. D. Carlo, L. Prodi, M. Montalti, N. Zaccheroni and K. M. Smith, *Tetrahedron*, 2004, **60**, 1099–1106.

274 C. Jiao, L. Zhu and J. Wu, *Chem. Eur. J.*, 2011, **17**, 6610–6614.

275 G. Ulrich, S. Goeb, A. De Nicola, P. Retailleau and R. Ziessel, *Synlett,*2007, **10**, 1517–1520.

276 G. Ulrich, S. Goeb, A. De Nicola, P. Retailleau and R. Ziessel, *J. Org. Chem.*, 2011, **76**, 4489–4505.

277 L. Jiao, C. Yu, M. Liu, Y. Wu, K. Cong, T. Meng, Y. Wang and E. Hao, *J. Org. Chem.*, 2010, **75**, 6035–6038.

278 Y. Kubo, Y. Minowa, T. Shoda and K. Takeshita, *Tetrahedron Lett.*, 2010, **51**, 1600–1602.

279 Y. Kubo, K. Watanabe, R. Nishiyabu, R. Hata, A. Murakami, T. Shoda and H. Ota, *Org. Lett.*, 2011, **13**, 4574–4577.

280 C. Yu, Y. Xu, L. Jiao, J. Zhou, Z. Wang, and E. Hao, *Chem. Eur. J.,* 2012, **18**, 6437–6442.

281 S. O. McDonnell and D. F. O'Shea, *Org. Lett.*, 2006, **8**, 3493–3496.

282 J. Killoran, S. O. McDonnell, J. F. Gallagher and D. F. O'Shea, *New J. Chem.*, 2008, **32**, 483–489.

283 A. Coskun, M. D. Yilmaz and E. U. Akkaya, *Org. Lett.*, 2007, **9**, 607–609.

284 R. Gresser, H. Hartmann, M. Wrackmeyer, K. Leo and M. Riede, *Tetrahedron*, 2011, **67**, 7148–7155.

285 X. Zhang, H. Yu and Y. Xiao, *J. Org. Chem.*, 2012, **77**, 669–673.

286 W. Zhao and E. M. Carreira, *Angew. Chem. Int. Ed.*, 2005, **44**, 1677–1679.

287 W. Zhao and E. M. Carreira, *Chem. Eur. J.*, 2006, **12**, 7254–7263.

288. Loudet, R. Bandichhor, L. Wu and K. Burgess, *Tetrahedron*, 2008, **64**, 3642–3654.

289 A. Loudet, R. Bandichhor, K. Burgess, A. Palma, S. O. McDonnell, M. J. Hall and D. F. O'Shea, *Org. Lett.*, 2008, **10**, 4771–4774.

290 H. Liu, J. Mack, Q. Guo, H. Lu, N. Kobayashi and Z. Shen, *Chem. Commun*., 2011, **47**, 12092–12094.

291 Y. Cakmak, S. Kolemen, S. Duman, Y. Dede, Y. Dolen, B. Kilic, Z. Kostereli, L. T. Yildirim, A. L. Dogan, D. Guc and E. U. Akkaya, *Angew. Chem., Int. Ed.*, 2011, **50**, 11937–11941.

292 W. Pang, X. F. Zhang, J. Zhou, C. Yu, E. Hao and L. Jiao, *Chem. Commun.*, 2012, **48**, 5437–5439.

293 M. T. Whited, N. M. Patel, S. T. Roberts, K. Allen, P. I. Djurovich, S. E. Bradforth and M. E. Thompson, *Chem. Commun.*, 2012, **48**, 284–286.

294 A. B. Nepomnyashchii, M. Bröring, J. Ahrens and A. J. Bard, *J. Am. Chem. Soc*., 2011, **133**, 19498–19504.

295 M. Bröring, R. Kruger, S. Link, C. Kleeberg, S. Kohler, X. Xie, B. Ventura and L. Flamigni, *Chem. Eur., J*., 2008, **14**, 2976–2983.

296 B. Ventura, G. Marconi, M. Bröring, R. Krüger and L. Flamigni, *New J. Chem*., 2009, **33**, 428–438.

297 A. B. Nepomnyashchii, M. Bröring, J. Ahrens and A. J. Bard, *J. Am. Chem. Soc.*, 2011, **133**, 8633–8645.

298 S. Rihn, M. Erdem, A. De Nicola, P. Retailleau and R. Ziessel, *Org. Lett*., 2011, **13**, 1916–1919.

299 Y. Hayashi, S. Yamaguchi, W. Y. Cha, D. Kim and H. Shinokubo, *Org. Lett.*, 2011, **13**, 2992–2995.

300 L. Gai, H. Lu, B. Zou, G. Lai, Z. Shen and Z. Li, *RSC Adv.,* 2012, **2**, 8840–8846.

301 G. M. Fischer, A. R. Ehlers, A. Zumbusch and E. Daltrozzo, *Angew. Chem., Int. Ed*., 2007, **46**, 3750–3753.

302 G. M. Fischer, M. Isomaki-Krondahl, I. Gottker-Schnetmann, E. Daltrozzo and A. Zumbusch, *Chem. Eur. J*., 2009, **15**, 4857–4864.

303 G. M. Fischer, C. Jungst, M. Isomaki-Krondahl, D. Gauss, H. M. Moller, E. Daltrozzo and A. Zumbusch, *Chem. Commun*., 2010, **46**, 5289–5291.

304 G. M. Fischer, M. K. Klein, E. Daltrozzo and A. Zumbusch, *Eur. J. Org. Chem*., 2011, **19**, 3421–3429.

305 S. Wiktorowski, G. M. Fischer, M. J. Winterhalder, E. Daltrozzo and A. Zumbusch, *Phys. Chem. Chem. Phys*., 2012, **14**, 2921–2928.

306 G. M. Fischer, E. Daltrozzo and A. Zumbusch, *Angew. Chem., Int. Ed*., 2011, **50**, 1406–1409.

307 S. Shimizu, T. Iino, Y. Arakib and N. Kobayashi, *Chem. Commun.,* 2013, **49**, 1621–1623.

308 M. Nakamura, H. Tahara, K. Takahashi, T. Nagata, H. Uoyama, D. Kuzuhara, S. Mori, T. Okujima, H. Yamada and H. Uno, *Org. Biomol. Chem*., 2012, **10**, 6840–6849.

309 Y. Cui and S. Wang, *J. Org. Chem.*, 2006, **71**, 6485–6496.

310 Y. Qin, I. Kiburu, S. Shah and F. Jäkle, *Org. Lett.*, 2006, **8**, 5227–5230.

311 Y. Nagata and Y. Chujo, *Macromolecules*, 2007, **40**, 6–8.

312 Y. Nagata, H. Otaka and Y. Chujo, *Macromolecules*, 2008, **41**, 737–740.

313 D. Li, H. Zhang and Y. Wang, *Chem. Soc. Rev.*, 2013, **42**, 8416–8433.

314 D. Zhao, G. Li, D. Wu, X. Qin, P. Neuhaus, Y. Cheng, S. Yang, Z. Lu, X. Pu, C. Long and J. You, *Angew. Chem. Int. Ed*., 2013, **52**, 13676–80.

315 Z. Zhang, H. Bi, Y. Zhang, D. Yao, H. Gao, Y. Fan, H. Zhang, Y. Wang, Y. Wang, Z. Chen and D. Ma, *Inorg. Chem.*, 2009, **48,** 7230–7236.

316 Y. Zhou, J. Kim, M. Kim, W. Son, S. Han, H. Kim, S. Han, Y. Kim, C. Lee, S. Kim, D. Kim, J. Kim and J. Yoon, *Org. Lett*., 2010, **12**, 1272–1275.

317 D. Frath, S. Azizi, G. Ulrich, P. Retailleau and R. Ziessel, *Org. Lett.*, 2011, **13**, 3414–3417.

318 Y. Kubota, T. Tsuzuki, K. Funabiki, M. Ebihara and M. Matsui, *Org. Lett.*, 2010, **12**, 4010–4013.

319 Y. Kubota, H. Hara, S. Tanaka, K. Funabiki and M. Matsui, *Org. Lett.*, 2011, **13**, 6544–6547.

320 Y. L. Rao and S. Wang, *Inorg. Chem.*, 2011, **50**, 12263–12274.

321 D. Frath, S. Azizi, G. Ulrich and R. Ziessel, *Org. Lett.*, 2012, **14**, 4774–4777.

322 R. Ma, Q. Yao, X. Yang and M. Xia, *J. Fluorine Chem.*, 2012, **137**, 93–98.

323 D. Curiel, M. Más-Montoya, L. Usea, A. Espinosa, R. A. Orenes, and P. Molina, *Org. Lett.*, 2012, **14**, 3360–3363.

324 M. Santra, H. Moon, M. Park, T. Lee, Y. K. Kim and K. H. Ahn, *Chem. Eur. J.*, 2012, **18**, 9886–9893.

325 J. Massue, D. Frath, G. Ulrich, P. Retailleau and R. Ziessel, *Org. Lett.*, 2012, **14**, 230–233.

326 J. Massue, D. Frath, P. Retailleau, G. Ulrich and R. Ziessel, *Chem. Eur. J.*, 2013, **19**, 5375–5386.

327 A. Zakrzewska, E. Kolehmainen, A. Valkonen, E. Haapaniemi, K. Rissanen, L. Chęcińska and B. Ośmiałowski, *J. Phys. Chem. A*., 2013, **117**, 252–256.

328 R. S. Singh, M. Yadav, R. K. Gupta, R. Pandey and D. S. Pandey, *Dalton Trans.*, 2013, **42**, 1696–1707.

329 B. Le Guennic,S. Chibani, A. Charaf-Eddin, J. Massue, R. Ziessel and G. Ulrich, D. Jacquemin, *Phys. Chem. Chem. Phys.,* 2013, **15**, 7534–7540.

330 J. Massue, P. Retailleau, G. Ulrich and R. Ziessel, *New J. Chem.*, 2013, **37**, 1224–1230.

331 Y. Zhou, Y. Xiao, S. Chi and X. Qian, *Org. Lett.*, 2008, **10**, 633–636.

332 J. Feng, B. Liang, D. Wang, L. Xue and X. Li, *Org. Lett.*, 2008, **10**, 4437–4440.

333 Y. Y. Wu, Y. Chen, G. Z. Gou, W. H. Mu, X. J. Lv, M. L. Du and W. F. Fu, *Org. Lett.*, 2012, **14**, 5226–5229.

334 Y. Zhou, Y. Xiao, D. Li, M. Fu and X. Qian, *J. Org. Chem*., 2008, **73**, 1571–1574.

335 H. Liu, H. Lu, J. Xu, J. Liu, Z. Li, J. Mack and Z. Shen, *Chem. Commun.*, 2014, **50**, 1074–1076.

336 W. Li, W. Lin, J. Wang and X. Guan, *Org. Lett.*, 2013, **15**, 1768–1771.

337 D. Frath, A. Poirel, G. Ulrich, A. De Nicola and R. Ziessel, *Chem. Commun.*, 2013, **49**, 4908–4910.

338 J. F. Araneda, W. E. Piers, B. Heyne, M. Parvez and R. McDonald, *Angew. Chem., Int. Ed.*, 2011, **50**, 12214–12217.

339 Y. Yang, X. Su, C. N. Carroll and I. Aprahamian, *Chem. Sci.*, 2012, **3**, 610–613.

340 L. Wu and K. Burgess, *J. Am. Chem. Soc.*, 2008, **130**, 4089–4096.

341 G. Nawn, S. R. Oakley, M. B. Majewski, R. McDonald, B. O. Patrickb and R. G. Hicks, *Chem. Sci.*, 2013, **4**, 612–621.

342 A. D. Quartarolo, N. Russo and E. Sicilia, *Chem. Eur. J.*, 2006, **12**, 6797–6803.

343 B. L. Guennic, O. Maurya and D. Jacquemin, *Chem. Chem. Phys*., 2012, **14**, 157–164.

344 B. L. Guennic, O. Maurya and D. Jacquemin, *Phys. Chem. Chem. Phys.*, 2012, **14**, 157–164

345 S. Chibani, A. Charaf-Eddin, B. L. Guennic and D. Jacquemin, *J. Chem. Theory Comput.*, 2013, **9**, 3127−3135

346 J. Mack and N. Kobayashi, *Chem. Rev.*, 2011, **111**, 281−321.

347 J. Mack, N. Kobayashi and Z. Shen, "*Handbook of Porphyrin Science*", K. Kadish, K. Smith and R. Guilard, Eds., 2012, World Scientific, Singapore, Vol. 23, Ch. 109, 281−371.

348 H. J. Xu, J. Mack, D. Wu, Z. L. Xue, A. B. Descalzo, K. Rurack, N. Kobayashi and Z. Shen, *Chem. Eur. J.*, 2012, **18**, 16844−16867.

349 H. J. Xu, J. Mack, A. B. Descalzo, Z. Shen, N. Kobayashi, X. Z. You and K. Rurack, *Chem. Eur. J.*, 2011, **17**, 8965−8983.

350 Z. Xue, J. Mack, H. Lu, L. Zhang, X̃.Z. You, D. Kuzuhara, M. Stillman, H. Yamada, S. Yamauchi, N. Kobayashi and Z. Shen, *Chem. Eur. J.*, 2011, **17**, 4396−4407.

351 S. Atilgan, T. Ozdemir and E. U. Akkaya, *Org. Lett*., 2008, **10**, 4065–4067.

352 S. Zhu, J Zhang,G Vegesna, F.T. Luo; S. A Green and H Liu, *Org. Lett*. 2011, **13**, 438–441.

353 M. Tasior and D. F. O'Shea, *Bioconjugate Chem.,* 2010, **21**, 1130–1133.

354 S. Atilgan, Z. Ekmekci, A. L. Dogan, D. Guc and E. U. Akkaya, *Chem. Commun.*, 2006, 4398–4400.

355 S. Zhu, J. Zhang, J. Janjanam, G. Vegesna, F. T. Luo, A. Tiwari and H. Liu, *J. Mater. Chem. B*, 2013, **1**, 1722–1728.

356 K. Griesser, D.Gohringer,. T Sabirov, and C. Richert, *Eur. J. Org. Chem*. 2010, **19**, 3611–3620.

357 S. L. Niu, G. Ulrich, R. Ziessel, A. Kiss, P. Y. Renard and A. Romieu, *Org. Lett*., 2009, **11**, 2049–2052.

358 N. J. Meltola, R. Wahlroos and A. E. Soini, J. *Fluoresc*., 2004, **14**, 635–647.

359 S. L. Niu, C. Massif, G. Ulrich, R. Ziessel, P. Y. Renard and A. Romieu, *Org. Biomol. Chem*., 2011, **9**, 66–69.

360 J. Jiang, H. Lu and Z. Shen, *Chin. J. Inorg. Chem.,* **2010**, 26, 1105–1108.

361 O. Dilek and S. L. Bane, Bioorg. *Med. Chem. Lett*., 2009, **19**, 6911–6913.

362 M. Brellier, G. Duportail and R. Baati, *Tetrahedron Lett*., 2010, **51**, 1269–1272.

363 C. Thivierge, R. Bandichhor and K. Burgess, *Org. Lett*. 2007, **9**, 2135–2138.

364 L. Li, J. Han, B. Nguyen and K. Burgess, *J. Org. Chem*. 2008, **73**, 1963–1970.

365 S. C Dodani, He, Q, Chang and C. J. *J. Am. Chem. Soc*., 2009, **131**, 18020–18021.

366 L. Li, B. Nguyen and K. Burgess, Bioorg., *Med. Chem. Lett*., 2008, **18**, 3112–3116.

367 M. Tasior, J. Murtagh, D. O. Frimannsson, S. O. McDonnell and D. F. O'Shea, *Org. Biomol. Chem*., 2010, **8**, 522–525.

368 S. Hoogendoorn, A. E. M. Blom, L. I. Willems, G. A. vander Marel and H. S. Overkleeft, *Org. Lett*., 2011, **13**, 5656–5659.

369 C. Massif, S. Dautrey, A. Haefele, R. Ziessel, P. Y. Renard and A. Romieu, *Org. Biomol. Chem*., 2012, **10**, 4330–4336.

370 J. Murtagh, D. O. Frimannsson and D. F. O'Shea, *Org. Lett*., 2009, **11**, 5386–5389.

371 T. Bura and R. Ziessel, *Org. Lett.*, 2011, **13**, 3072–3075.

372 S. L. Niu, G. Ulrich, P. Retailleau, J. Harrowfield and R. Ziessel, *Tetrahedron Lett.*, 2009, **50**, 3840–3844.

373 A. Romieu, C. Massif, S. Rihn, G. Ulrich, R. Ziessel and P. Y. Renarda, *New J. Chem.*, 2013, **37**, 1016–1027.

374 S. L. Niu, C. Massif, G. Ulrich, P. Y. Renard, A. Romieu and R. Ziessel, *Chem. Eur. J.*, 2012, **18**, 7229–7231.

375 J. Zhao, W. Wu, J. Sun and S. Guo, *Chem. Soc. Rev.*, 2013, **42**, 5323–5351.

376 Y. Yang, R. P. Hughes and I. Aprahamian, *J. Am. Chem. Soc.*, 2012, **134**, 15221−15224.

377 X. Wang, H. Liu, J. Cui, Y. Wu, H. Lu, J. Lu, Z. Liu and W. He, *New J. Chem.*, 2014, **38**, 1277−1283.

Structural modification strategies for the rational design of Red/NIR region BODIPYs

Hua Lu,[a,b] John Mack,[c] Yongchao Yang,[a] Zhen Shen*[a]

Structure-property relationships of red/NIR region BODIPY dyes are analyzed, so that trends in their photophysical properties can be readily compared.